ELECTROSTATIC PROPULSION BEAM DIVERGENCE EFFECTS ON SPACECRAFT SURFACES

FINAL REPORT
VOLUME I

David F. Hall

17 AUGUST 1970

CONTRACT NO. 952350

"This work was performed for the Jet Propulsion Laboratory, California Institute of Technology, as sponsored by the National Aeronautics and Space Administration under Contract NAS7-100."

TRW
SYSTEMS GROUP
ONE SPACE PARK
REDONDO BEACH, CALIFORNIA 90278

ACKNOWLEDGEMENT

The technical work reported herein was accomplished by the following individuals:

Chemistry	R. A. Meyers E. R. Wilson
Metallurgy	M. E. Kirkpatrick R. A. Mendelson
Thermophysics	L. R. Kelley E. E. Luedke
Surface and Vacuum Physics	D. F. Hall H. Shelton

Substantial support was provided by M. Billingsley, W. Goldstein and P. Faville. The JPL Technical Manager was J. R. Womack. He was aided by W. Carroll.

TABLE OF CONTENTS

TABLE OF CONTENTS (Cont'd)

ABSTRACT

The second phase of a program to develop understanding of and tolerance-level criteria for the deleterious effects of electrostatic rocket exhaust (Cs, Cs^+, Hg, Hg^+) impinging on typical classes of spacecraft (S/C) surfaces is completed. Prior work was done under Contract No. NAS7-575. This phase included fabrication of necessary experimental fixtures and exploratory experiments. Fixture design, fabrication, and testing is reported along with experimental and analytical results obtained to date. Recommendations are made for the next phase. Immersion at approximately 20°C of Teflon FEP and Kapton (H-film) in liquid Cs, and of Pb/Sn solder in both Cs and Hg produced notable degradation of sample properties. Sylgard 182, Delrin, GT-100 and SMRD 745, which are representative of additional organic matrices found in S/C materials appeared uneffected by immersion in Hg and Cs. Silver reacted with Hg rather slowly. Ultimate tensile strength of Ag was unaffected by surface coatings of Hg and up to four weeks of reaction time. Addition of up to 10% Ag to soft solder apparently does not improve its resistance to Hg attack. Atomic Hg beams did not significantly affect the absorptivity (α) or emittance (ε) of ten typical S/C coatings or the sputtering rate of aluminum under conditions where at most one monolayer of Hg could be adsorbed. Very high fluxes and large doses of 3 Kev Hg^+ produced marked increases in α of white paints and RTV samples, but not of black paints, Al, Au, and glasses. Emittances of all samples remained relatively constant. Analysis shows that sputtered accelerator grid material is an important thruster effluent to S/C surfaces.

I. INTRODUCTION

A. Background

Electrostatic rockets emit propellant particles into at least 2π steradians. Spacecraft (S/C) designers therefore require tolerance-level criteria for the almost inevitable interception of propellant particles by S/C surfaces. During Phase I of this program, under Contract NAS7-575, a systematic analytical study was made of the deleterious effects of Hg, Hg^+, Cs, and Cs^+ on spacecraft surfaces. Erosion of non-metallic surfaces by sputtering, degradation of thermal control coatings, chemical degradation of non-metallic surfaces, and propellant condensation on solar cell cover glasses were identified as likely to pose the most restrictive design constraints. Of the above areas, quantitative constraints were generated for condensation subsequent to the adsorption of the first monolayer; the others were at the qualitative stage and required experimental study. During the course of the present phase, the Phase I work was summarized and extended first in a presentation to the electric propulsion community[2] and then in an archival publication.[3]

B. Program Approach and Scope

Table I-1 summarizes the potential problem areas of degradation of spacecraft components by propellant interactions. Since the fields of solar-electric spacecraft design and component construction are constantly evolving, a series of engineering material tests in each of these areas is not indicated. Rather, physical models of degradation effects and extrapolatable data are needed to provide the bases for tradeoff calculations and consideration of new materials and designs. It is the goal of this multi-phase program to provide these models and data with respect to cesium and mercury ion thrusters. For both of these propellant species, the effects of neutrals, ions, and mixtures of neutrals and ions are important.

Table I-1. Potential degradation of spacecraft components from impinging propellants.

DEGRADATION MECHANISM ↓ / SPACECRAFT COMPONENTS AFFECTED →	THERMAL CONTROL COATINGS	OPTICAL ELEMENTS AND COATINGS	STRUCTURAL MATERIALS	INSULATORS AND ELECTRODE GAPS	CONDUCTORS	ADHESIVES	MOVING JOINTS	SOLID STATE COMPONENTS
PROPELLANT CONDENSATION AND/OR THRUSTER MATERIAL DEPOSITION	X	X		X				
CHEMICAL REACTION	X	X	X	X		X	X	
METALLURGICAL REACTION	X		X		X		X	
SPUTTERING EROSION	X	X	X	X	X	X	X	X
RADIATION DAMAGE (DEPOSITION OF ENERGY WITHIN SOLIDS, E.G. IONS)	X							X

X POTENTIAL PROBLEM AREA

The program contains four work units; Metallurgy, Chemistry, Thermophysics, and Low Thrust Propulsion. The metallurgy group is charged with elucidating reactions between the propellants and S/C metals. The chemistry group is responsible for elucidating reactions between the rocket efflux and non-metallic S/C materials. The thermophysics group determines the surface thermal changes which occur in various thermal control coatings. The low thrust propulsion group is responsible for sputtering experiments, operation of the primary facility in which most experiments are performed, and program management.

C. Program Status

The program goals of Phase II were: 1) to fabricate experimental fixtures needed, and 2) to perform exploratory experiments to determine in which areas future emphasis should lie. These program goals have been met. The major experimental fixtures -- the surface thermal sample holder, the multipurpose sample holder, and the quartz crystal microbalance -- were fabricated and successfully tested, and numerous improvements have been made in the basic experimental facility. Exploratory chemical, metallurgical, thermophysical and sputtering experiments have provided a basis for dismissing portions of some potential problem areas, have suggested definitive experiments in other areas, and have shown that still other areas require more complete exploration. Additional analysis of potential problem areas demonstrates that our concern should extend beyond the efflux of propellant particles from thrusters. A presentation of the experimental aspects of the program to the electric propulsion community is presently in preparation.[4]

D. Report Organization

This "Volume I" of the Final Report is an account of work accomplished during Phase II. (Volume II will be issued at the completion of Phase III.) Its structure reflects the program approach. The technical discussion is divided into six sections which represent major program elements. Every section contains a brief introduction linking it with Phase I, an account of progress made during Phase II, specific conclusions, and recommendations for future work. Section VIII draws some general conclusions from the program results to date, and Section IX contains general recommendations for future work. Appendix A describes how the rate of mercury flowing through the experimental beam source is determined. Appendix B contains the spectral reflectance data taken on control samples of thermal control coating materials.

II. CHEMISTRY

During Phase I it was determined that relatively little information was available in the literature regarding the chemistry of organic spacecraft surface materials and the propellants cesium and mercury. It was therefore recommended that an exploratory series of immersion tests be conducted to characterize sample material reactions preliminary to propellant beam exposures. The results of these immersion tests are described following a discussion of seven polymeric materials not considered in Phase I.

A. Evaluation of Additional Spacecraft Materials

The feasibility study of a 30 watt/lb roll-up solar array by the General Electric Co.[1] proposed the use of seven polymeric materials not evaluated in Phase I. Since this array concept was selected for further development these materials were evaluated on the basis of structure reactivity relationships with regard to use in cesium and mercury neutral and ion environments. Table II-1 lists the materials, their intended use on the GE array, and other pertinent information.

Table II-1

Material	Manufacturer	Type	Use on GE Array
Epon 934	Shell	Aromatic epoxy polymer	bonding beryllium
Delrin	Dupont	Polyacetal	Neg'ator take-up spool
Sylgard-182	Dow Corning	Polydimethylsiloxane with vinyl groups cured with Pt & silane materials	Cell-to-cover glass bond
RTV-560	G.E.	Polymethylphenylsiloxane	Cushioning buttons
SMRD 745	G.E.	Aromatic epoxy polymer	Cell-to-substrate bond
Epiall 1914	Allied	Epoxy, novolac-amine cured	Drum power feed-thru slip ring dielectric
GT-100	Schjeldahl	Polyester	Bus strip-to-substrate bond

Several of these materials were selected for immersion testing; reactions between propellant and untested materials were predicted on the bases of the chemical structure of these materials, immersion tests of similar materials, and chemical theory. The status of each nonmetallic spacecraft material studied to date is summarized in Table II-2.

B. Selection of Representative Samples

The 13 organic plastics in Table II-2 may be classified in six categories according to the chemical structure of their organic matrices. These matrices, which make up the reactive and property conferring portions of these spacecraft materials, are: polyester, polyacetal, epoxy, polyimide, silicone and polyperflorethylenepropylene. In order to avoid the cost of screening each spacecraft material individually, six spacecraft materials which are representative of each of the six organic structures present in the total group were selected for immersion in propellant and analysis. These are: Sylgard 182 (a methylphenylvinyl silicone similar in structure to both RTV resins S-13G, and to a portion of the matrix of PV100), GT 100 (a polyester which is also representative of a part of the structure of PV100), SMRD 745 (an epoxy resin which is similar in structure to Epon 934, Epiall 1914, and Cat-a-lac black), Teflon FEP (a perfluorinated carbon chain), Kapton H-film (a polyimide), and Delrin (a polyacetal). Each of the resins selected were unfilled and colorless, which greatly facilitates analysis.

C. Initial Immersion Test

Kapton (H-film) was chosen as the first material for chemical evaluation as Kapton is the major plastic construction material for the 30 watt/lb General Electric roll-up solar array concept.

A one liter resin kettle was fitted with a lid sealed with Apiezon wax and connected to a vacuum system consisting of a roughing pump, and LN_2 cooled trap. The system was evacuated to 25 μ and the kettle was heated to approximately 100°C and held overnight to insure drying of the glass.

The following morning the resin kettle, still evacuated, was transferred to a dry box, along with the Kapton film and cesium to be used in the experi-

Table II-2. Chemical effects of Cs, Cs^+, Hg, and Hg^+ on typical spacecraft materials.

MATERIAL	TYPE	EXTENT OF DEGRADATION[a] BY			
		Cs	Cs^+, Hg^+	CsOH[b],	Hg
H-FILM[c] (KAPTON)	POLYIMIDE	TURNS DEEP VIOLET DUE TO ONE ELECTRON OXIDATION-REDUCTION (PRODUCT PROBABLY HIGHLY CONDUCTIVE AND PHOTOCONDUCTIVE)	(MODERATE)[d]	(SEVERE HYDROLYSIS WITH CHAIN SCISSION)	NONE
TEFLON FEP[c]	POLY (PERFLUORO-ETHYLENE PROPYLENE)	TURNS BLACK; C & CsF FORMS AT SURFACE	(SEVERE, LOSS OF FLUORINE)[d]	(NONE)	NONE
RTV 40	AMINE CURED SILICONE	(LITTLE OR NONE)	(MODERATE)[d]	(MODERATE BY HYDROLYSIS)	(NONE)
CAT-A-LAC BLACK	AMINE CURED EPOXY	(LITTLE OR NONE)	(MODERATE)[d]	(MODERATE)	(NONE)
PV-100	SILICONE-ALKYD RESIN; TiO_2 PIGMENT	(LITTLE OR NONE OF RESIN; POSSIBLE PIGMENT DISSOLUTION)	(MODERATE, WITH DARKENING)[d]	(MODERATE TO SEVERE DUE TO HYDROLYSIS)	(NONE)
DELRIN[c]	POLYACETAL	LITTLE OR NONE	(MODERATE)[e]	(NONE)	NONE
SYLGARD 182[c]	SILICONE	LITTLE OR NONE	(MODERATE)[d]	(MODERATE)	NONE
SMRD 745[c]	EPOXY	LITTLE OR NONE	(MODERATE)[d]	(LITTLE OR NONE)	NONE
GT-100[c]	POLYESTER	LITTLE OR NONE	(MODERATE)[d]	(SLIGHT TO SEVERE DUE TO HYDROLYSIS)	NONE
EPON 934	AROMATIC EPOXY	(LITTLE OR NONE)	(MODERATE)	(SLIGHT)	(NONE)
RTV-560	POLYMETHYLPHENYL-SILOXANE	(LITTLE OR NONE)	(MODERATE)	(NONE)	(NONE)
EPIALL 1914	EPOXY NOVOLAC	(LITTLE OR NONE)	(MODERATE)	(SLIGHT)	(NONE)
S-13G	METHYL SILICONE +ZnO	(LITTLE OR NONE OF RESIN POSSIBLE DARKENING OF PIGMENT)	(MODERATE, PROBABLE DARKENING DUE TO PIGMENT REACTION)[e]	(MODERATE)	(SLIGHT OR NONE)
Z-93	POTASSIUM SILICATE +ZnO	(SLIGHT AT STRAIN POINTS, MODERATE DARKENING)	(MODERATE, WITH DARKENING)	(MODERATE ETCHING)	(SLIGHT OR NONE)
Al_2O_3		(SLIGHT TO MODERATE AT STRAIN POINTS)	(SLIGHT)	(SLIGHT ETCHING)	(SLIGHT OR NONE)
BeO		(SLIGHT TO MODERATE AT STRAIN POINTS)	(SLIGHT)	(SLIGHT ETCHING)	(SLIGHT OR NONE)
CORNING 7740	PYREX	(SLIGHT TO MODERATE AT STRAIN POINTS)	(SLIGHT TO NONE)	(SLIGHT ETCHING)	(SLIGHT OR NONE)
CORNING 0211	PYREX	(SLIGHT TO MODERATE AT STRAIN POINTS)	(SLIGHT TO NONE)	(SLIGHT ETCHING)	(SLIGHT OR NONE)

a. INFORMATION IN PARENTHESES IS POSTULATED, BASED ON ANALOGOUS LITERATURE DATA, INFORMATION WITHOUT PARENTHESES IS DATA FROM LITERATURE AND IMMERSION TESTS.

b. CsOH IS ANTICIPATED WHEN Cs ARRIVES AT SURFACES HAVING ABSORBED WATER VAPOR.

c. IMMERSION TESTED IN Cs AND Hg FOR 48 HOURS.

d. SURFACE CHAIN DEGRADATION AND CROSS-LINKING.

e. SURFACE CHAIN SCISSION.

ment. The entrance chamber of the dry box was evacuated to ∿1 μ, and held there for one hour and then back filled with high purity argon. The kettle was opened to the argon atmosphere and the sample was placed inside of it, followed by enough cesium to immerse the film completely. The kettle was taken out of the dry box, evacuated to 25 μ, and stored at room temperature for 24 hours. At the end of this time, the kettle was replaced in the dry box and the sample was withdrawn and quenched with methanol.

During the withdrawl of the film, it tore into several fragments, and after quenching it was noted that the tear strength was almost nil.

The Kapton film was not well dried using the above experimental method and it was hypothesized that the film decomposition was due to the reaction of Kapton with cesium hydroxide rather than cesium metal. An improved apparatus was designed which allows exposure of very dry materials to distilled cesium metal at the temperature of choice. Kapton tested in this apparatus did not lose tensile strength.

D. Improved Apparatus

The improved apparatus was designed (Figure II-1) and assembled. It allows anhydrous and oxygen free exposure of samples to distilled cesium.

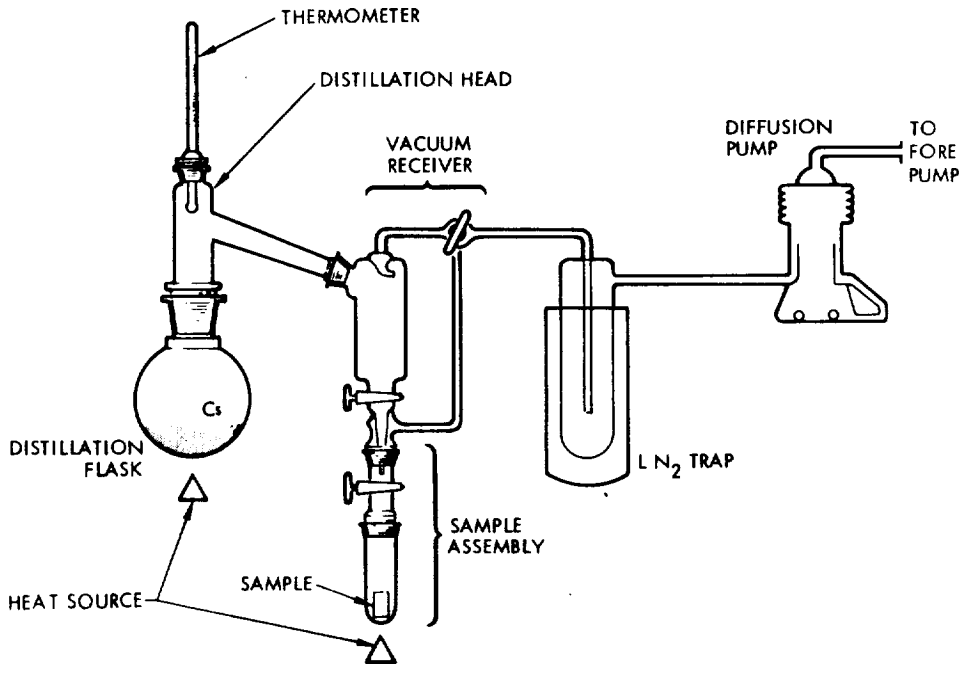

Figure II-1. Cesium distilling apparatus

Operation.

(1) Apparatus is placed under a vacuum of 25 microns.

(2) Sample is dried by heating at 70°C for two hours.

(3) Cesium is distilled (240-250°C) onto sample (at temperature of choice), covering sample.

(4) Sample assembly is removed, still under vacuum, and transferred to a glove box where it is stored for duration of exposure.

(5) Sample is removed from assembly in glove box and immediately immersed in quench solution.

E. Cesium/Kapton Immersion Tests.

The improved apparatus and procedure described above was utilized to expose well dried Kapton film to distilled cesium. The film was exposed to cesium at room temperature for a period of 48 hours. The film rapidly turned to a dark purple color where exposed to cesium, but after removal of the film from the cesium environment and quenching (destruction of cesium) the tensile strength of the film had not changed (25,000 psi); in addition chemical analysis of the quench solution by thin layer chromatography showed that no organic portion of the Kapton film had been chemically reacted. The formation of the purple color, however, is highly significant.

Aromatic organic compounds (those containing phenyl or fused phenyl rings) form one electron oxidation-reduction salts with strong alkali metal reducing agents such as sodium, potassium and lithium as shown in the figure for cesium:

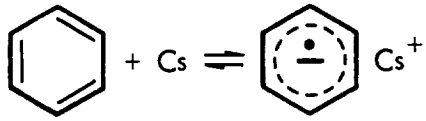

These salts are highly colored due to low energy electronic transistions which become possible by virtue of the one electron oxidation reduction reaction. The salts are semiconductors, whereas the original organic compound

structures may have been excellent insulators. Resistivities of the order of 10^1 to 10^{13} ohm·cm are common for these complexes in the dark or feeble light and many of them exhibit photoconductivity, where the resistivity may be lowered by an additional order of magnitude on exposure to visible light.

Although one electron oxidation-reduction reactions have not previously been observed between polymeric materials and alkali metals, the color formation described above strongly suggests a reaction analogous to that which is known to occur between aromatic organics and alkali metals. Thus, it is contended that while the Kapton film is not chemically degraded by contact with Cs, the one electron oxidation-reduction salt is formed, thereby increasing the dark and light conductivity of the film by several orders of magnitude.

In view of the importance of Kapton as a spacecraft surface material, two additional immersion tests were performed. In both a 2-mil-thick sample was placed under approximately 3000 psi tension with a spring device during 48 hours of immersion. The tests differed in the cesium temperature; one was performed at room temperature whereas the other was at 60°C.

The results of all three dry-Kapton exposures were similar. In all cases exposure of the H-film produced a deep violet color where the Cs touched the surface of the material. No differences were noted between the tension and 60°C test results and the 22°C, 48 hour exposure. The physical properties of the exposed film had not changed after quenching. As long as the samples were protected from moisture the color remained, but when they were exposed to laboratory air, the color disappeared over a period of days.

F. Additional Cesium Immersion Tests

The five remaining representative organic spacecraft materials were immersion tested in cesium. Each of these materials was dried in a sample tube at 90-100°C/25 μ for one hour just prior to distillation of the Cs onto it. Each material was left in the liquid metal at approximately 30°C for 48 hours. At the end of the exposure period each material was washed with reagent n-Hexane and then quenched in reagent methanol. The samples were dried and weighed to determine weight loss or gain. Quantitative results are listed in Table II-3. Control samples were given identical treatment except for cesium exposure. Infrared spectrograms were made of all samples using the ATR device.

TABLE II-3. Preliminary Analysis of Cesium Exposed Spacecraft Materials

Material	Initial wt., g	Final wt., g	Percent wt. Changes	Comments
Delrin[1]	1.2145	1.2153	+0.066	no visible change
Delrin[2]	1.3263	1.3272	+0.068	no visible change
Sylgard 182[1]	0.1262	0.1255	-0.55	
Sylgard 182[2]	0.1164	0.1154	-086	
Teflon FEP[1]	0.2601	0.2543	-2.23	sample turned black
Teflon FEP[2]	0.2481	0.2480	-0.04	
SMRD 745[1]	0.5982	0.5844	-2.31	no visible change
SMRD 745[2]	0.6056	0.5930	-2.08	
GT 100[1]	0.0624	0.0587	-5.02	no visible change
GT 100[2]	0.0638	0.0624	-2.19	TLC shows no organic materials

1. Exposed (immersed in cesium, then immersed in quench solution and dried).
2. Standard unexposed (immersed in quench solution and dried).

The exposure of SMRD 745, Delrin, Sylgard 182, and GT-100 produced little if any change in the appearance of the materials. The exposure of Teflon FEP produced a major and lasting change in the surface properties of this material. The surface of this material had turned black and the sample lost approximately 2% of its weight. The infrared spectrum of the exposed sample indicated the destruction of the C-F bonds at the surface.

The reaction of Cs with the Teflon FEP film apparently proceeds with the extraction of fluorine from the surface of the polymer. This leaves a carbon surface which will conduct electricity and also provides a breakdown path for high voltages after short reaction times. The blackening of the surface should radically affect the emission-absorption properties of the material.

The thin film chromatographic analysis of the condensed wash and quench solutions did not show the presence of organic materials in them. Acidification of these solutions did not change this. Thus, in none of the cases did organic residues break off the polymer chains nor was there any extensive lowering of molecular weight.

The conclusion is that of the six materials tested, only H-film and Teflon FEP undergo rapid degradation by cesium.

G. Mercury Immersion Tests

Weighed samples of each of the six representative materials were placed in clean reaction tubes and covered with freshly filtered triple distilled mercury. At the end of 48 hours, the mercury was decanted from the tubes and the samples were flushed with reagent hexane. After drying, each sample was visually inspected and reweighed. The data appears in Table II-4.

Table II-4. Weight changes of mercury exposed spacecraft materials

Sample	Weight g		% Change
	Before Exp.	After Exp.	
H-film	0.0582	0.0584	+0.35
GT-100	0.0575	0.0582	+1.22
Sylgard-182	0.1111	0.1114	+0.27
Delrin	1.2156	1.2157	+0.008
Teflon FEP	0.1105	0.1108	+0.27
SMRD 745	0.5597	0.5606	+0.16

Visually there were no indications of reaction between the materials and the metal. Small increases in the weight of each sample were noted. This is probably due to the adherence of small amounts of mercury to the surface of the samples. The surface of the GT-100 is rougher than those of the others and it also has a larger surface to weight ratio. This explains the larger weight change for this sample.

These experiments indicate that there is little or no reaction between the selected materials and metallic mercury at room temperature for the time interval of the tests.

H. Adhesive Experiments

A short investigation was undertaken to determine a good adhesive to fix samples to the aluminum substrate of the multipurpose sample holder. This holder, described in Section VI, will be used to expose samples to propellant beams during Phase III. The adhesive criteria was that a good bond be formed, but the sample be capable of being freed without damage.

Experiments were carried out with H-film. Films (3/4" x 1") of this material were glued to aluminum sheet and tested for adherence manually. The samples were subjected to shear and peeling tests.

Three materials were tested, vinyl alcohol (dissolved in water), ethyl cellulose (dissolved in ethyl alcohol), and vinyl acetate emulsion to which ethyl alcohol was added.

The aluminum plate was coated with the desired adhesive and the film was pressed firmly down on it. The sample was then dried at 40-50°C approximately 1/2 hour, and then given a manual shear test, which consisted of taking the sample in the right hand and producing a shear stress on the adhered film with the right thumb.

It was found that the vinyl acetate emulsion gave the best bond. The vinyl alcohol material did not dry even after several hours and the ethyl cellulose gave a poor bond.

A final test was conducted on the vinyl acetate material. A well handled sample was placed in a vacuum chamber and held for 24 hours at approximately 25 μ pressure. At the end of this period, the sample was well bonded to the aluminum sheet, but could be peeled from the substrate without damage.

I. Conclusions

Immersion tests of six organic spacecraft materials , Sylgard 182, Delrin, GT100, SMRD 745, Teflon FEP, and Kapton (H-film), which are representative of six organic matrices (silicone, polyacetal, polyester, epoxy, polyperflorethylenepropylene, and polyimide) in mercury and cesium indicate that Kapton and Teflon FEP are subject to rapid chemical attack by cesium. The remaining four materials immersed in cesium and all materials immersed in mercury were not measurably affected. Consequently, it is expected that chemical effects of atomic beams impinging on these (and similar) materials will be either subtle or nonexistent.

Immersion of Teflon FEP in cesium for 24 hours at approximately 20°C produced a black, carbon surface layer through destruction of C-F bonds at the surface. This layer will conduct electricity and it provides a breakdown path for high voltages. If it is produced when Teflon is exposed to atomic cesium beams, then Teflon's use as an electrical insulator and/or first surface thermal control coating on spacecraft surfaces must be correspondingly restricted.

Immersion of Kapton in liquid cesium has raised questions regarding their compatibility. If the Kapton is completely dry, it turns purple where contacted by cesium. It is believed that a one electron oxidation-reduction, semiconductive, photoconductive salt layer is formed. In addition to this reaction, if residual water is present in the Kapton, as might be the case for several hours following array unrolling, liquid cesium seriously reduces Kapton's tensile strength. These are not desirable properties for solar cell substrates.

An adhesive suitable for mounting film materials to aluminum multipurpose sample holder substrates has been identified.

J. Recommendations for Future Work

As expected, the work accomplished during Phase II permits identification of those areas which require additional experimental effort and those which do not. Specifically, it is believed that:

1) Mercury atom beam multipurpose sample holder exposures are not required on organic materials.

2) Of the samples immersion tested, cesium atom beam multipurpose sample holder exposures are only of interest in the cases of Kapton and Teflon FEP.

3) Ion beam multipurpose sample holder exposures of representative organic spacecraft materials are required for the reasons outlined in Section 5.4.2 of Reference II-2.

4) Evaluation should be made of the purple colored complex which is produced when cesium contacts Kapton.

5) Immersion tests are cost effective. Therefore, additional tests should be performed a) whenever possible degradation of S/C surface materials by atomic propellant is predicted, e.g., Cs/S13G, Cs/Z93, and b) on all organic materials which may receive propellant by virtue of specific spacecraft designs.

III. METALLURGY

In Phase I it was determined that two classes of experiments were required on certain spacecraft metals, viz., measurement of changes in surface thermal properties, and determination of bulk effects. The surface thermal measurements are described in Section IV. Immersion and surface coating experiments designed to qualitatively determine the bulk effects of mercury on solder and silver and of cesium on solder are described below.

A. Immersion Tests

1. Test Vessel Design. The vessel that was used for the immersion tests is a modified, flat bottom test tube which provides a sealed test chamber. Figure III-1 shows the vessel design. The glass rod on the axis of the chamber provides a viewing platform on which the sample sits when the tube is inverted. In the mercury immersion tests, the rod insures that the sample will remain submerged. The fill port valve and fitting are compatible with the cesium distilling apparatus described in Section II, which was used for cesium immersion tests.

2. Mercury/Solder.

a. Experimental procedure. The solder used for the immersion tests was a rosin core 63 w/o Sn solder. It was cast into a cylindrical shape 0.4900" in diameter in a quartz test tube. The solder was then remelted under an argon atmosphere in an induction furnace and kept molten long enough to allow the bulk of the rosin to float to the top of the liquid pool. After the solder solidified samples were taken from the lower half of the remelted section. No residual rosin was observed on cut sample. The solder sample was then ground so that both ends were flat, solvent cleaned, weighed, and measured. The sample was then placed in the cleaned test vessel and the glass was sealed. Figure III-2a is a photograph of the sample in the sealed test vessel. Fifty grams of triple distilled mercury was then added to the test vessel through the glass valve. The test vessel was placed in a vertical position so that the mercury completely covered the solder sample.

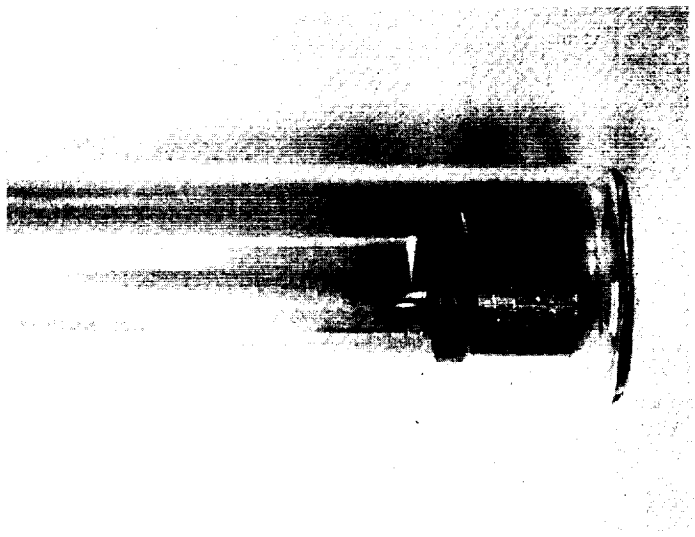

Figure III-2a. Solder sample prior to addition of mercury.

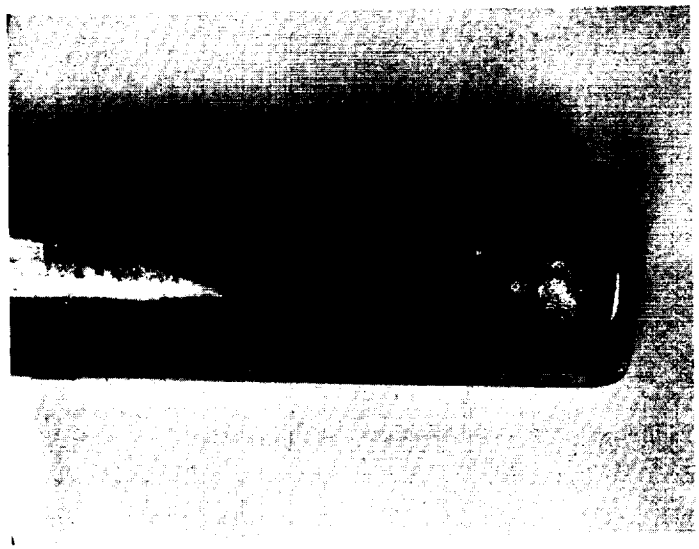

Figure III-2b. Solder sample after one week exposure to mercury.

b. Observations. Upon addition of the mercury to the test vessel, an immediate surface reaction with the solder seemed to take place. The surface appeared to be completely wet by the mercury. Examination of the solder sample was performed on a daily schedule for one week, during which time an increasing amount of solder was dissolved from the sample. After the first two days a precipitate was seen at the upper end of the test vessel. Figures III-2b and III-3 show the test vessel after 1 week of exposure. At this point the sample was eroded quite severely but still had the shape of a cylinder. The equilibrium diagrams of a lead/mercury and tin/mercury revealed that the liquid mercury will hold only about 1 to 2% of either constituent in solution, so that the precipitated material would be expected. After the first week of exposure the reaction rate seemed to slow considerably. After two additional weeks no further change could be seen in the solder sample. The test was terminated after 6 weeks, at which time the sample volume was approximately 1/2 its initial value.

Metallographic examination of this sample was not possible because the solder had taken a substantial amount of mercury into solution and did not have sufficient mechanical strength to be mounted and polished. Visual examination of the sample verified that it contained a large amount of mercury. This result is consistent with the phase diagrams for the combinations Pb/Hg and Hg/Sn. These phase diagrams show that Pb will take up to 24% Hg in solution and Sn will take up to 10% Hg at room temperature. The phase diagrams do not indicate rates of reaction; they indicate what will result after reactions are complete. The immersion tests demonstrated that a six week exposure of solder to excess mercury produces a structure with little or no mechanical strength.

3. Mercury/Silver. The silver-mercury immersion test duration was 4 weeks. Upon removal of the silver sample from the mercury, a surface coating of mercury was still present. The sample was cleaned by rubbing it in sulfur, which formed a Hg-S compound, washing this compound off with water, and then briefly immersing it in dilute nitric acid. The sample was then measured and weighed. There was no apparent change in physical dimensions of the sample but there was a slight weight gain due either to incomplete removal of the surface coating of mercury or to mercury being dissolved into the silver. According

Figure III-3. Photo of upper end of test vessel showing metallic deposit.

to the Ag/Hg phase diagram, silver can take approximately 30% mercury into solution.

Cross sections of the silver sample before and after mercury exposure are shown in Figure III-4. Surface irregularities such as that appearing in Figure III-4b were also seen in the unexposed sample. Therefore, they are not ascribed to mercury exposure. Most of the outer edge of the exposed sample has approximately 0.2 mil layer of porous-appearing material. Occasionally there are local regions where this layer is approximately 2 mils thick, such as the one shown in Figure III-4b. The zone underneath the surface layer, which is defined by the dark band, has an average depth of approximately 3 mils. Interpreting these preparations in terms of the phase diagram, one expects that the other layer is ε phase (containing approximately 45% (atomic percent) Hg), and that the zone underneath is a solid solution ranging in mercury concentration from 36% at the interface with the ε down to approximately 0% somewhere in the vicinity of the dark band. A series of microhardness measurements were performed on the silver sample after exposure to the mercury. Table III-2 lists the relative hardness of the sample from the center toward the edge. As predicted from the interpretation above, the hardness increases as the traverse is taken, with the hardest point at the edge of the sample. Figure III-5 shows the microhardness indentations.

This immersion test showed that the reaction time of silver with excess mercury at room temperature is long compared with a month.

4. Cesium/Solder.

a. First test. The eutectic solder/cesium immersion test sample was a 6 gram cylindrical casting. The sample was sealed in a test vessel, and the vessel was loaded with approximately 7 grams of cesium using the distillation system described in Section II. This quantity of cesium completely immersed the sample. Within the first hour after filling, a dark precipitate was seen to form on the internal glass surfaces. Visibility of the sample was lost due to cesium wetting the glass in the sample area. An attempt was made to remove this cesium by heating the vessel with a hot air gun. This attempt was only partially successful; however, the sample appeared to have only a surface coating of cesium.

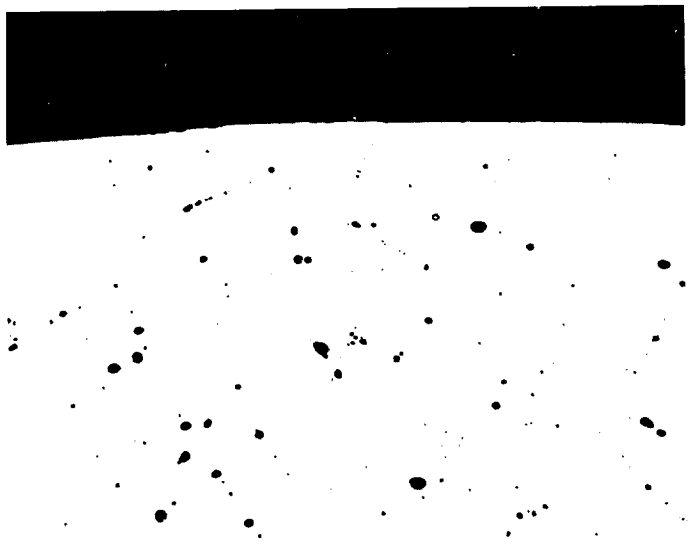

Figure III-4a. Cross section of silver casting before exposure to mercury. 100X.

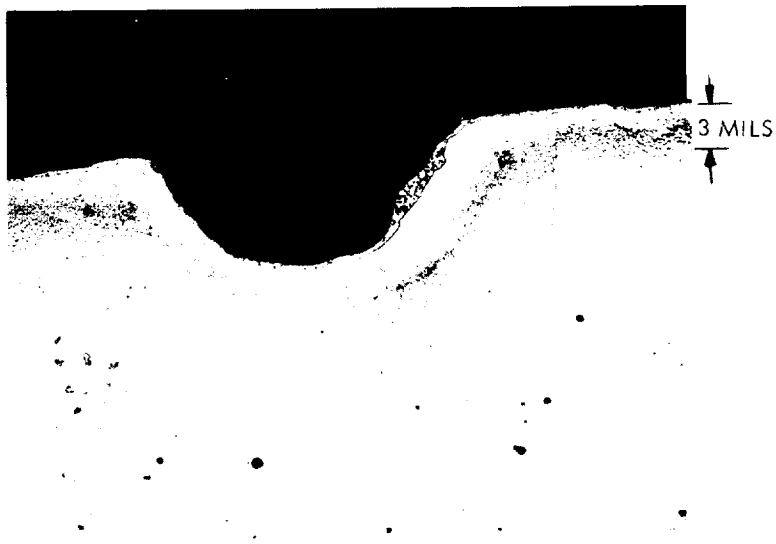

Figure III-4b. Cross section of silver casting after 4 week exposure to mercury. 100X.

Table III-1. Microhardness of silver sample after 4 week immersion in mercury.

Location	Knoop Hardness
Center of sample	49.23
Middle of silver area	48.3
Interface	49.23
Diffusion zone	48.65
	59.23
	63.24

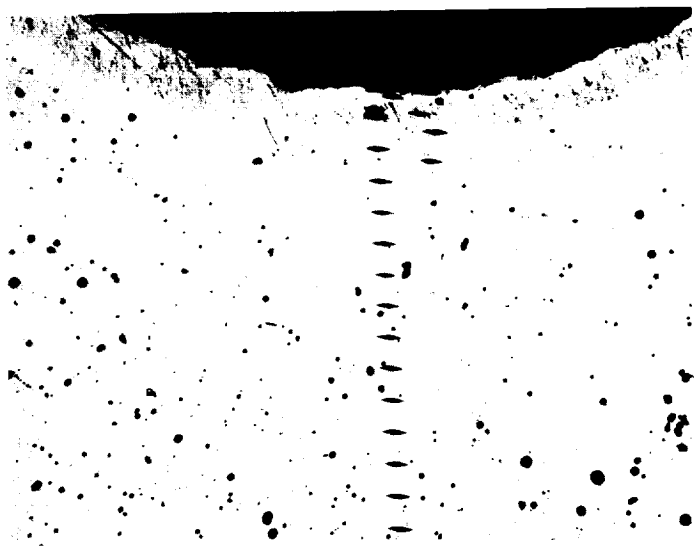

Figure III-5. Microhardness indentation performed on Ag/Hg sample. 100X.

No reaction was visible at this time. Sometime within the next 72 hours a catastrophic reaction took place, breaking the glass vessel. It is not clear if the reaction was solely that of solder with cesium, or a partial reaction which caused the glass to crack, thereby exposing the cesium to air and causing a cesium fire which melted the solder. There was some evidence that a cesium fire had occurred and only a small amount of the solder sample remained. It was a melted button. The balance of the solder had reacted to form what appeared to be a cesium-metal hydroxide.

b. Second Test. A repeat test of the solder/cesium was performed to clarify the reaction of this combination. For this test, the test vessel (see Figure III-1a) was modified by shortening the support rod to leave a reaction chamber that was approximately 3 inches long. After sealing in the sample, the vessel was then loaded with approximately 8 grams of cesium using the distillation system. The cesium completely covered the solder sample and filled approximately 1/3 of the reaction chamber. Since the sample was covered with cesium no reaction could be seen; however, the cesium appeared to change in color from a metallic silver to a straw yellow. This color change was accompanied by a volume increase. No heat was applied to the test vessel and the dark precipitate was not seen. After 72 hours of exposure no apparent change could be seen in the sample. At this time the test vessel was heated to approximately 100°F. The yellow compound melted exposing what appeared to be the reacted solder slug. Upon removal of the heat the cesium compound resolidified with the same straw yellow color. After 5 days the test vessel was opened to air, which resulted in a cesium fire. However, the solder sample was removed before melting could occur. Examination of the solder revealed that it had been severely attacked by the cesium but not in the manner as the previous sample. A photograph of the sample is shown in Figure III-6. The remaining sample was then prepared for metallographic analysis. Photographs of the cross section is shown in Figure III-7. The sample was prepared using standard metallographic techniques and was etched with a HNO_3 - CH_3COOH mixture. The edges appear to have been attacked at a relatively uniform rate and no intergranular corrosion was noted. The cause of the catastrophic reaction that was observed in the

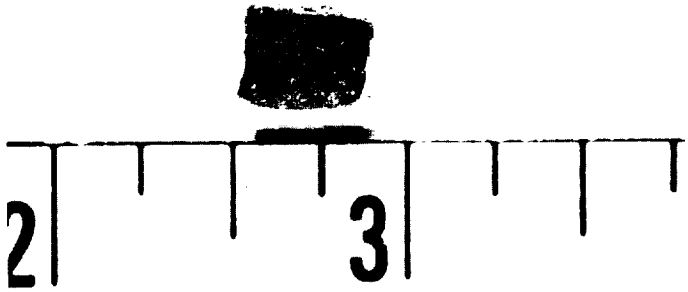

Figure III-6. Solder sample after 5 day exposure to cesium.

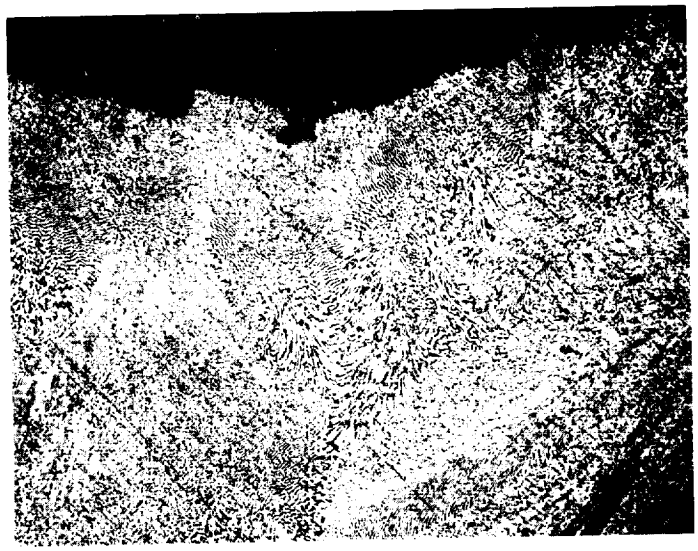

Figure III-7. Cross section of solder sample after exposure to cesium. 100X.

first test was apparently expansion of the solder/cesium compound against the test vessel and its support column which caused the glass to crack exposing the cesium to air. However, in both experiments the cesium attacked the solder at a rate which would probably preclude the use of solder at locations on the spacecraft which receive high arrival rates of cesium.

B. Surface Coating Tests

In view of the relatively rapid attack of solder by mercury, and the poor mechanical properties of the reacted solder, additional tests were devised to explore this metallurgical couple. A repeatable method for exposing test samples to much more modest quantities of mercury was desired, along with a means of quantifying changes in sample mechanical properties. After these procedures were developed on solder samples, they were also used on silver and solder/silver samples.

1. Test Design. Tensile properties, as measured on a standard tester with a crosshead speed of 0.5 in/min., were used to characterize changes in the mechanical properties of samples. Some test bars were machined into a standard 4 inch long, 1/4 inch thick, 1/4 inch wide "dog bone" configuration. Other test bars were thin (.007 inch); as it happened, none of the thin bars were run on the tester.

Both the thick and thin sample bars were surface coated with mercury, but the techniques employed were different. The thick bars were solvent cleaned, forced to the bottom of a container of mercury, and released. The buoyant force expelled the bar and it was immediately removed from the container. The thin bars, which would have deformed during such a procedure, were placed in a test tube. The tube was then filled with mercury while held at approximately 45° to the vertical and emptied immediately. Thus, with both techniques the samples were immersed for only a matter of seconds and the mercury exposure consisted of that quantity of mercury which adhered to the sample surface.

A complete test sequence consisted of machining several identical test bars, tensile testing one bar as machined, surface coating the remaining bars, and tensile testing these bars after varying periods of room temperature storage.

Comparison was made between the tensile properties of the virgin material and those of the material after exposure to a fixed quantity of mercury over varying reaction periods.

2. Mercury/Solder. Three 1/4 inch thick tensile bars were machined from solder. One was tensile tested as machined; the other two were briefly immersed in mercury. They were wet completely with a thin surface coating of mercury and appeared as a front surface mirror when withdrawn. The coated samples were then stored at room temperature for one week and one month, respectively, and tensile tested. Before testing, visual observation indicated that the thin surface coating of mercury had diffused into the bulk of the sample. The surface at this time was a dull solder gray. Table III-2 presents the results of the tensile tests. The small variations in results between the one week sample and the unexposed sample may be largely statistical scatter. However, the third sample shows a marked decrease in elongation, decrease in tensile strength, and an order of magnitude change in modulus. These changes in mechanical properties indicate a change in the structure of the material with only a small coating of propellant.

Table III-2. Tensile properties of solder test bars.

Sample (Reaction Period)	Yield Strength	Ultimate Tensile Strength	Elongation	Modulus (psi)
Uncoated Bar	2,200 psi	4,200 psi	90%	36.4×10^4
Surface coated w/Hg 1 wk reaction time	2,600	4,600	90	32.5×10^4
Surface coated w/Hg 4 wks reaction time	2,450	3,300	29	28×10^5

A further study of the mechanical behavior of solder in mercury was performed on a thin sheet (.007") tensile bars of eutectic solder. This solder was

surface treated in the same manner described above, so that only a small amount of mercury would come in contact with the solder strip. The appearance of the strip after coating was identical to the large samples. However, in trying to move the samples after coating it was found that the samples would not support their own weight. The total time between coating and failure being less than 20 seconds. Figure III-8 and III-9 show solder samples after coating and then after fracture. Repeated tests showed that the longest period of time for the 7 mil sheet to fracture was less than one minute.

3. Mercury/Silver Solder Alloy. Both immersion and surface coating tests of solder in mercury clearly indicated that solder had very low physical strength properties after exposure to mercury. In contrast, silver showed some attack after four weeks of immersion but appeared to have sufficient properties to be used in the mercury environment. Furthermore, silver is sometimes employed as a solder constituent in solar array designs. Therefore, two silver solder alloys were made for testing. Both of the alloys made contained 10% silver, but they were made in two different ways. The first alloy contained $57^{W}/o$ (weight percent) Pb and 10% Ag while the second was 61.9% Sn, 38.1% Pb to which $10^{W}/o$ Ag was added. Both of these alloys were melted without flux in an argon atmosphere. After melting, a 7 mil strip was rolled from each of the alloys and tensile samples were cut. The samples were then surface coated with mercury in the usual manner. These 7 mil alloy samples reacted to the surface mercury coating in the same way as eutectic solder. That is, the samples would not support their own weight and the longest time period between coating and failure was less than one minute.

4. Mercury/Silver. Tensile tests were made on 1/4 x 1/4 inch silver bars. Table III-3 presents the data from these tests. Ultimate tensile strength of the bars was unaffected by up to four weeks of reaction time following surface coating with mercury. The modulus of the four-week bar is significantly lower than recorded for the one-week bar and the uncoated bar. This result is not understood in the light of the four week immersion test (see Section III.A.3).

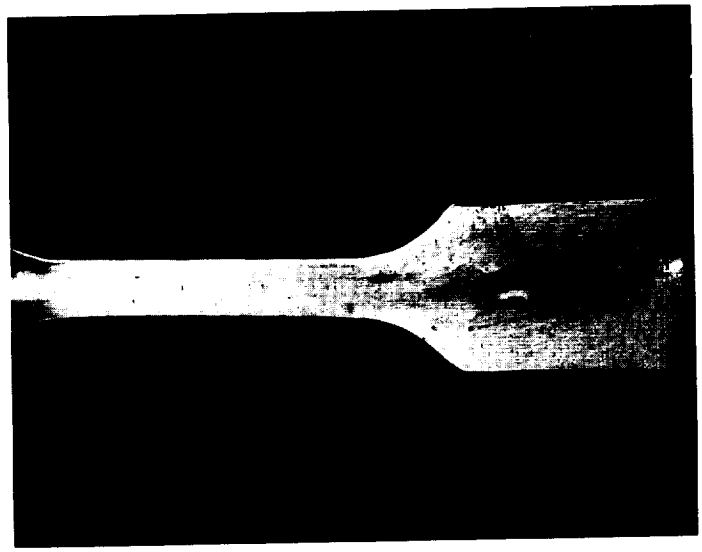

Figure III-8. 7 mil solder sample after surface coating of mercury.

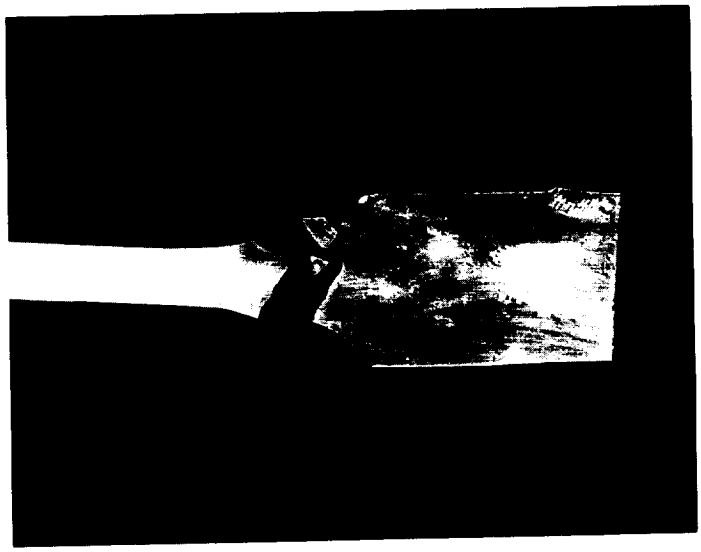

Figure III-9. Fractured 7 mil solder samples.

That test indicated no more than a 3 mil deep reaction zone with higher microhardness values than the sample interior. Variations in modulus between samples are usually associated with variations in sample composition or structure.

However, the effects of mercury on the mechanical properties of silver do not appear, on the bases of these tests, to exclude the use of silver on spacecraft surfaces which intercept mercury propellant.

Table III-3. Tensile properties of silver test bars.

Sample (Reaction Period)	Ultimate Tensile Strength	Modulus
Uncoated Bar	41,050 psi	13.2×10^6 psi
Surface Coated with Hg 1 week reaction time	40,400	14.4×10^6
Surface Coated with Hg 4 weeks reaction time	40,600	9.7×10^6

C. Conclusions

1. Mercury/Solder. In considering the results of the three types of tests with solder and mercury -- long term immersion, surface coating of massive bars, and surface coating of thin bars -- the following picture emerges. When small quantities of mercury are present in solder, the solder is embrittled, as was shown by the fragility of the thin bars and the measured properties of the four-week, thick bar. However when the mercury concentration becomes large, solder has little mechanical integrity: The sample which underwent 6 weeks of immersion was so "mushy" it couldn't be mounted and polished for metallographic examination.

The results of surface coating thin silver solder alloy samples with mercury were identical to that of coating thin silver-free solder samples, indicating that in concentrations of 10% or less silver do not significantly reduce degradation of solder strength by mercury.

Solder used on light weight solar arrays must be able to sustain both residual strain present at a joint after fabrication and strain introduced by handling, deployment and flexing. These experiments show 1) mercury "wets" solder so no advantage may be expected from low fractional monolayer adsorption energy and 2) limits will have to be imposed on the total amount of mercury arriving at exposed solder surfaces on solar-electric spacecraft.

2. Cesium/Solder. Immersion of eutectic solder in cesium results in rapid, heavy attack. Thus, as in the case of mercury/solder, damage rates of solder on warm spacecraft surfaces will be controlled by cesium arrival rates.

3. Mercury/Silver. A metallurgical reaction between silver and mercury has been observed. However the reaction rate is not rapid nor the properties of the reaction products obviously unacceptable.

D. Recommendations for Future Work

Since solder was not unaffected by the relatively severe immersion and surface coating exposures to propellant, experiments should be performed which will more closely simulate the spacecraft surface environment. This can be accomplished by exposing samples on the multipurpose sample holder to propellant beams, followed by ex situ tests and analysis. Electrical and mechanical specification requirements of lightweight solar arrays on solder should be determined and used in developing these experiments.

IV. SURFACE THERMAL DEGRADATION MEASUREMENTS

The Phase I study[1] identified thermal control coatings as one of the classes of spacecraft surfaces most likely to be sensitive to electrostatic rocket exhaust. Although degradation of various coatings by photons, noble gas ions, and micrometeroids had received extensive study, these studies were not an adequate basis for predicting the extent of electrostatic rocket exhaust effects. They did warn that damaged surfaces often heal when exposed to oxygen. Therefore, electrostatic rocket exhaust experiments would require detection of changes in sample properties while they remained within the vacuum environment following beam exposure, i.e., in situ.

A. Experimental Design

The experiment which was devised to measure the effects of electrostatic rocket exhaust particles on thermal control coatings is shown schematically in Figure IV-1. This is a top view of a 4 foot by 8 foot vacuum chamber. A 15-cm electron bombardment (E-B) thruster is supported from the front chamber door port cover. It is the source of ion and atom beams. As shown, a titanium ion beam collector divides the chamber into two sections. Samples are exposed to the E-B engine exhaust through a cut-out in the collector center and then rotated 180° for property measurements which require illumination from a xenon lamp shining through a quartz window in the rear door of the tank. These two experimental sections of the chamber are almost completely surrounded by a combination of cylindrical shrouds and planar surfaces, all of which may be cooled with LN_2. The interior surfaces of the rear section have been painted with 3M Type 401-C-10 Velvet Black paint.

Figure IV-2 is a photograph of the surface thermal sample holder in place behind the collector. It is turned toward the solar simulator, in the measurement position. The holder accepts up to 5 separate samples for simultaneous exposure to propellant beams. In this photograph, each sample happens to be black paint. The holder can rotate 180° in the collector-mounted bracket (at the right in Figure IV-2) into the propellant beam exposure

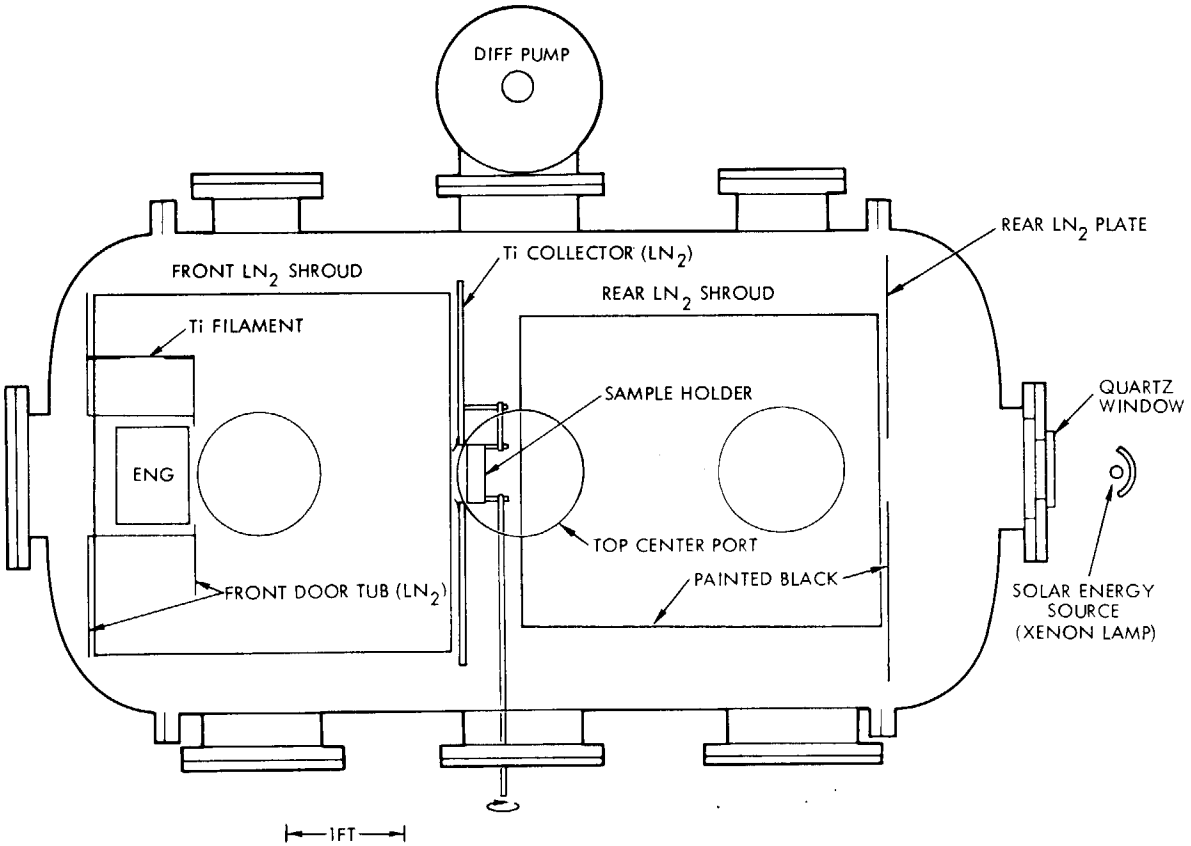

Figure IV-1. Overall schematic of 4 foot x 8 foot vacuum chamber as viewed from above and showing the surface thermal sample holder.

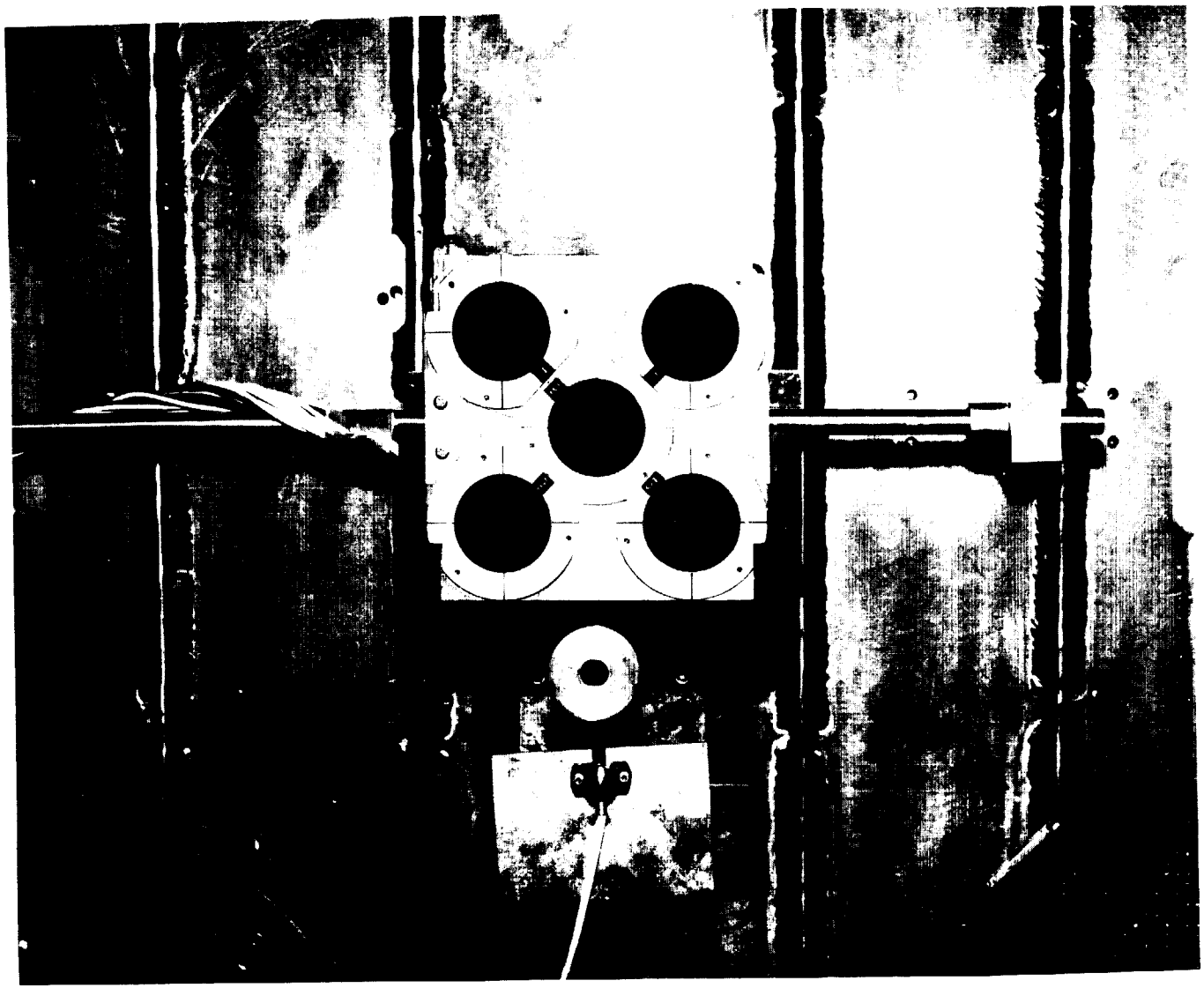

Figure IV-2. Surface thermal sample holder in measurement position. Radiometer appears below sample holder.

position, as shown in Figure IV-3. The "window frame" around the sample area is a set of carefully designed shields which prevent foreign metal particles from arriving at the samples. They are described in Section VI.C.1.

Since the thruster cannot be turned on and off rapidly, the sample shutter shown in Figure IV-4 is used to initiate and terminate beam exposures. The shutter is actuated through a rotary motion feed thru in less than two seconds. In the closed position it is a few inches in front of the sample plane, and its thermal design permits thruster operation when closed without significant outgassing in the direction of the samples.

The critical elements of the experiment are discussed below.

1. In situ Measurement Method. An electrical substitution method was selected for the in situ measurements because of its high accuracy, wide range of linearity, and ability to maintain almost constant sample temperature during exposure and measurement. This method provides an absolute measurement of sample hemispherical emittance and an absorptance measurement relative to the spectrum of the solar simulator used.

Figure IV-5 illustrates the construction of one of the five identical measurement units. The sample is attached to a very thin electrical heater of the same diameter as the sample (1.75 inches). Cemented to the other side of the heater is a very thin equal diameter thermopile-type-heat flux meter which in turn is permanently bonded to a water cooled plate. An annular shaped aluminum ring surrounds and lays flush with the sample to minimize edge radiation and protect electrical connections from ion beam erosion. Clearance between the sample edge and the ion shield is approximately 0.01 inch.

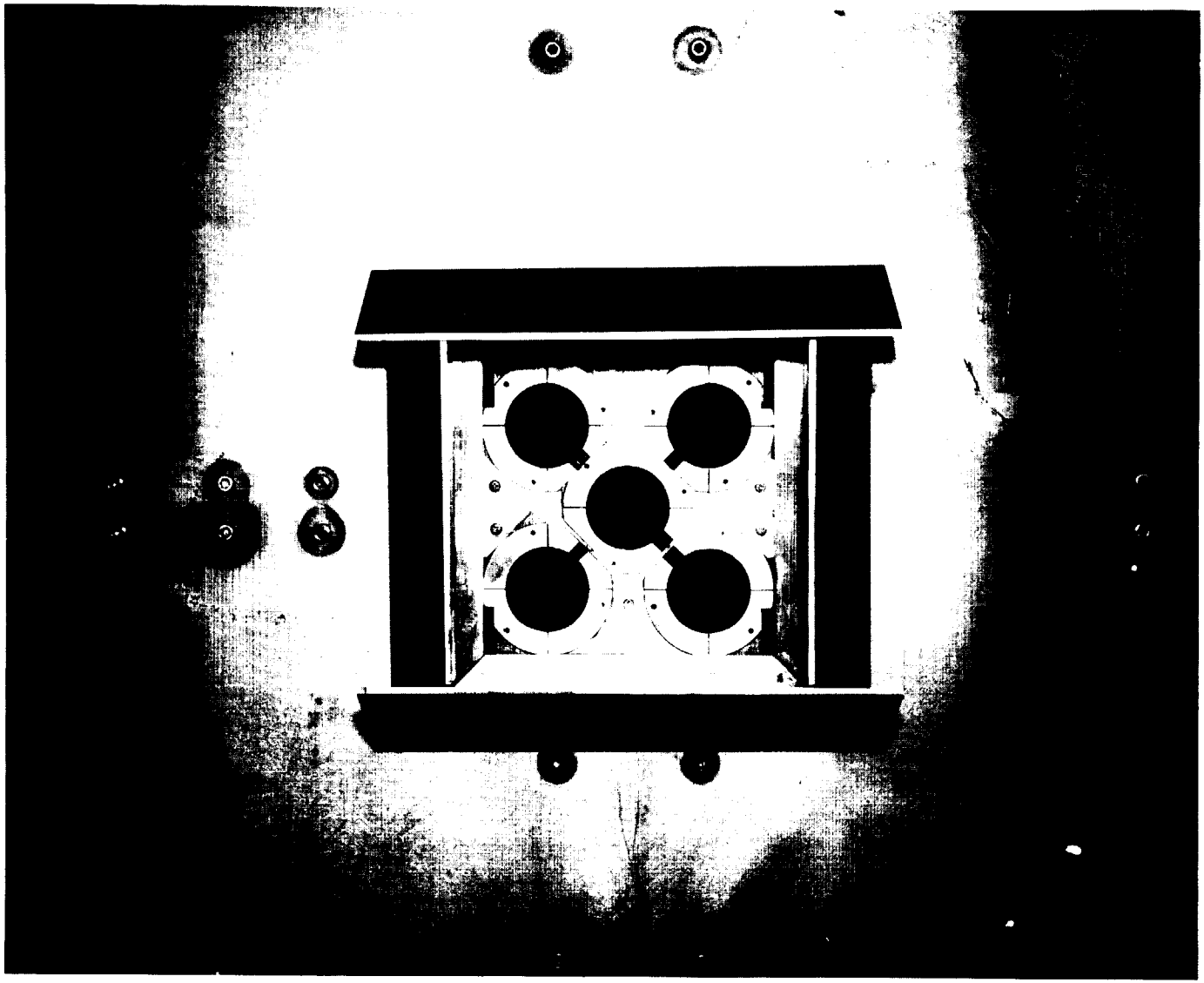

Figure IV-3. Closeup of sputtering shields and surface thermal sample holder.

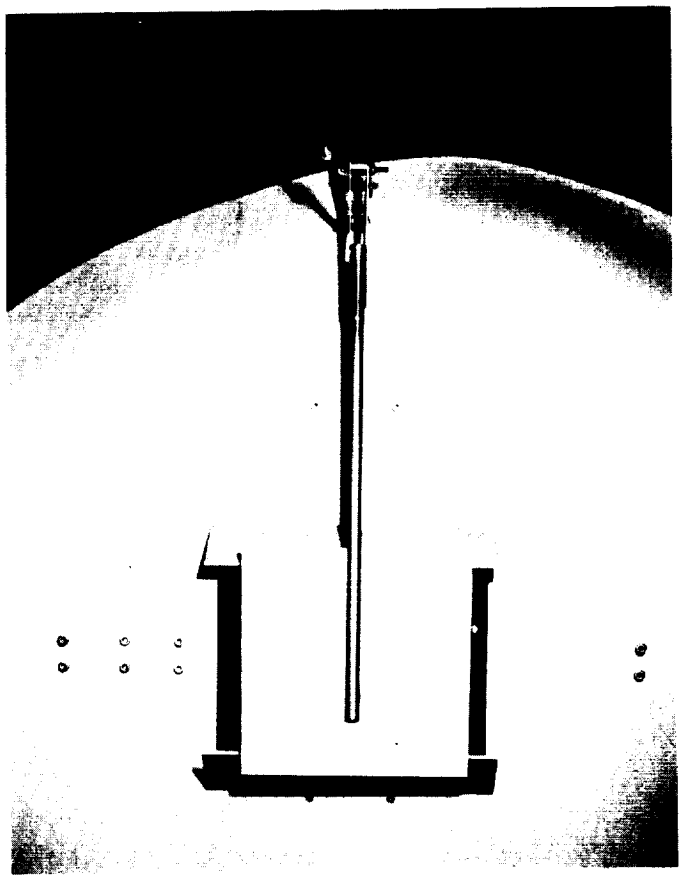

Figure IV-4. Sample shutter in closed position.

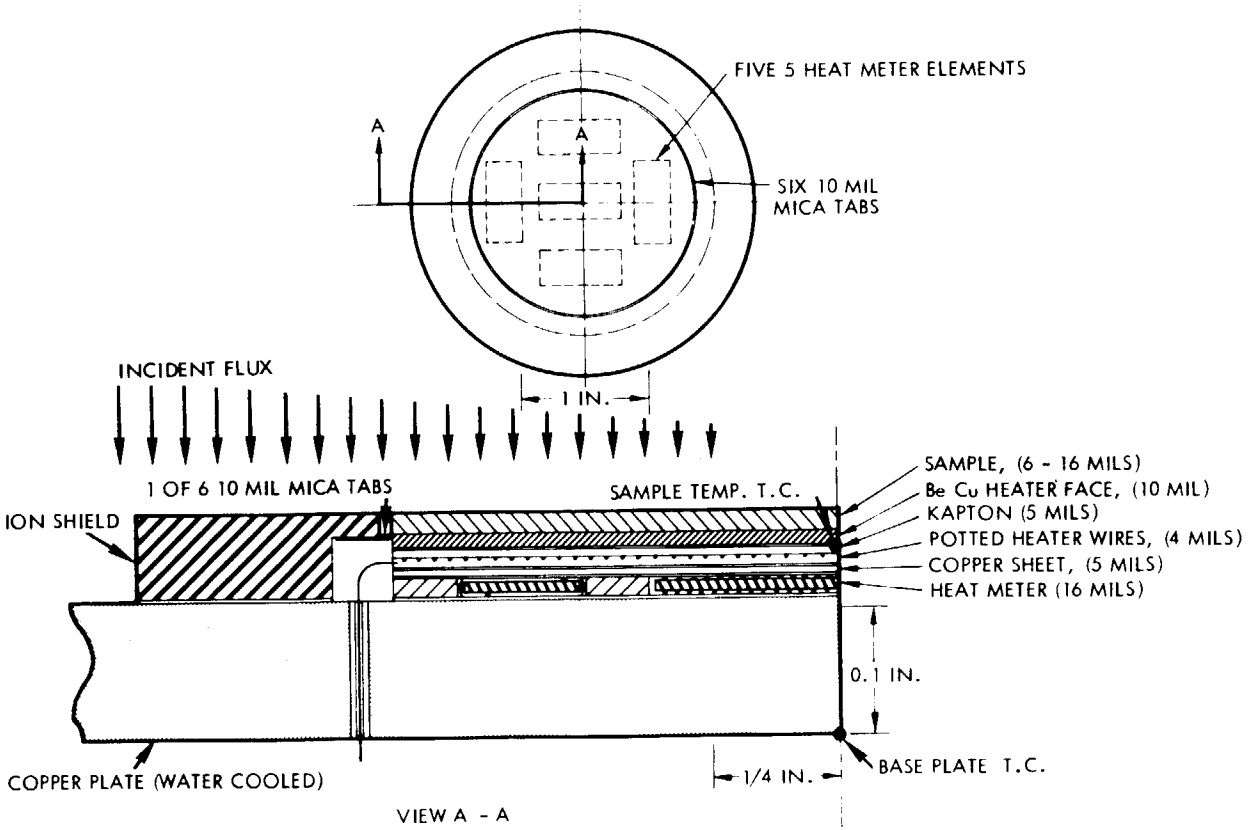

Figure IV-5. Cross section of one surface thermal property measurement unit.

During property measurements, the samples view only an LN_2 cooled shroud and a quartz port through which a xenon lamp solar simulator beam can be projected. With the solar simulation beam off, the electrical power to each sample heater is adjusted so that the corresponding heat meter is nulled. Under this condition, almost all of the measured electrical power to a sample heater is emitted by its sample. A small amount of the power (which can be computed and corrected for) is lost by radiation from the edge and conduction through the lead wires. The temperature of each sample is measured by a thermocouple placed between the sample and the heater, and a correction is made for the small temperature drop through the sample. Since sample area is known and temperature and emitted power are measured, total hemispherical emittance is computed from the heat balance equation:

$$\varepsilon_H = \frac{Q_e}{A\sigma[T_e^4 - T_W^4]} \tag{1}$$

where Q_e = electrical power to the heater during emittance measurement

A = sample area

σ = Stefan-Boltzman constant

T_e = sample temperature during emittance measurement, °K

T_W = temperature of chamber walls, °K

After the emittance readings are taken, the xenon lamp is turned on and the power to each sample heater is reduced until the heat meters are again nulled. The new electrical power dissipation and sample temperature readings are taken and corrected as before. In addition, the incident flux density (G) of the solar simulator beam is measured with a radiometer before and after illuminating each sample position. (The radiometer appears below the sample assembly in Figure IV-2.) Sample absorptivity with respect to xenon spectrum can then be computed from the new heat balance equation:

$$\alpha_{Xe} = \frac{\varepsilon_H A\sigma[T_a^4 - T_W^4] - Q_a}{AG} \tag{2}$$

where Q_a = electrical power to the heater during absorptance measurement

T_a = sample temperature during absorptance measurement.

It is estimated that the in situ measurements are accurate to within ± 0.03 (absolute number) in emittance and $\pm .05$ (absolute number) in absorptance. These estimates are based on a detailed error analysis[1] of a similar sample holder configuration and agreement obtained between in situ and ex situ measurements to date.

2. Heat Meter Sensitivity. Successful performance of the sample holder unit hinges on proper design of the heat meters. These units must be extremely thin to both minimize edge effects and reduce thermal resistance in the normal direction. The heat flux density during sample exposure to ion beams is typically 500 mw/cm^2 and can be as high as 1 watt/cm^2. Thus, unless the thermal resistance between the sample surface and the water cooled plate is small, sample temperature during exposure would vary strongly with beam power and even elevate enough to affect sample properties. Stabilization time during measurement is also reduced by minimizing the thermal resistance.

In spite of its thinness and low thermal resistance, the heat meter must produce a measurable signal (2-3 μv) for a heat flow that (ideally) is negligible compared to the heat radiated by the sample. This was accomplished by utilizing a thermopile with approximately 365 junction pairs in each heat meter.

The junctions were formed by first winding 0.002 inch diameter constantan wire on 0.007-inch-thick 1/4-inch-wide Texolite (epoxy impregnated fiberglass) with 0.006 center to center wire spacing. Approximately 1/3 of the 1/4 inch width was then silver plated so as to form one silver-constantan junction pair per turn of wire. Five 3/4 inch long strips were mounted individually in 1/4 by 3/4 inch cut-outs in a 0.010 inch thick 1.75 inch diameter Texolite wafer, as shown in Figure IV-5. The five windings were then connected in series and the wafer and strips were potted with TBS758 silicone rubber to form a 0.016 inch thick heat meter.

Calibration measurements were made by reading the heat meter output for a black sample of known emittance with no electrical power applied to the sample heater. These measurements indicate that the heat meter sensitivity is approximately 3.95 mv/watt. An automatic controller was able to maintain null within $\pm$ 4 μv. The uncertainty of heat flow through the heat meter was therefore approximately 0.001 watt. This is quite small, even when compared to the approximatly 0.037 watts emitted from a 1.75-inch-diameter low emissivity (ε_H = 0.05) sample at 20°C. In fact, the heat meters are so sensitive that minor fluctuations in cooling water temperature and/or pressure

introduced noise (20-50 μv) in the heat meter output signal. This problem was solved by installing a thermally insulated constant-head gravity-feed cooling system.

3. Solar Simulator. A Christie model UF 30K projector with a 1600 watt xenon short arc lamp and a fused quartz lens assembly provided the simulated solar radiation beam. In order to obtain sufficiently high beam flux density (150 mw/cm^2) at the sample plane to accurately measure α_{Xe} on low $\alpha_{Xe}/\varepsilon_H$ samples (such as white paints or second surface mirrors), the simulator beam had to be focused down to approximately a 10 inch diameter circle at the target plane. As a result, the beam was spacially and spectrally non-uniform, so only the center 2 inch diameter core was used for measurement purposes. This center core was accurately aimed first at the radiometer, then at one of the five samples, and then back at the radiometer using a telescope sight rigidly attached to the simulator. The simulator was mounted on an adjustable platform shown in Figure IV-6. Cross hairs in the telescope were "sighted in" during beam intensity calibration measurements so that at the sample plane the line of sight through the telescope intersected the simulator beam axis. Sighting aids placed on each sample holder (see Figure IV-2) were used to accurately position the center of the beam onto the center of each sample.

Low beam flux densities (3 mw/cm^2) at the sample plane were obtained by removing the entire projection lens assembly. A permanent clamp was placed on the lens assembly to assure that it would be replaced in the same position each time. Intermediate flux densities were obtained by introducing 60 mesh brass wire screens with the lens assembly in place. Minor intensity adjustments were also made by varying the lamp current.

a. Spectral distribution measurement. Spectral distribution of the solar simulator beam was measured between 0.26 and 2.9 microns using a Beckman DK2A double beam spectrophotometer using essentially the method described in Reference 2. Magnesium oxide diffusing plates were interposed in both beams to reduce directional effects. An NBS calibrated tungsten-halogen lamp was used

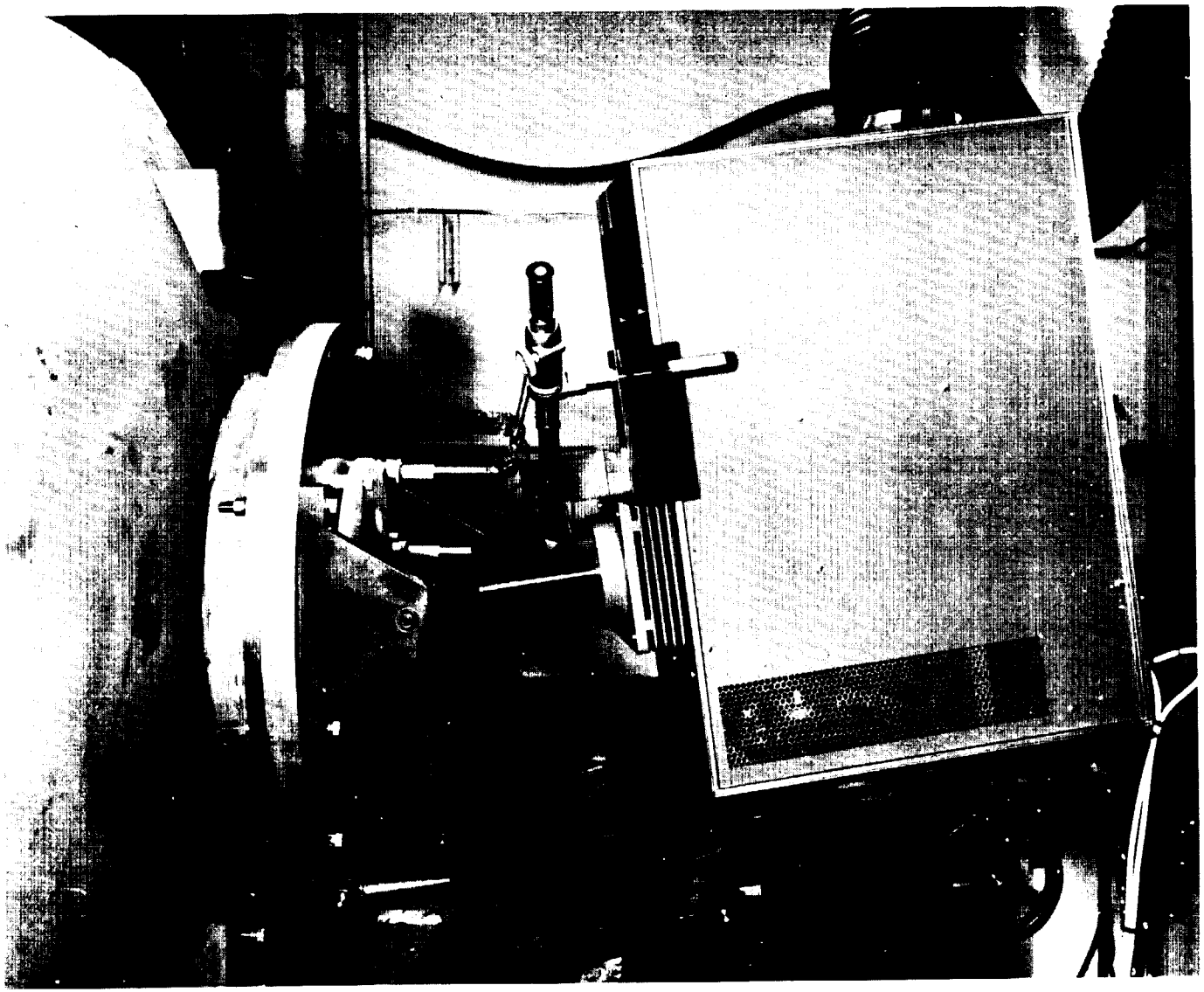

Figure IV-6. Solar simulator on adjustable mount.

as the reference source. Neither insertion of wire screens in the beam nor variation of the xenon arc lamp current had any significant effect on the measured spectral distribution. Removal of the lens assembly, however resulted in a considerably different spectral distribution. Figures IV-7 and IV-8 show the normalized spectral distribution with lens in and lens out respectively. Lens configuration is indicated in in situ data tables by footnotes.

b. Spacial distribution measurement. Flux density distribution throughout the center 4 inch diameter of the beam was mapped with and without the projection lens assembly in place by traversing the beam in the x and y directions across the radiometer. With the lens out the distribution is flat. Figure IV-9 shows the lens-in distribution. The flux density drops off about 10% symmetrically from the center of the beam to a radius corresponding to the edge of a sample. Table IV-1 shows the integration of this curve to obtain the appropriate correction factor, 0.94, for the total flux incident on the sample based on the radiometer reading on the beam axis.

c. Reference radiometer. The TRW EC-1 was selected as the reference radiometer. This is an electrically compensated radiometer which consists of two identical foils housed in identical enclosures. One foil is exposed to the unknown beam intensity through a 1.3 cm diameter quartz window. The other foil is heated electrically at a rate that will just null a differential thermocouple operating between the two foils. The beam intensity can be determined approximately from the measured electrical power, the window aperture area, the absorptance of the receiving foil, and the transmittance of the window. For greater accuracy however, several identical instruments have been calibrated in vacuum against a laboratory standard radiometer whose calibration is traceable to the National Bureau of Standards.

Figure IV-2 shows the radiometer as installed within the chamber. The radiometer aperture is in the same plane as the samples.

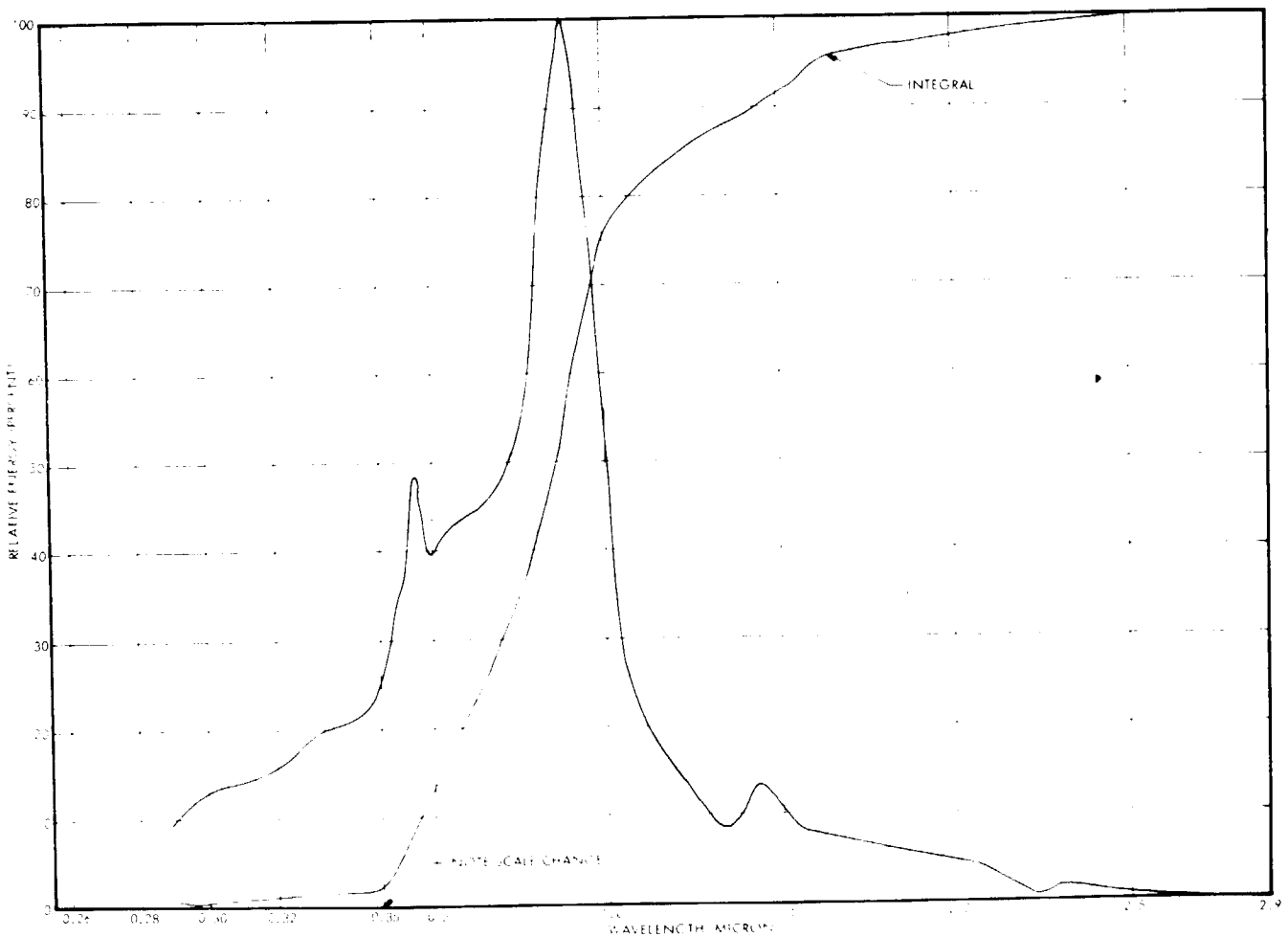

Figure IV-7. Normalized spectral distribution provided at the sample by the Christie Xenon Arc System with the lens in place.

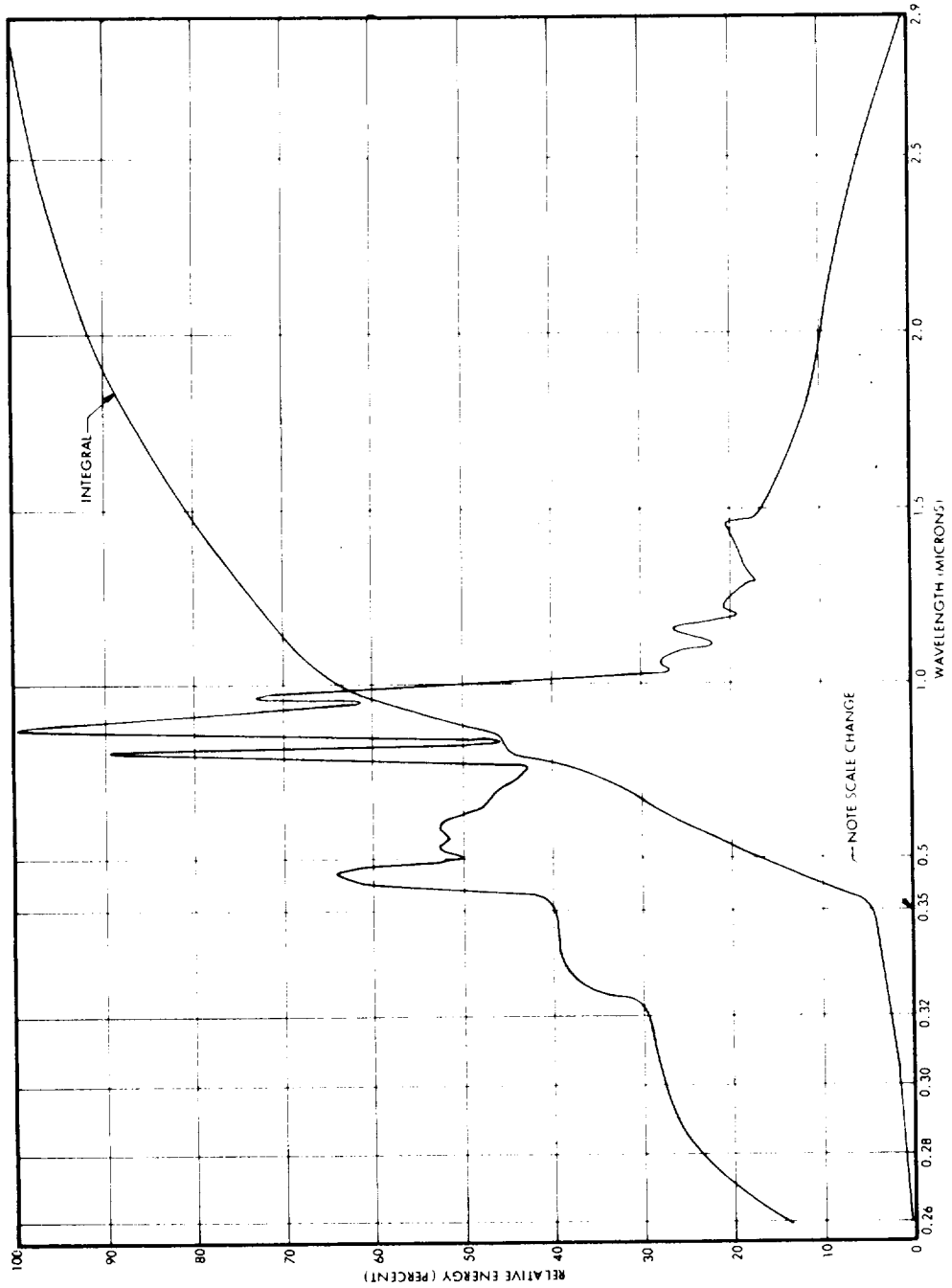

Figure IV-8. Normalized spectral distribution provided at the sample by the Christie Xenon Arc System with the lens removed.

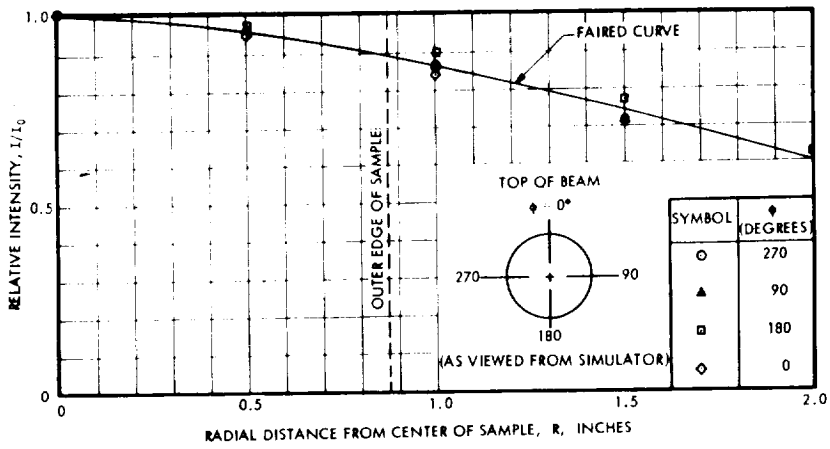

Figure IV-9. Total intensity distribution at 60.3 inches from the front face of the Christie lamp housing.

Table IV-1. Computation of effective beam intensity.

$(\bar{R})$ (inches)	(I/I_0)	ΔR (inches)	$(\bar{R})(I/I_0)(\Delta R)$
.05	.995	.10	.004975
.15	.990	.10	.01485
.25	.982	.10	.02455
.35	.975	.10	.034125
.45	.960	.10	.04320
.55	.949	.10	.052195
.65	.940	.10	.0611
.75	.912	.10	.0684
.8375	.899	.075	.05647
SUM		.875	.359865

$$\frac{I_{effective}}{I_{center}} = \frac{2\sum(\bar{R})(I/I_0)(\Delta R)}{R^2_{max}} = \frac{(2)(.359865)}{(.875)^2} = 0.94$$

4. In Situ Instrumentation. The in situ electrical and temperature measurements are made with a Darcy Model 440 digital voltmeter (DVM) with low noise mV option (random variation $\pm$ 2 μV) through a specially designed signal switching console. Switch S2 in the console circuit, shown in Figure IV-10, permits switching an electronic controller (which automatically nulls its input signal) between samples and radiometer. Switch S1 selects which of the five sample units or radiometer signal sets will be available to the DVM, and S3 switches the DVM through the signal set. Figure IV-11 shows the entire electronics rack including the switching console, and a HP 425A microvoltmeter which is part of the electronic controller. Also visible in the figure is the vacuum port cover which supports the sample holder package and electrical hermetic seal pass-throughs.

During in situ property measurements the DVM readings are recorded by hand in a systematic way on specially prepared data sheets. Sample, run, beam exposure, and solar simulator configuration codes are also recorded. Immediately following data recording, the data is punched onto paper tape with a nearby teletypewriter. The teletypewriter is then connected to a timesharing digital computer which has the data reduction program in memory. Within seconds after the paper data tape is read into a computer file, values of α_{Xe}, ε_H and several instrument diagnostic numbers are computed for each sample. This rapid procedure for data reduction permits the sequence of experimental steps to be modified in response to current results while the experiment is in progress. For instance, if a property measurement seems questionable it is repeated before going on; when a 0.3 hour atom beam exposure had little effect, a much larger period was chosen for the next exposure.

5. Ex Situ Measurements. Spectral distributions of two samples of each material were measured between 0.28 and 2.5 microns on a modified Beckman DK2A double beam ratio recording spectrophotometer[3] and between 2.0 and 26.0 microns on a Gier Dunkle Heated Cavity Reflectometer.[4] These data are presented in Appendix B.

All ex situ spectral data taken during the program was manually reduced by the equal energy band method. Values for α_{Xe} were obtained by using a 25-band overlay with each band representing 4% of the total integrated energy under the measured spectral distribuiton of the Christie xenon lamp unit. During runs requiring low thermal flux density, the Christie lens system was removed. Since the spectral distribution with the lens out is somewhat

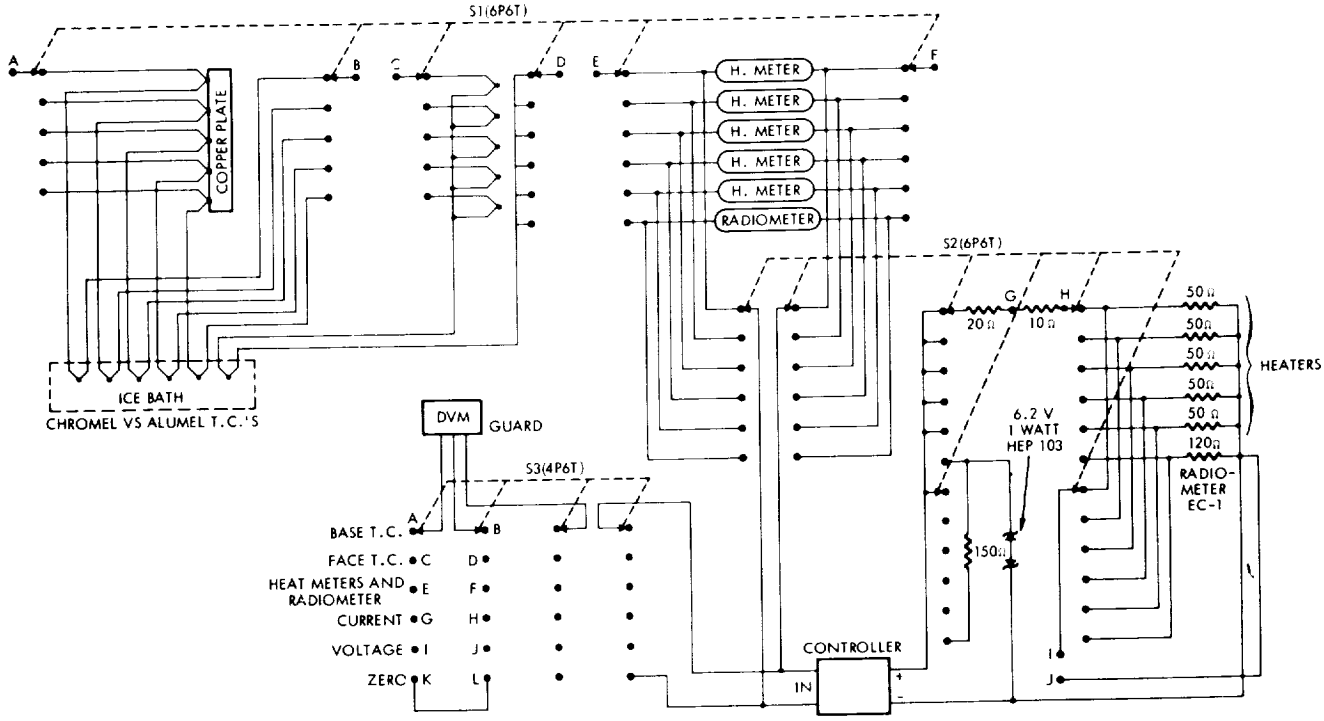

Figure IV-10. Schematic diagram of signal and controller switch console.

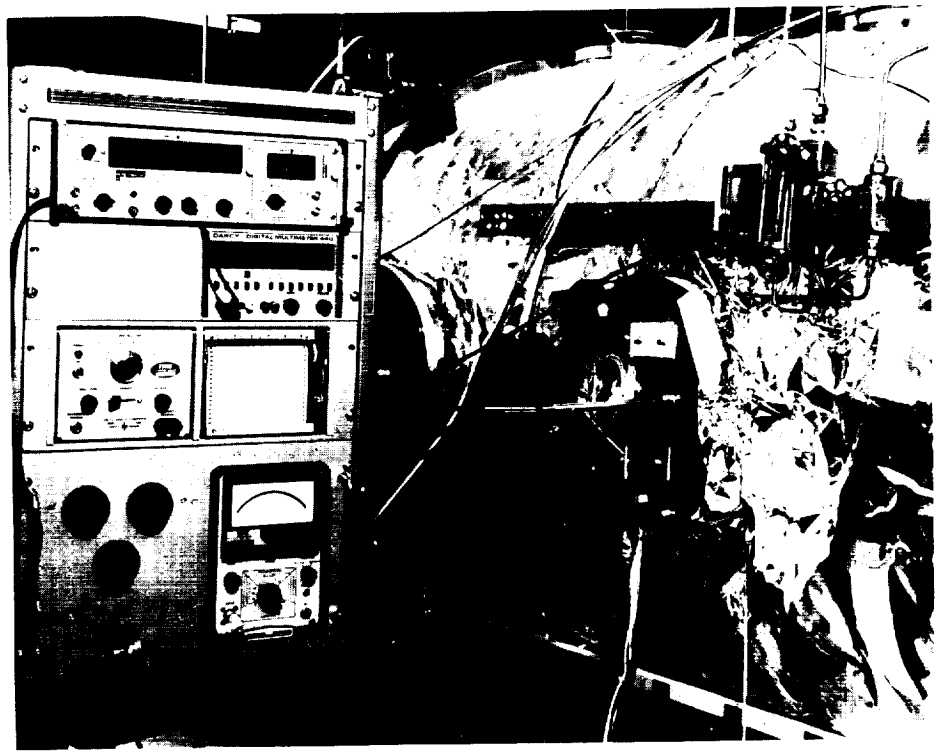

Figure IV-11. Exterior view of port plate, electronics, and water cooling system.

different from that with the lens in, a separate overlay was made for each of the two optical configurations. Values for α_s were obtained by using a 25-band overlay based on the Johnson zero-air-mass solar curve.[5] These data are tabulated in Table IV-2.

In addition to the spectral measurements, ex situ quick inspection total measurements of α_s and ε_N were made on each sample before and after exposure to the ion engine exhaust. These measurements were made with the sample in place of the sample holders using a Gier Dunkle Model MS 250 Mobile Solar Reflectometer for α_s and a Gier Dunkle Model DB100 Mobile Infrared Emittance Inspection Device[6] for ε_N.

B. Results and Discussion

1. Mercury Atom Beam Experiments. Two sets of five sample materials were tested in situ before and after exposure to a mercury atom beam. The samples of the first set were all paints, 3M velvet black, Cat-a-Lac black, PV100 white, Z93 white, and S13G white. All in situ emittance data and the in situ absorptance data on the white paints appear valid; however difficulties with low intensity operation of the solar simulator produced inconsistent absorptance data on the black paints. Because of the questionable validity of this portion of the data, rerunning a duplicate set of paint samples is planned for Phase III. Accordingly, none of the values from the first data set are tabulated in this report. The valid data showed that 4 hours exposure to approximately 10^{14} Hg atoms/cm^2-sec at a sample temperature of approximately 22°C produced no significant change in either α_{xe} or ε_H of the white paints, or in ε_H of the black paints. These in situ results were confirmed by comparing before and after ex situ measurements made with the quick inspection devices.

Results for the second set of five sample materials (polished aluminum, gold plated aluminum, 6-mil second surface aluminized microsheet, 20-mil second surface aluminized fused quartz, and RTV41 on aluminum) appear to be consistent and valid in their entirety. Table IV-3 shows in situ values of α_{xe} and ε_H after various periods of accumulated exposure compared to the ex situ

Table IV-2.

SUMMARY OF RESULTS OF PRE-EXPOSURE

EX SITU MEASUREMENTS ‡

SAMPLE NO.		α_s(a)	α_{xe}(a)	ε_N(b)	ε_H(c)
454-69	Gold Plated Aluminum	.220	.160*	.010	.013
455-69	Gold Plated Aluminum	.196	.140*	.010	.013
456-69	S13G White Paint	.190	.148	.903	.853
457-69	S13G White Paint	.188	.142	.899	.850
458-69	PV100 White Paint	.188	.142	.866	.823
459-69	PV100 White Paint	.190	.139	.864	.820
460-69	Z93 White Paint	.159	.117	.918	.869
461-69	Z93 White Paint	.162	.117	.923	.873
462-69	Polished Aluminum	.181	.166*	.018	.023
463-69	Polished Aluminum	.169	.155*	.021	.027
464-69	3M Black Paint	.982	.982	.909	.858
465-69	3M Black Paint	.986	.986	.918	.866
554-69	6-mil Microsheet†	.138	.133	.817	.785
555-69	6-mil Microsheet†	.142	.135	--	--
556-69	20-mil Quartz†	.118	.114	.779	.751
557-69	20-mil Quartz†	.118	.114	--	--
613-69A	Cat-a-lac Black	.956	.956	.872	.828
613-69B	Cat-a-lac Black	.954	.954	.868	.825
672-69	RTV 41	.305	.265	.892	.846
673-69	RTV 41	.327	.291	.887	.843
794-69	RTV 566	.652	—	—	—
795-69	RTV 566	.652	—	—	—

‡Accuracy within $\pm$.02 in α and $\pm$.03 in ε; repeatability $\pm$.005; therefore third figure shows data trends.

†Vacuum deposited aluminum on second surface.

*Based on lens-out spectrum.

(a) Measured on modified Beckman DK2A.

(b) Measured on Gier Dunkle Heated Cavity Reflectometer.

(c) Calculated from normal emittance and theoretical correction given in Eckert and Drake, "Heat and Mass Transfer," 2nd Edition.

Table IV-3. Surface thermal degradation test results, mercury neutrals.

(SAMPLE TEMPERATURE ~ 22°C, BEAM FLUX DENSITY ~ 1 X 10^{14} ATOMS/CM^2 SEC)

SAMPLE MATERIAL	EX SITU PRE EXPOSURE†				IN SITU MEASUREMENTS†										EX SITU POST EXPOSURE†			
					T = 0 HR		T = 0.333 HR		T = 2.37 HR		T = 3.37 HR		POST O_2					
	α_S (a)	α_{Xe} (a)	ϵ_N (b)	ϵ_H (c)	α_{Xe}	ϵ_H	α_{Xe}	ϵ_H	α_{Xe}	ϵ_N	α_{Xe}	ϵ_H	α_{Xe}	ϵ_H	α_S (a)	α_{Xe} (a)	ϵ_N (b)	ϵ_H (c)
POLISHED 6061-T6 ALUMINUM	0.175	0.173 0.161*	0.035	0.045	0.146* 0.121*	0.058 0.056	0.147*	0.058	0.157*	0.060	0.137*	0.059	-	-	0.184	0.182 0.169*	0.029	0.037
GOLD PLATING ON POLISHED ALUMINUM	0.220	0.138 0.160*	0.025	0.032	0.130* 0.110*	0.053 0.056	0.170*	0.063	0.152*	0.069	0.147*	0.068	-	-	0.224	0.140 0.162*	0.018	0.023
6-MIL MICROSHEET 2ND SURFACE V D ALUMINUM	0.138	0.133	0.842	0.802	0.153 0.151	0.790 0.789	0.157	0.795	0.148	0.798	0.153	0.798	-	-	0.131	0.129	0.845	0.804
20-MIL QUARTZ 2ND SURFACE V D ALUMINUM	0.118	0.114	0.811	0.778	0.139 0.139	0.765 0.766	0.139	0.773	0.142	0.776	0.140	0.775	-	-	0.113	0.124	0.809	0.775
RTV 41 SILICONE RUBBER	0.305	0.265	0.909	0.860	0.237 0.236	0.877 0.874	0.245	0.883	0.245	0.888	0.239	0.887	-	-	0.271	0.235	0.909	0.859

(a) MEASURED ON BECKMAN (MODIFIED DK2A).

(b) MEASURED ON GIER DUNKLE QUICK EMITTANCE INSPECTION DEVICE.

(c) CALCULATED FROM NORMAL EMITTANCE AND THEORETICAL CORRECTION GIVEN IN ECKERT AND DRAKE, HEAT AND MASS TRANSFER, 2ND EDITION.

† THIRD FIGURE INCLUDED TO SHOW DATA TRENDS; NOT FULLY SIGNIFICANT.

* BASED ON LENS-OUT SPECTRUM.

measurements. The impinging beam was again mercury atoms (neutrals) at a constant rate of about 1 x 10^{14} atoms/cm^2-sec and the sample temperatures were again about 22°C.

In general, it can be said that the absolute values of α_{Xe} and ε_H as determined in situ for all five samples are in excellent agreement with the corresponding ex situ values. The apparent scatter of in situ values for any given sample is approximately of the same magnitude as scatter observed in the ex situ measurements. Therefore the effect of beam exposure on sample optical properties can be examined.

A comparison in Table IV-3 of in situ measurements of α_{Xe} or ε_H after various exposure times indicates that no significant change occurred with up to an accumulated 1.2x10^{19} Hg^+/cm^2 dose. Pre- and post-exposure ex situ measurements ε_H tends to substantiate this conclusion. Post exposure α_{Xe} was not measured on the Beckman for this set of samples because of time limitations, so that comparison is unavailable.

Results from these two sets of five samples should be examined in light of Figure VII-2, which indicates that bulk condensation of mercury will not occur under the conditions of exposure employed. Thus, if an effect had been observed on any of the samples, it would have been the result of fractional monolayer coverage, either as an adsorbed film or through reaction with the sample material. Reaction of mercury with the paint samples was not expected in light of the chemical immersion tests discussed in Section II.G. It is common knowledge that glass and mercury do not react at 22°C. Since gold's affinity for mercury is well known, it is a most interesting result of these measurements that gold was affected only slightly, if at all.

a. Conclusions and recommendations. It appears on the basis of these first experiments, with the possible exception of the black paints, that either 1) the 10 materials tested do not react with mercury in a manner which produces significant change in thermophysical properties, or 2) even fractional monolayer mercury adsorption did not occur. The obvious next step in this investigation is to expose these sample materials to mercury atoms under conditions which will result in bulk mercury condensation, reevaporate

the bulk mercury, and then look for sample property changes. If no changes are found, it will then be possible to dismiss mercury atom damage to these (and perhaps similar) thermal control coatings as a deleterious effect to be considered in spacecraft design.

Such an experiment might provide a secondary but interesting result if an in situ measurement of ε_H and α_{Xe} of the mercury layer could be made before the mercury is reevaporated. The experimental difficulty of maintaining a constant sample temperature well below room temperature and accounting for heat of sublimation would undoubtedly reduce the accuracy of the measurement. It would be valuable, however, to compare even an approximate measurement with the semi-theoretical values computed in Phase I.

2. Mercury Ion Beam Experiments. Ten sample materials were exposed to various doses of 3 Kev mercury ions and the properties were measured in situ. The ion flux used in these tests was approximately 1×10^{15} ions/cm^2-sec and the samples were maintained at approximately 22°C. The results are presented in Table IV-4a and 4b. The experimental sequence employed was to pump down the vacuum chamber overnight, cool the LN_2 cold shroud to its steady state temperature, make in situ pre-exposure measurements of ε_H and α_{Xe} (labeled "t=0" in the tables), turn the samples 180° for a timed exposure to the ion beam, return the samples to the measurement position and remeasure the properties (labeled "t=X.XXX hrs" in the tables), turn and expose again, turn and measure again, and repeat this sequence until the samples had received 3 Hg^+ doses. Throughout these measurements tank pressure was typically less than 2×10^{-7} torr and consisted of gases not condensed at LN_2 temperatures (mainly CO and H_2).

The second set of measurements shown after 0.667 hours of ion beam exposure of the samples listed in Table IV-4a were made approximately 18 hours following the first set. The excellent agreement between the two sets demonstrates that the sample optical properties were stable in vacuo, even in the cases where ion exposure had caused drastic changes in property values.

Table IV-4a. Surface thermal degradation test results, mercury ions.

(SAMPLE TEMPERATURE ~ 22°C, BEAM FLUX DENSITY ~ 1×10^{15} IONS/CM^2 SEC)

SAMPLE MATERIAL	EX SITU PRE EXPOSURE†				IN SITU MEASUREMENTS †										EX SITU POST EXPOSURE†			
					T = 0 HR		T = 0.167 HR		T = 0.667 HR		T = 3.25 HR		POST O_2					
	α_S (a)	α_{Xe} (a)	ϵ_N (b)	ϵ_H (c)	α_{Xe}	ϵ_H	α_{Xe}	ϵ_H	α_{Xe}	ϵ_N	α_{Xe}	ϵ_H	α_{Xe}	ϵ_H	α_S (a)	α_{Xe} (a)	ϵ_N (b)	ϵ_H (c)
6-MIL MICROSHEET 2ND SURFACE V D ALUMINUM	0.138	0.133	0.842	0.802	0.152 0.170	0.805 0.804	0.187	0.805	0.186 0.182I	0.804 0.811I	0.142	(u)	0.169	0.865	0.166	0.173	0.845	0.804
20-MIL QUARTZ 2ND SURFACE V D ALUMINUM	0.118	0.114	0.811	0.778	0.151 0.179	0.779 0.777	0.165	0.779	0.165 0.159I	0.780 0.803I	0.155	0.811	0.147	0.807	-	-	0.809	0.776
3M VELVET BLACK PAINT	0.982	0.982	0.919	0.870	0.888 0.877	0.889 0.885	0.884	0.883	0.876 0.878I	0.886 0.887I	0.900	0.895	0.861	0.889	0.960	0.970	0.915	0.869
RTV41 SILICONE RUBBER	0.305	0.265	0.909	0.860	0.244 0.253	0.881 0.878	0.450	0.873	0.446 0.420I	0.874 0.878I	0.486	0.865	0.451	0.857	0.460	0.420	0.909	0.860
Z93 WHITE PAINT	0.171	0.117	0.932	0.883	0.147 0.148	0.924 0.904	0.660	0.915	0.762 0.763I	0.915 0.916I	0.841	0.912	0.808	0.912	0.871	0.864	0.938	0.889

(a) MEASURED ON BECKMAN (MODIFIED DK2A).

(b) MEASURED ON GIER DUNKLE QUICK EMITTANCE INSPECTION DEVICE.

(c) CALCULATED FROM NORMAL EMITTANCE AND THEORETICAL CORRECTION GIVEN IN ECKERT AND DRAKE, HEAT AND MASS TRANSFER , 2ND EDITION.

(u) DATA UNRELIABLE DUE TO INSTRUMENTATION INSTABILITY.

† THIRD FIGURE INCLUDED TO SHOW DATA TRENDS; NOT FULLY SIGNIFICANT.

I REMEASURED ~ 18 HOURS LATER

Table IV-4b. Surface thermal degradation test results, mercury ions.

(SAMPLE TEMPERATURE ~ 22°C, BEAM FLUX DENSITY ~ 1 X 10^{15} IONS/CM^2 SEC)

SAMPLE MATERIAL	EX SITU PRE EXPOSURE †				IN SITU MEASUREMENTS †										EX SITU POST EXPOSURE†			
					T = 0 HR		T = 0.017 HR		T = 0.167 HR		T = 0.667 HR		POST O_2					
	α_S (a)	α_{Xe} (a)	ϵ_N (b)	ϵ_H (c)	α_{Xe}	ϵ_H	α_{Xe}	ϵ_H	α_{Xe}	ϵ_H	α_{Xe}	ϵ_H	α_{Xe}	ϵ_H	α_S (a)	α_{Xe} (a)	ϵ_N (b)	ϵ_H (c)
GOLD PLATING ON POLISHED ALUMINUM	0.220	0.138 0.160*	0.025	0.032	0.135*	0.067	(u)	(u)	0.131*	(u)	0.126	(u)	-	-	0.203	0.131 0.152*	0.025	0.032
CAT-A-LAC BLACK PAINT	0.956	0.956	0.890	0.842	0.881	0.862	0.826	0.852	0.868	0.882	0.852	0.890	-	-	0.952	0.955	0.892	0.844
P V 100 WHITE PAINT	0.188	0.142	0.873	0.827	0.165	0.808	0.573	0.802	0.663	0.804	0.632	0.816	-	-	0.562	0.522	0.884	0.837
RTV 566 SILICONE RUBBER	0.652	0.605	0.898	0.849	0.575	0.853	0.626	0.848	0.655	0.845	0.649	0.851	-	-	0.698	0.659	0.895	0.847
S13G WHITE PAINT	0.190	0.148	0.713	0.864	0.163	0.880	0.309	0.872	0.344	0.877	0.338	0.876	-	-	0.331	0.270	0.915	0.866

(a) MEASURED ON BECKMAN (MODIFIED DK2A).

(b) MEASURED ON GIER DUNKLE QUICK EMITTANCE INSPECTION DEVICE.

(c) CALCULATED FROM NORMAL EMITTANCE AND THEORETICAL CORRECTION GIVEN IN ECKERT AND DRAKE, HEAT AND MASS TRANSFER, 2ND EDITION.

(u) DATA UNRELIABLE DUE TO INSTRUMENTATION INSTABILITY.

† THIRD FIGURE INCLUDED TO SHOW DATA TRENDS; NOT FULLY SIGNIFICANT.

* BASED ON LENS-OUT SPECTRUM.

As seen in Tables IV-4 there were significant changes in some of the test surfaces, notably the Z-93; after a 10 minute exposure its absorptance had increased from 0.15 to 0.66. Two other white paints, PV-100 and S13G, and both RTV samples also showed increase in α_{Xe} when exposed to Hg^{+}, a trend which was also confirmed by visual inspection. The α_{Xe} of the black paints and the ϵ_H of all samples were not significantly affected. Both the quartz and microsheet second surface mirrors exhibited essentially stable properties (within measurement accuracy).

The five samples of Table IV-4a were tested for oxygen-linked recovery. After in situ property measurements were made following the final ion beam exposure, the chamber pressure was raised to approximately 700 torr for approximately 15 minutes. (In addition, pressurization consumed approximately 15 minutes and reevacuation 48 minutes.) Throughout the entire procedure the LN_2 liners were kept cold to prevent desorption of Hg and H_2O, but above LN_2 temperature to limit condensation of O_2. At the higher pressures a thick oxygen fog was produced within the chamber.

As the "Post O_2" column of Table IV-4a indicates, this procedure had, at most, a very minor effect on the total property values of these samples. This result may or may not be sustained with other sample materials, or sample temperatures, or with other thruster propellants, but it does tend to enhance the value of the ex situ spectral reflectance measurements made for the current series. Pre- and post-exposure spectral reflectance distributions (from ex situ measurements) are therefore presented in Figure IV-12 for gold, all of the tested samples that exhibited noticeable degradation in total properties as measured in situ, and 6 mil microsheet.

The gold sample underwent a visual color change; its post-test appearance could best be described as "coppery." A comparison of pre- and post-exposure spectral reflectance (Figure IV-12a), however, indicates no significant change in total absorptance and the spectral distribution still exhibits the gold characteristics. The surface is most likely a gold-mercury amalgam, but primarily gold.

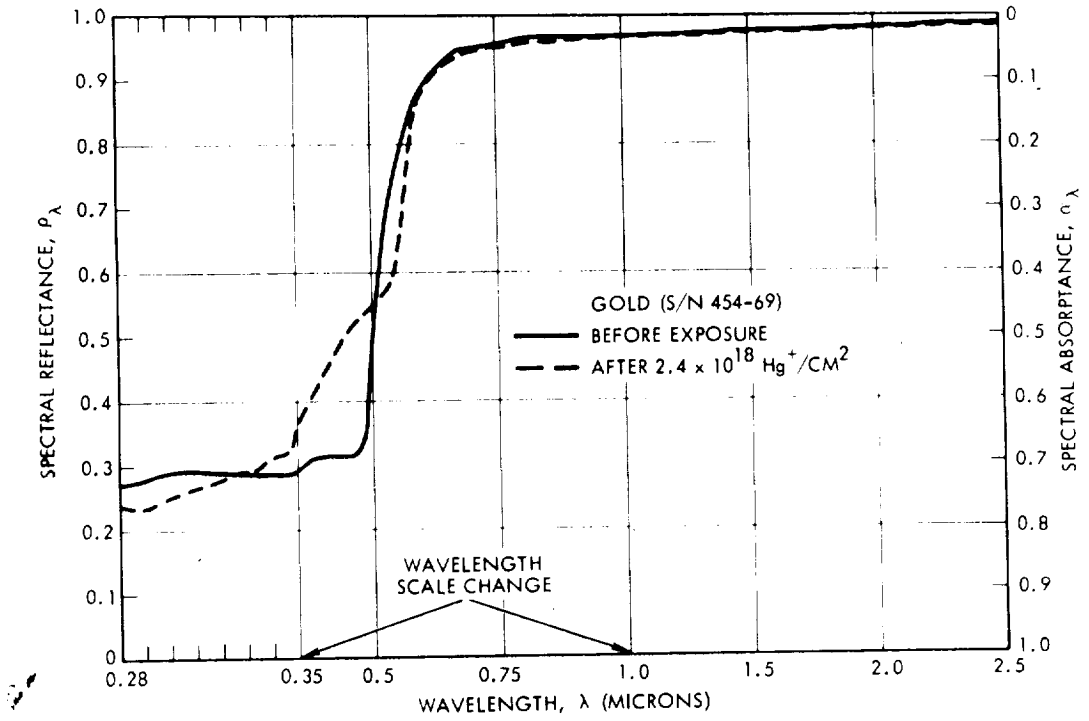

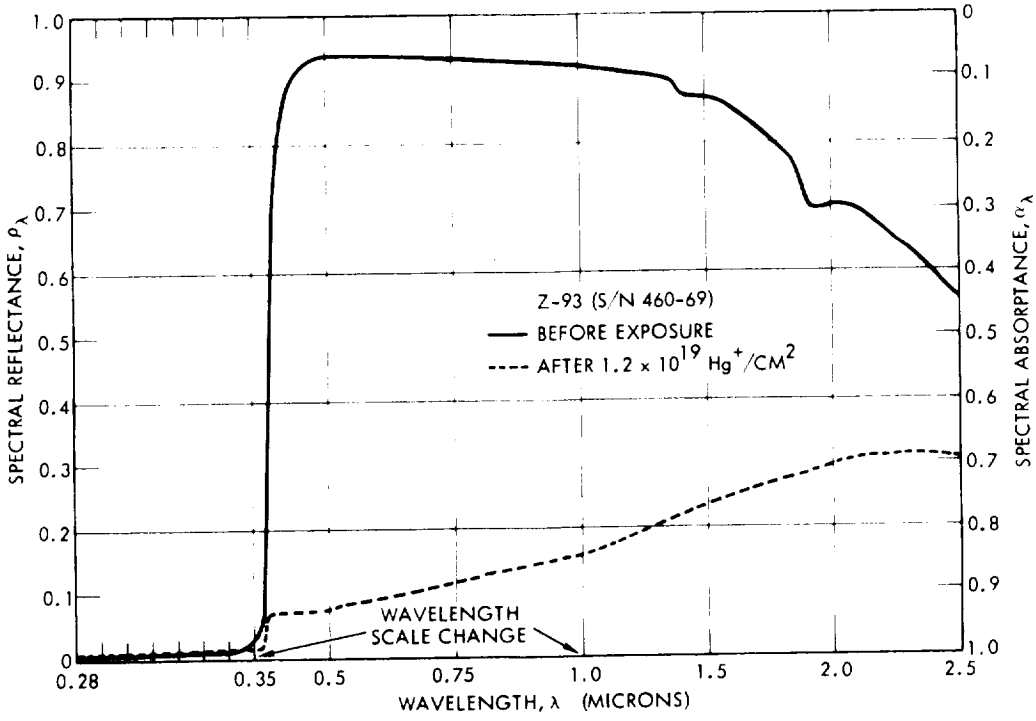

Figure IV-12a and b. Spectral reflectance of gold and Z93 white paint vs wavelength before and after exposure to 3 KeV mercury ions.

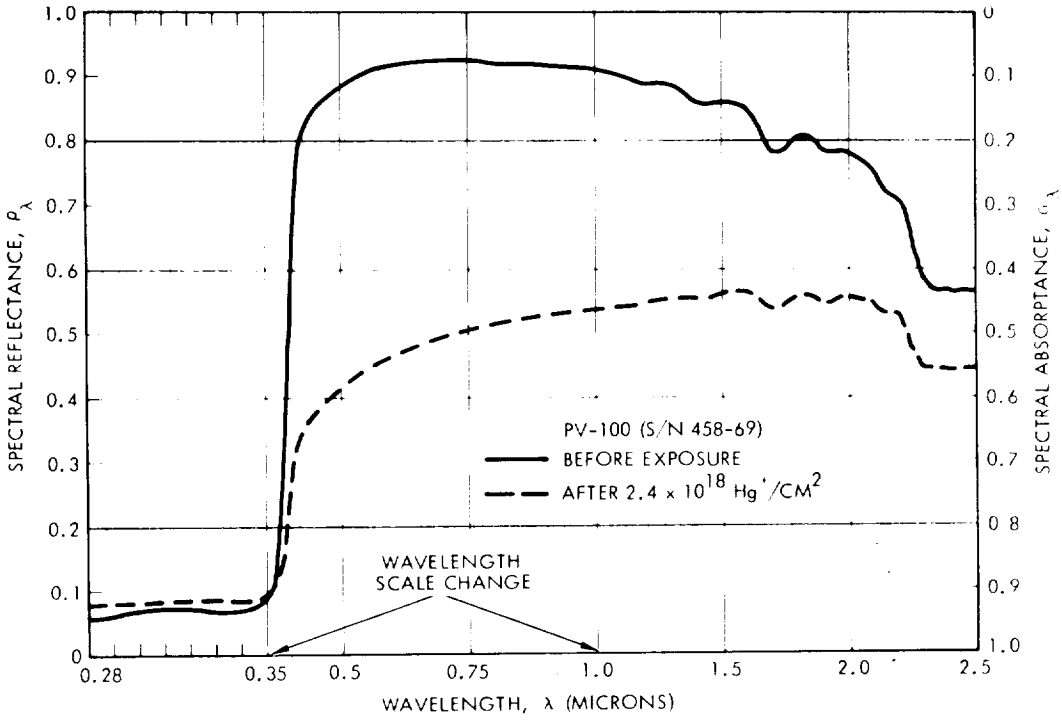

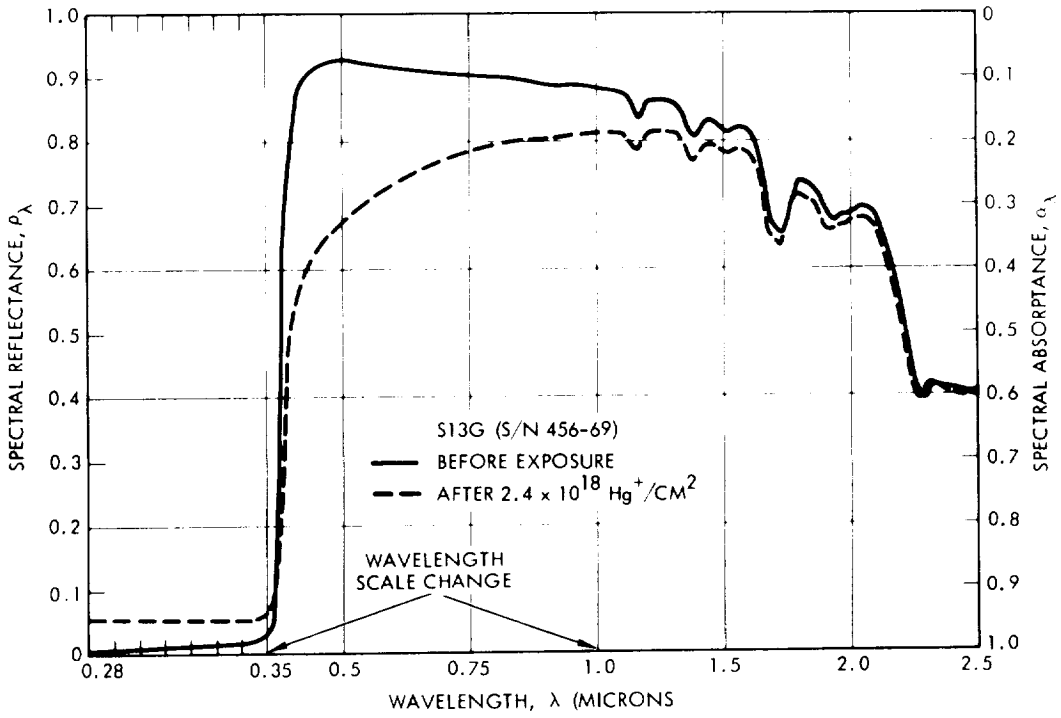

Figure IV-12c and d. Spectral reflectance of PV100 and S13G white paints vs wavelength before and after exposure to 3 KeV mercury ions.

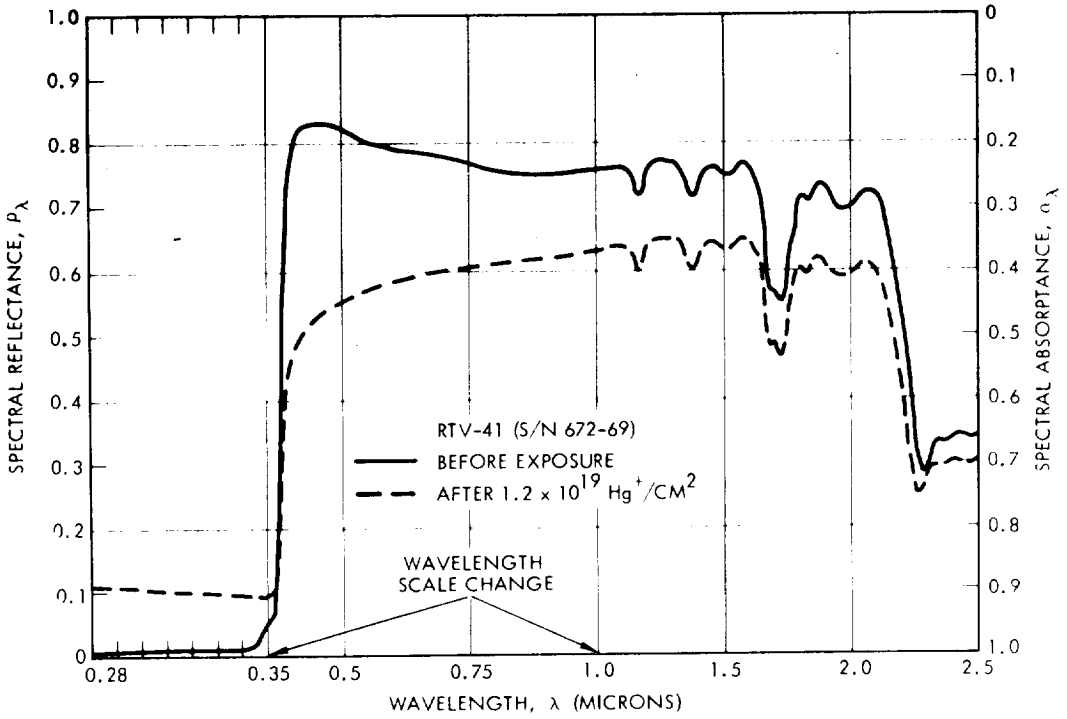

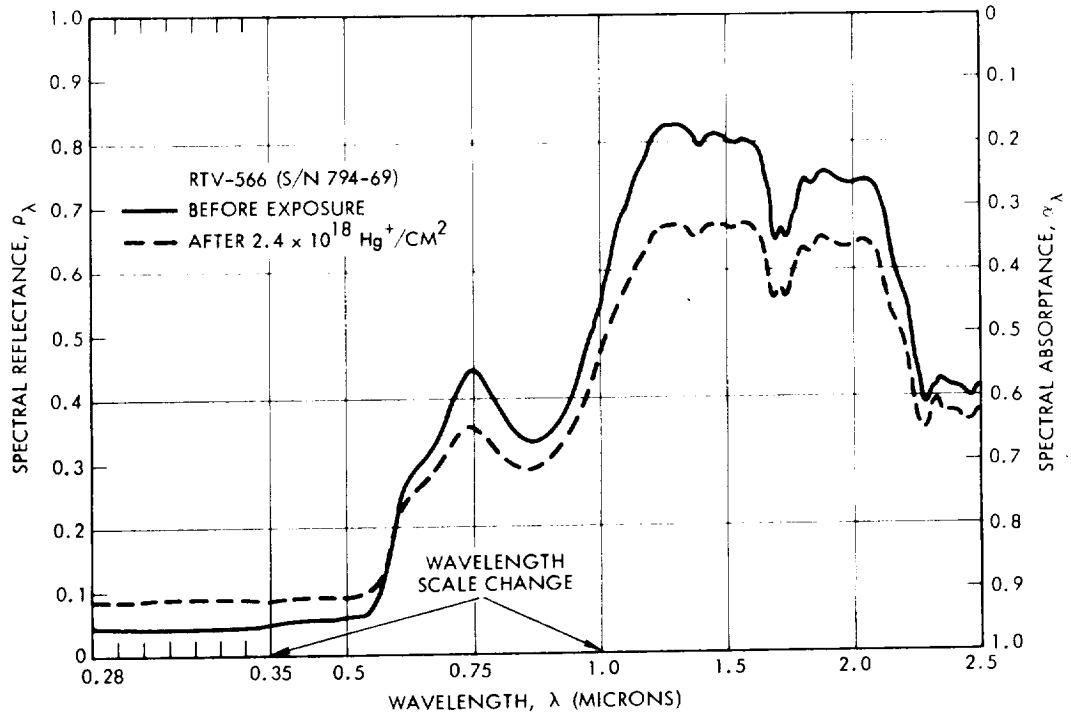

Figure IV-12e and f. Spectral reflectance of RTV41 and RTV566 vs wavelength before and after exposure to 3 KeV mercury ions.

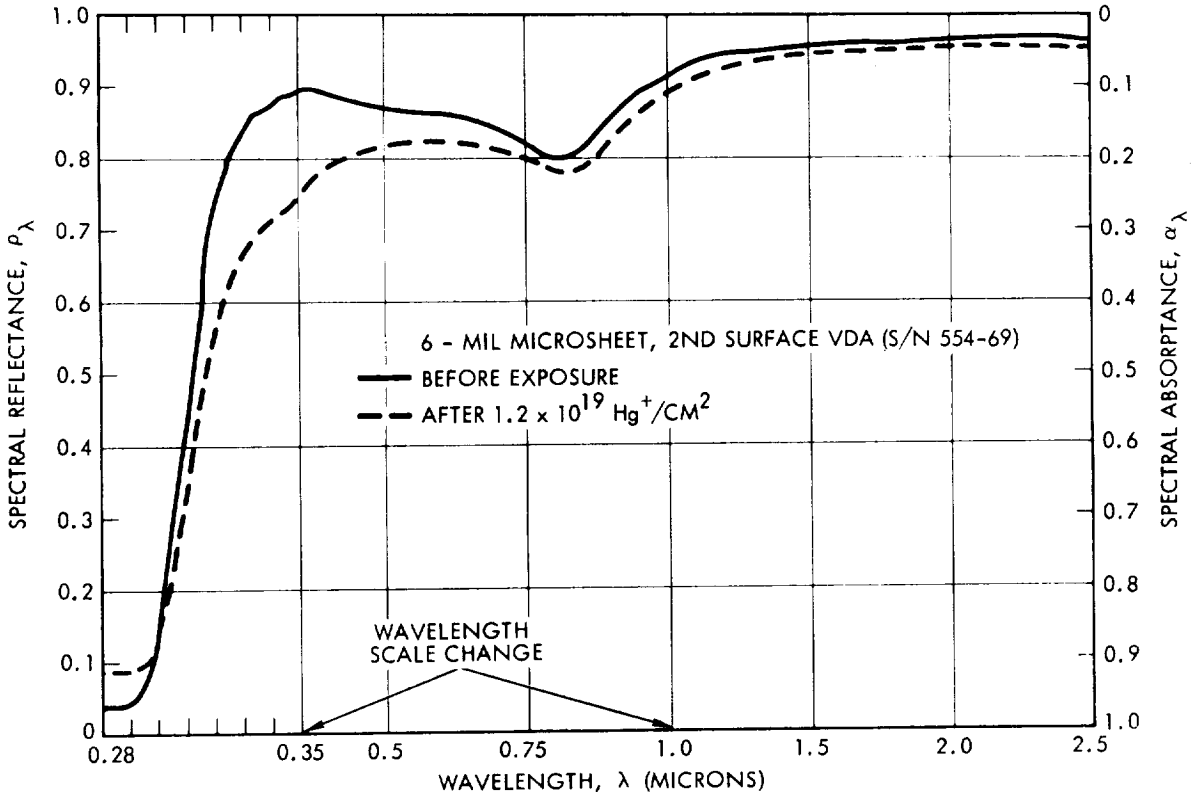

Figure IV-12g. Spectral reflectance of 6-mil-thick Corning 0211 microsheet with second surface vacuum deposited with aluminum vs wavelength before and after exposure to 3 KeV mercury ions.

A comparison of pre- and post-exposure Z93 spectral data, (Figure IV-12b), is interesting in that the absorptance edge of ZnO is still evident at 0.37 microns even though the surface is nearly "black" at that wavelength. However, this is the only spectral feature remaining. The other two white paints, which suffered less drastic change in α_{Xe}, preserved much more of their spectral features as well, as is seen in Figures IV-12c and d. The spectral signature between 1.0 and 2.5 microns arises from the silicone binder of these paints; it is seen again in Figures IV-12e and f of the silicone based RTV's.

a. Conclusions and recommendations. Note that the test results are for greatly accelerated arrival rates, and the effects of flux rate have not yet been evaluated. A typical arrival rate of high divergence angle ions to a spacecraft surface would be 10^9 ions/cm^2-sec as compared with the 10^{14} in these experiments. Furthermore, the Hg^+ dose was large in comparison to most practical missions. A 10^9 arrival rate during a 10^4 hour thrust period corresponds to a 3×10^{16} ions/cm^2 dose, whereas in these experiments 6×10^{16} ions/cm^2 arrive in 1 minute. Clearly, Phase III experiments should include exposing these samples at lower arrival rates and measurements after smaller doses.

Nonetheless, the following tentative conclusions may be drawn from these severe tests of thermal control coatings with respect to solar-electric spacecraft:

(1) With the probable exception of degradation of their optical coatings, if any, ion damage to solar cell cover glass properties will probably proceed at ion erosion rates, i.e., very slowly. Thus, thermophysical attention regarding the front surface of a solar array should focus on the materials exposed to the thruster exhaust by virtue of cover glass discontinuity and on propellant condensation effects.

(2) On the rear surface of solar arrays, where only ε_H is of interest, ion damage will also proceed slowly for many if not all coatings.

(3) Use of white paint as a low α_s/ε_H thermal control coating in areas exposed to the exhaust of ion engines should be avoided. Second surface quartz or glass mirrors appear to be a suitable substitute. Second surface aluminized (or silvered) Teflon may also be a stable substitute, (it does not degrade in uv as badly as Mylar), but ion engine exhaust effects on Teflon have not yet been determined.

V. SPUTTERING EXPERIMENTS

A. Introduction and Summary

Two kinds of sputtering experiments were proposed in the Phase I Final Report[1]: Gross erosion rate measurements using the multipurpose sample holder and protection effect studies using the quartz crystal microbalance (QCM). The multipurpose sample holder has been fabricated (see Section VI) and erosion rate measurements will be made with it in Phase III. Initial QCM experiments are reported in this section. Additional QCM experiments are in progress.

"Protection effect" refers to the fact that targets undergoing ion impingement can be at least partially, and sometimes fully, protected from sputtering, if a flux of atoms arrives at the surface simultaneously with the ions, adsorbs, and is sputtered in lieu of target atoms. Section 4.2.4 of Ref. 1 details the conditions under which protective effects might be expected and refers to accounts in the literature of experiments where they have been observed, sometimes unexpectedly. The bases for interest in protection effects in this program is that the ratio of ion to propellant atom flux emanating from an electrostatic thruster is a continuous function of angle from zero to 90 degrees with the thrust beam axis. At small angles the ratio is high, but drops to low values outside the primary beam. Hence, spacecraft surfaces located within the thruster exhaust hemisphere but outside the primary beam might be subject to protection effects.

The first series of experiments were performed with a $\sim$ 22°C aluminum target and total mercury arrival rates well below the minimum required for bulk condensation. Therefore, protection, if observed, would arise from the absorption of a monolayer or less of mercury. As explained in Section 3 of Ref. 1, the desorption energy of mercury from most surfaces (E_D^o) is less than from itself (E_D^f) and so if conditions for bulk condensation are not met, then the surface coverage of adsorbed mercury is likely to be minute. However, the condition of the surface is critical in adsorption; a surface under simultaneous atom and ion bombardment could have $E_D^o > E_D^f$ and therefore have a large fraction of a monolayer adsorbed even with low arrival rates.

In the experiments the ratio of mercury atoms to ions arriving at the target was varied from run to run to see if this ratio influenced target sputtering yield. No significant sputtering protection was afforded this target by arriving atom fluxes as high as 2 1/2 times arriving ion fluxes. This result, together with early results from a second series of experiments now in progress, in which bulk condensation of mercury on the QCM has been achieved, allow the following conclusions:

- Aluminum targets will not exhibit the protection effect when mercury arrival rates are insufficient to permit bulk condensation. (As a practical matter, such conditions are unlikely to occur on sun-illuminated surfaces at solar distances smaller than 3 AU.)
- Even when bulk mercury condensation has occurred, on aluminum it is so easily removed by ion bombardment that the level of protection is insignificant.
- Mercury protection effect experiments should be continued with a gold or silver target when priority permits.

B. Apparatus

The basic operation of the QCM is described in Appendix C of Ref. 1. Briefly, minute quantities of mass which accumulate on, or are removed from, a vibrating piezoelectric crystal are detected as changes in the crystal's resonant frequency. QCM improvements incorporated in Phase II were crystal temperature sensors (both a thermistor and a thermocouple) and an electrical heater capable of rapidly elevating the crystal temperature above that of its water cooled mounting-plate.

Figure V-1 is a front and back view of the QCM assembly in the experimental position. The electromechanical crystal shutter is in the "open" position. About one inch below the crystal is the ion current density (j_+) probe.

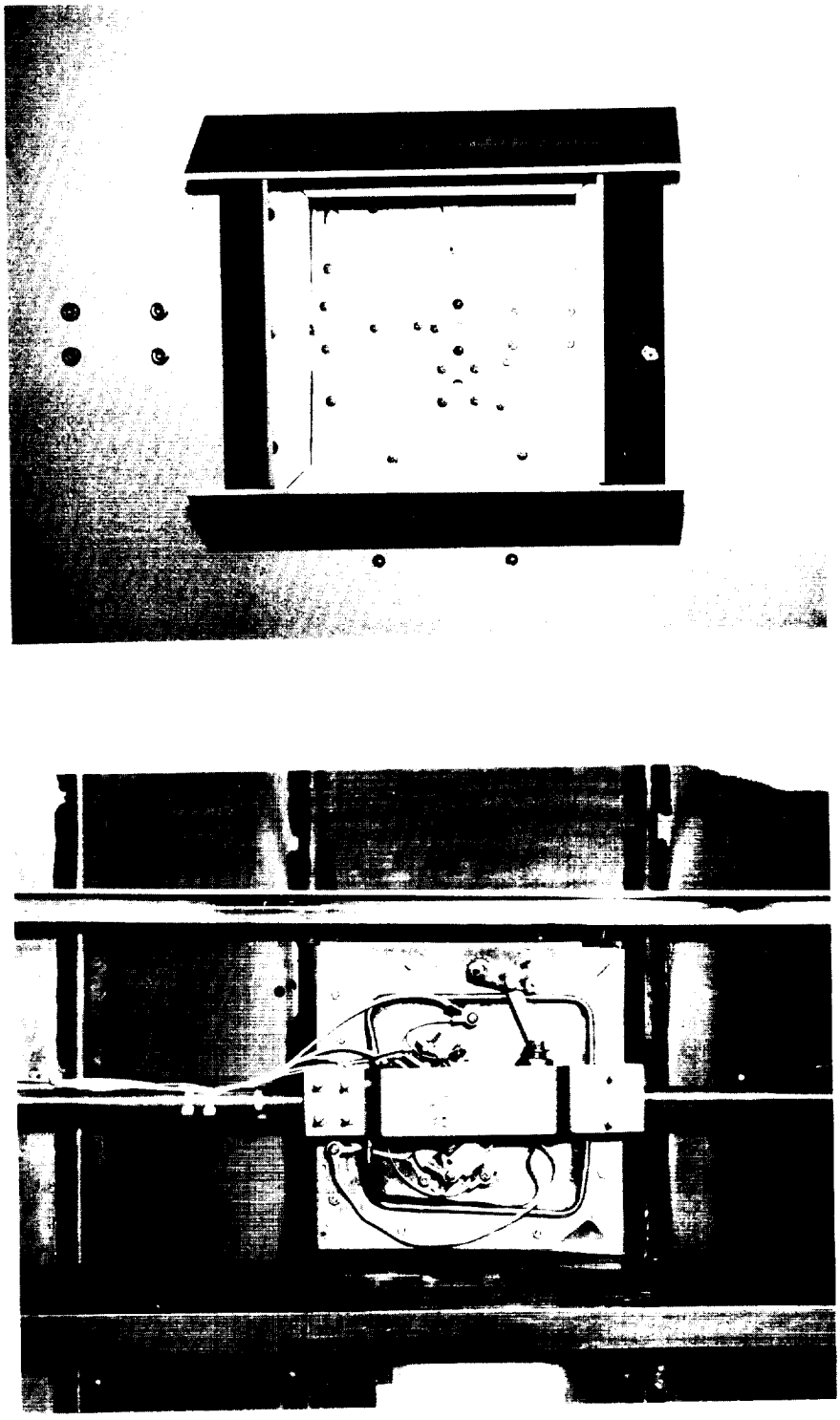

Figure V-1. Front and rear views of quartz crystal microbalance apparatus in experimental position.

The series of QCM experiments performed in Phase I removed nearly the entire aluminum coating on the crystal. It was therefore necessary to recoat the crystal. A laboratory vacuum chamber was fitted for this purpose. Aluminum in an externally heated beryllia crucible is the evaporative source. The crystal holder is mounted on a heat-sink two inches above the crucible. Interposed between the source and crystal are an LN_2 cooled aperture plate to reduce contaminants and radiant energy arriving at the crystal, and a shutter to allow preheating and cleaning of the aluminum before starting deposition on the crystal.

The mounted crystal was coated with this apparatus with enough aluminum to produce approximately 100 kHz frequency change.

C. Experimental Procedure

The ion source is first brought to the desired operating point and stabilized. Meanwhile the water cooling the QCM plate is turned on so that its temperature stabilizes. The frequency of the crystal is measured with a HP5245L frequency counter, the last 2 or 3 digits converted to an analog signal with a HP581A digital to analog converter, and this analog signal is displayed on a Varian G-4000 10-inch strip chart recorder. The other pen of this recorder displays the ion current density signal from the j_+ probe.

To commence an exposure, the flag shutter in front of the crystal is opened with a solenoid. During the next 30 seconds or so the crystal frequency changes rapidly in response to the thermal transient associated with application of the ion beam power. Thereafter the value of df/dt is nearly constant, and an impressively linear sawtooth pattern is produced on the chart paper. The exposure is continued until the crystal frequency has changed at least 1 kHz. Then the exposure is terminated by closing the shutter, and another thermal transient is observed.

In the data reduction process the early portion of frequency vs time curve is given less weight than the final portion, since it is sometimes found that the initial erosion rate is slightly lower than that subsequently recorded. This is understood as the result of a surface coverage of aluminum oxide which has a lower sputtering yield than aluminum. Thus, in a 2 kHz exposure, the second sawtooth is used. A straight edge is laid along the chart line, and

a parallel line drawn with a pencil. The slope of this line is noted and divided by the average value of j_+ during this period, and multiplied by the square of the ratio of current crystal frequency to the frequency of the crystal at the beginning of the experimental series, which adjusts the erosion rate quantity for the slowly changing sensitivity of the QCM with frequency:

$$R = \frac{\Delta f}{K_1 j_+'} \quad \frac{K_2}{L} \quad (f_o/f)^2 \tag{1}$$

Here K_1 converts the chart reading j_+' into current density, K_2 is the chart speed, and L is the chart length consumed in producing Δf frequency change. This normalized erosion rate is then compared to values obtained under various exposure conditions.

The ion to atom arrival rate ratio is calculated from the following considerations. The ion arrival rate is simply

$$\Gamma_+ = j_+/q \tag{2}$$

where j_+ is the ion current density at the QCM and q is the electronic charge. The atom arrival rate at the QCM is

$$\Gamma = K_3 \Gamma_o \tag{3}$$

where Γ_o is the atom flux density at the thruster and K_3 is the geometric dilution of this flux. The value of K_3 is 10^{-2}, which may be determined from the thruster-target distance (30 inches) and Figure A-2 of Ref. 1. The value of Γ_o is

$$\Gamma_o = \frac{I_t - I_b}{A_s q} \tag{4}$$

where I_t = the total boiler flux in equivalent ma.

I_b = the total ion beam current

and A_s = the area of the source (177 cm^2)

The value of I_t is obtained from the gravimetric boiler calibration, found in Appendix A of this report, together with the relation

$$I_t \text{ (ma)} = 133\ \dot{m}\ \left(\frac{gm}{hr}\right) \tag{5}$$

Thus the desired ratio is found from Eqs. 2, 4 and 6:

$$\frac{\Gamma_+}{\Gamma} = \frac{A_s\ j_+}{K_3\ (I_t - I_b)} = 1.77 \times 10^4\ \frac{j_+\ (ma/cm^2)}{133\ \dot{m}\ (gm/m) - I_b\ (ma)} \tag{6}$$

Another quantity of interest is the arrival rate ratio of ions to the total arriving flux:

$$\frac{\Gamma_+}{\Gamma + \Gamma_+} \equiv \frac{1}{\Gamma/\Gamma_+ + 1} \tag{7}$$

A small computer program was written to perform the calculations of Eqs. 1, 6 and 7 from a standardized format of the raw data.

D. Discussion of Results

1. Summary of results. Approximately 40 ion beam exposures of the $\sim$ 22°C aluminum coated QCM were made at ion current densities ranging between 20 and 190 $\mu a/cm^2$ and ion to atom arrival rate ratios of 0.4 to 40. No evidence of target protection was obtained under these experimental conditions of low propellant arrival rate (as compared with that which could be required for bulk condensation). Therefore a second series of experiments is underway in which propellant arrival rates are high by this measure. This is accomplished by lowering the QCM temperature, since further increases in propellant flux lead to increasing experimental uncertainty, as discussed below.

Two qualitative results of the second series which bear on the interpretation of the first series results are:

1) It is usually necessary to sputter the target in order to initiate the condensation process, even when the mercury arrival rate substantially exceeds that required for subsequent layer growth.

2) Mercury condensed on the aluminum coated crystal is removed at enormous rates when bombarded with mercury ion beams. The reasons for this is under investigation, but the fact is pertinent regardless of its cause.

Thus, the following simple picture emerges. Mercury will only adsorb on aluminum if the substrate is relatively clean, and even then it adheres very poorly. Hence, the conclusions in Section V.A.

The absence of the protection effect in the first series does not mean that the normalized erosion rate R (see Eq. 1) was found to be absolutely constant as the experimental parameters were varied. Indeed, a 40% range of R was obtained from the data. Rather, it means that no correlation was observed with protection-effect related parameters, and in any case, the range obtained is relatively small.

2. Effects of charge exchange. The value of R did have a positive correlation with mass flow from the boiler; $R(\dot{m})$ was a positive, approximately linear function. Such a relationship would result if a significant amount of charge exchange between fast ions and slow atoms occurred: The resulting fast atoms would sputter the target but would not be recorded as current to the j_+ probe. This hypothesis was tested as follows:

Assume that the normalized erosion rate is constant when both the fast ions and fast atoms are accounted for. Assume further that the production of fast atoms is simply proportional to the product of the ion beam current and the atom beam current. Then

$$\frac{\dot{\Delta f}}{j_+ + K\, I_+ I_n} = C \qquad (8)$$

Since R has previously been defined as

$$R \equiv \frac{\dot{\Delta f}}{j_+} \tag{9}$$

(from which Eq. 1 is derived),

$$R = C\ (1 + K \frac{I_+ I_n}{j_+}) \tag{10}$$

Thus, a plot of R vs I_+I_n/j_+ should yield a linear curve of slope CK and y intercept C.

Data points selected to represent the range of experimental values obtained for these variables are plotted in Fig. V-2. These points show that R increases with the charge exchange production parameter as predicted by the hypothesis. The lack of perfect linearity, especially at higher values of I_+I_n/j_+, probably reflects inadequacy in expressing the fast atom current density simply as $K\ I_+I_n$. At least two additional effects may be influencing the data somewhat. These effects, chamber residual gas injestion/protection and a varying component of double charged ions, are discussed in later sections.

Charge exchange calculations have been made, again based on simplifying assumptions, and approximately half of the increase in R with I_+I_n/j_+ has been accounted for. The most questionable assumptions made were that the flux atoms leaving the thruster was constant across its exit plane and that these atoms had angular distribution of a distributed cosine source. If the neutral and the ion flux are both high in the same region, and/or if the neutral distribution is peaked in the forward direction by the grid system, the calculated charge exchange production is low.

The important point, insofar as the experiments are concerned is that charge exchange creates experimental uncertainty, since charge exchange results in a fast neutral atom component in the beam which is neither measured nor accurately calculated. The larger the total mercury flux from the thruster, the larger this component. Therefore, increasing total mercury flux to the QCM is unattractive. Since limits exist on how small I_+ may be and still obtain stable thruster operation, I_n must be increased if increases in the atom to ion arrival

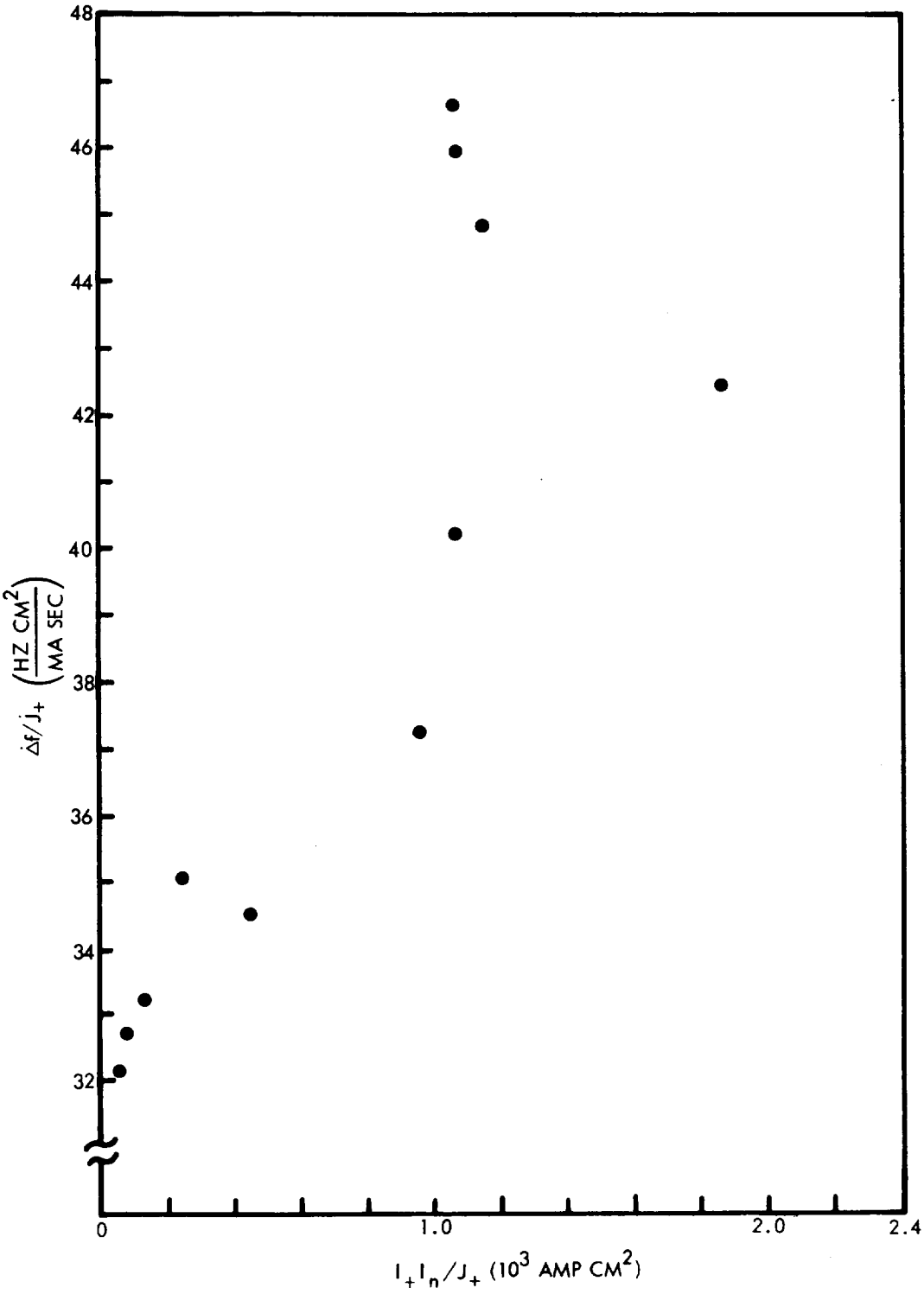

Figure V-2. Target erosion rate vs charge exchange production parameter, both normalized to incident ion current density. Data points were selected to indicate the range obtained in these variables.

rate ratio above 2 1/2 are sought. Increasing I_n with fixed I_+ also increases the charge exchange rate. It was these considerations which led to adopting the alternative approach of the second series of experiments, i.e., lower the target temperature in order to increase the residence time of mercury atoms on its surface, thereby increasing the probability that these atoms will be removed by sputtering instead of evaporation.

3. Effects of residual vacuum chamber gases. Experiments on the effects of residual vacuum chamber gases on ion erosion rates were reported in Appendix C of Ref. 1. Briefly, it was found that an indicated 2×10^{-7} torr partial pressure of CO reduced the erosion rate of Al by 250 microamp/cm^2 3 Kev Hg^+ beam approximately 1%. In the present experiments, indicated chamber pressure was approximately 2×10^{-7} torr, and the beam current density ranged between 200 and 20 microamp/cm^2. As a result, R values could be 1 to 10% low. It is difficult to determine from the data whether this effect is in fact present, but the possibility of its presence discourages further reductions in j_+ even if stable thruster operation could be obtained.

4. Effects of doubly ionized beam components. The ion beam of an electron bombardment mercury thruster operating at its design point contains approximately 6% Hg^{++} (see Appendix A, Ref. 1). Presumably this component decreases with decreasing anode potential. Since a Hg^{++} is recorded by the j_+ probe as two Hg^+, as long as $S_{Hg^{++}} < 2\, S_{Hg^+}$, where S is the sputtering yield, the value of R will decrease as the anode potential is decreased. Review of published energy dependence data of S for Hg^+ over the 3 to 6 Kev range indicates that $S_{Hg^{++}} \simeq 1.6\, S_{Hg^+}$. In these QCM experiments, low values of j_+ at high $\dot{m}$ have mainly been obtained by reducing the anode potential. It is calculated that this effect would at most lower the value of R by 2%.

VI. MULTIPURPOSE SAMPLE HOLDER

A major task completed during Phase II was the detailed design, fabrication, integration, and testing of the multipurpose sample holder. As its name implies, this fixture will be used in several experiments. Samples on the holder exposed to propellant beams will provide data on erosion rate as a function of angle, and chemical and metallurgical reactions as a function of both sample temperature and beam arrival rate. The motivation for these experiments is discussed in Ref. VI-1.

A. Basic Design Concept

The multipurpose sample holder, like the surface thermal sample holder, mounts behind the beam collector cutout, as shown in Figure IV-1. The basic design concept, developed in Phase I, is shown in Figure VI-1. It has a large sample capacity, sample temperature control, shielded areas on each sample (for the erosion depth measurements), a multiplicity of sample orientations with respect to an incident beam, and provision for making negligible the incidence of foreign particles on sample surfaces. The sample holder can be removed from vacuum chamber in an inert atmosphere following cesium beam exposures. The philosophy behind the basic design concept is presented in Ref. VI-1.

B. Requirements of Detailed Design

In preparing a detailed design of the sample holder, the following requirements were identified as critical:

1) Effective location and cooling of sputtering shields.
2) Sample holder positioning in and removability from the chamber.
3) Easy removability of sample pipes without endangering samples.
4) Obtaining good registration of sample pipes in holder.
5) Minimizing thermal shorts between sample pipes.
6) Simple sample substrate design with provision for erosion depth measurement reference surfaces.
7) Compatibility of the system with the surface thermal sample holder system.

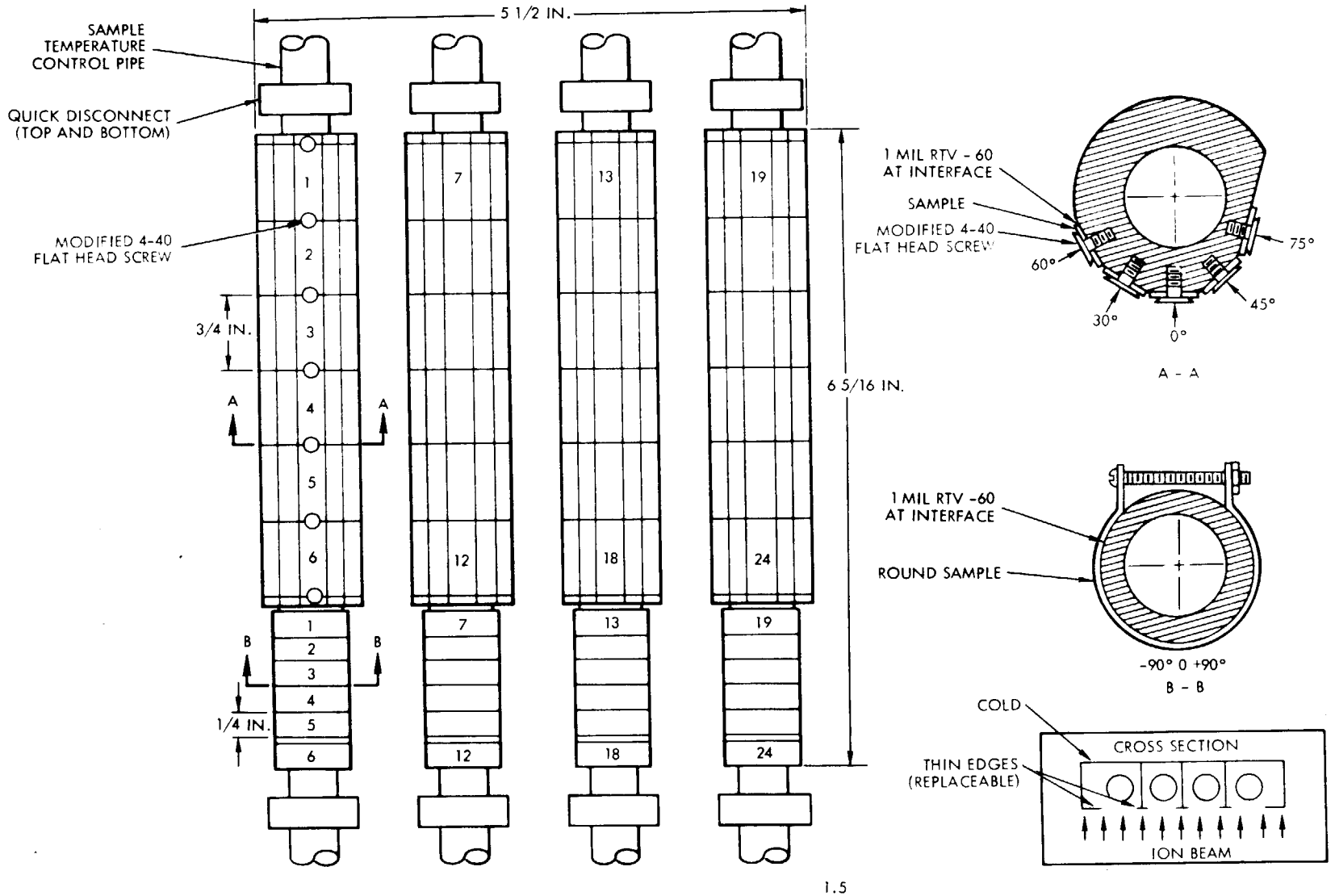

Figure VI-1. Conceptual design of multipurpose sample holder.

Most of these requirements interact with each other, so an iterative design process was necessary.

C. Design and Fabrication

1. Collector Plate Sputtering Shields. This portion of the sputtering shield system is mounted on the beam collector and is therefore common to all sample holders. Figure VI-2 shows the collector plate shields (and the surface thermal sample holder loaded with 5 black paint samples); Figure VI-3 is a closeup with the sample area blanked off with white paper. The forward (most prominent) shield set shadow the sample area from copper sputtered from the rear half of the cylindrical LN_2 liner shown in Figure VI-2. The inner set of shields precisely define the sample area and prevent ions from striking the sides of the cut-out in the 5/8 inch thick titanium collector plate. In their absence, sputtered titanium would reach the samples. Both sets of shields have their inside edges beveled to make the edge area, and therefore copper sputtered onto the samples, negligible.

2. Sample Removal System. Figure VI-4 shows systematically how the sample holder will be removed from vacuum chamber following cesium exposures. The sample holder, which is mounted on a port plate, is loaded behind the square cutout in the collector. To facilitate the insertion and positioning of the sample holder, two horizontal tracks were installed in the tank. When it comes time to remove the assembly, a large glove bag is attached to the port and a support table positioned adjacent. The assembly is rolled out on the internal tracks and table until it is entirely within the glove bag. Then the four sample containing pipes are disconnected, placed in an air tight transfer box, and carried to a nearby glove box. In the glove box the samples are demounted from the pipes and measurements begun.

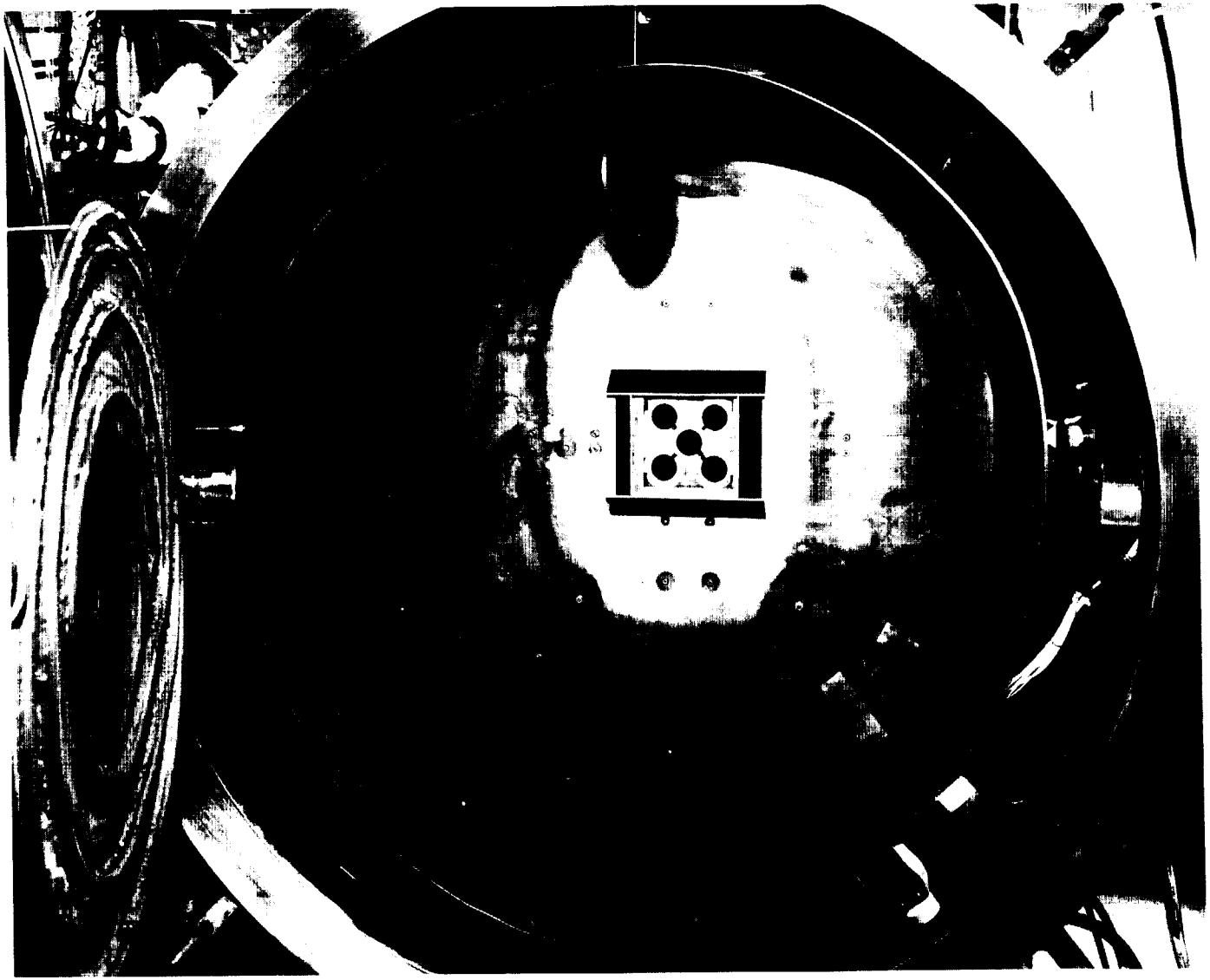

Figure VI-2. Forward interior section of 4 x 8 chamber showing front liner, titanium collector, sputtering shields, and surface thermal sample holder in beam exposure position.

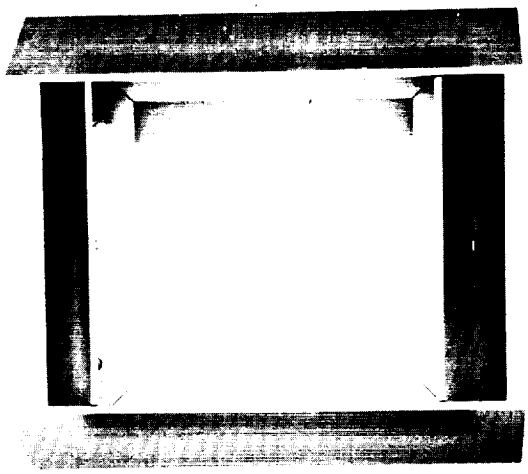

Figure VI-3. Closeup photograph of collector plate sample-area-cut-out sputtering shields.

3. Sample Holder. The sample holder design satisfies each of the requirements listed in Section VI.B. In the following series of photographs, many of the design features are evident.

The basic parts of the sample holder are shown disassembled in Figure VI-5, partially assembled in Figure VI-6, and fully assembled in Figure VI-7. Removal of individual sample holder "pipes" (following exposure) will be accomplished by removing the screws in the fittings on each end of the pipe and then sliding the pipes forward in the two slotted guide plates. Interposed between adjacent pipes are shields which prevent exchange of sputtered material

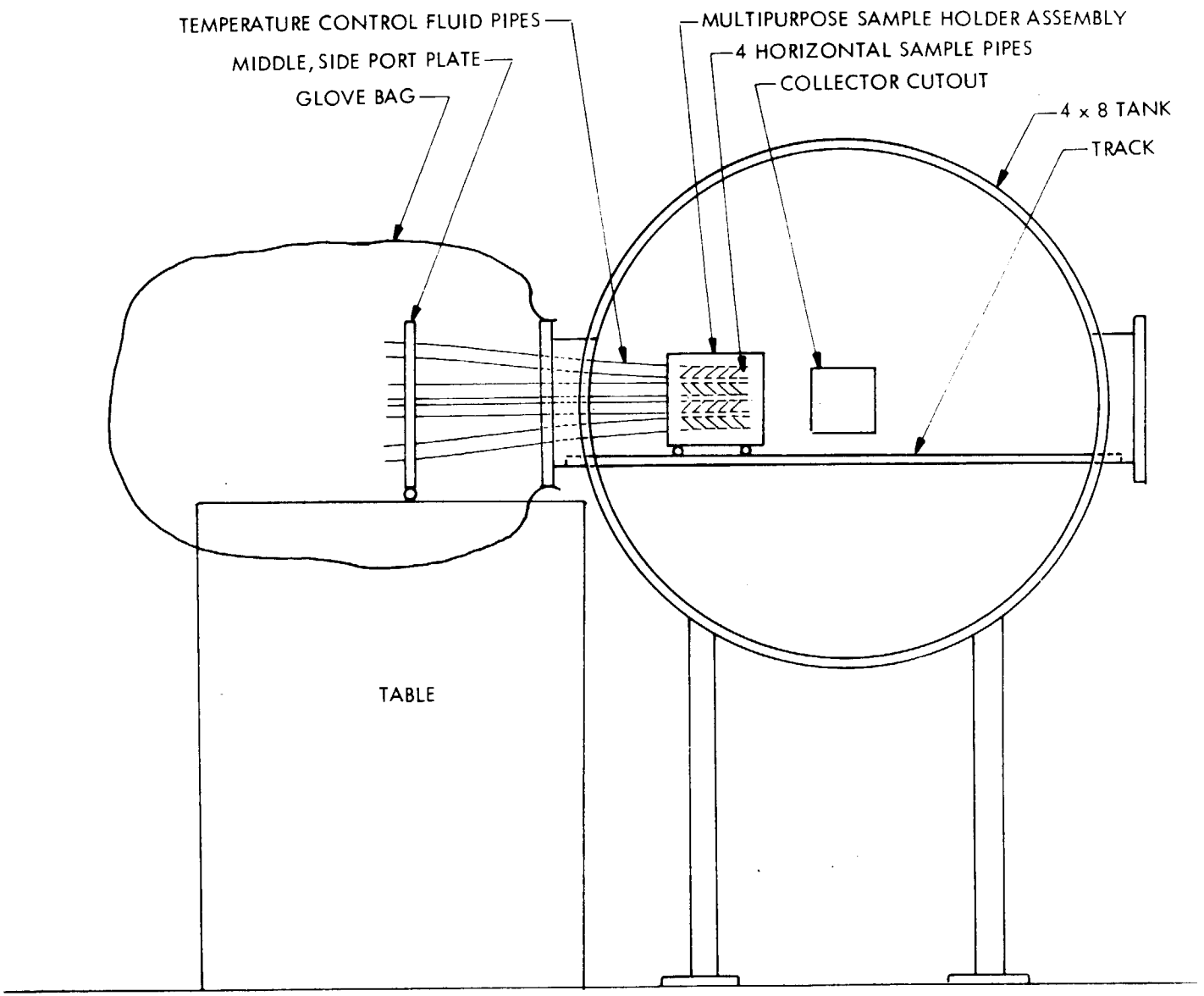

Figure VI-4. Scheme for removing multipurpose sample holder into inert atmosphere. (Viewed from rear of chamber.)

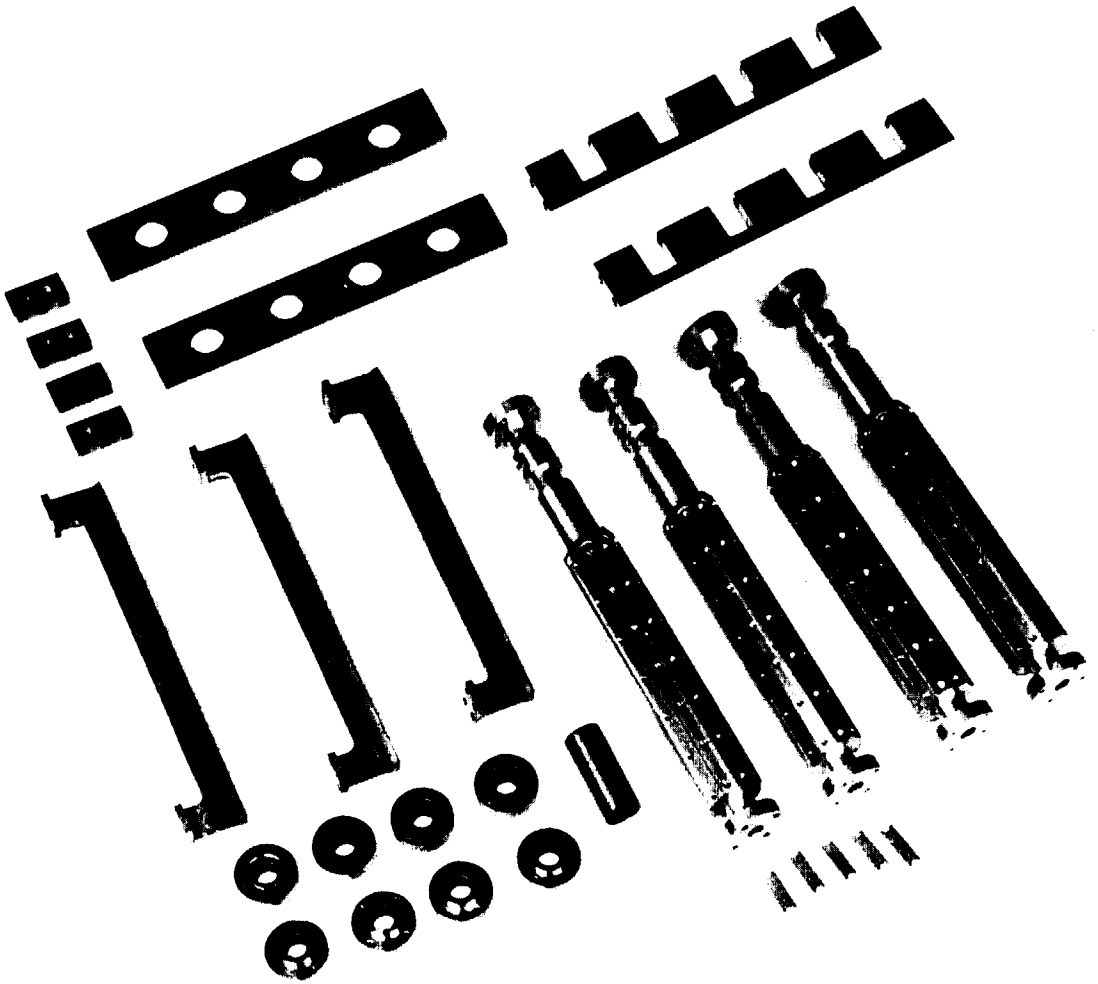

Figure VI-5. Principal parts of the multipurpose sample holder.

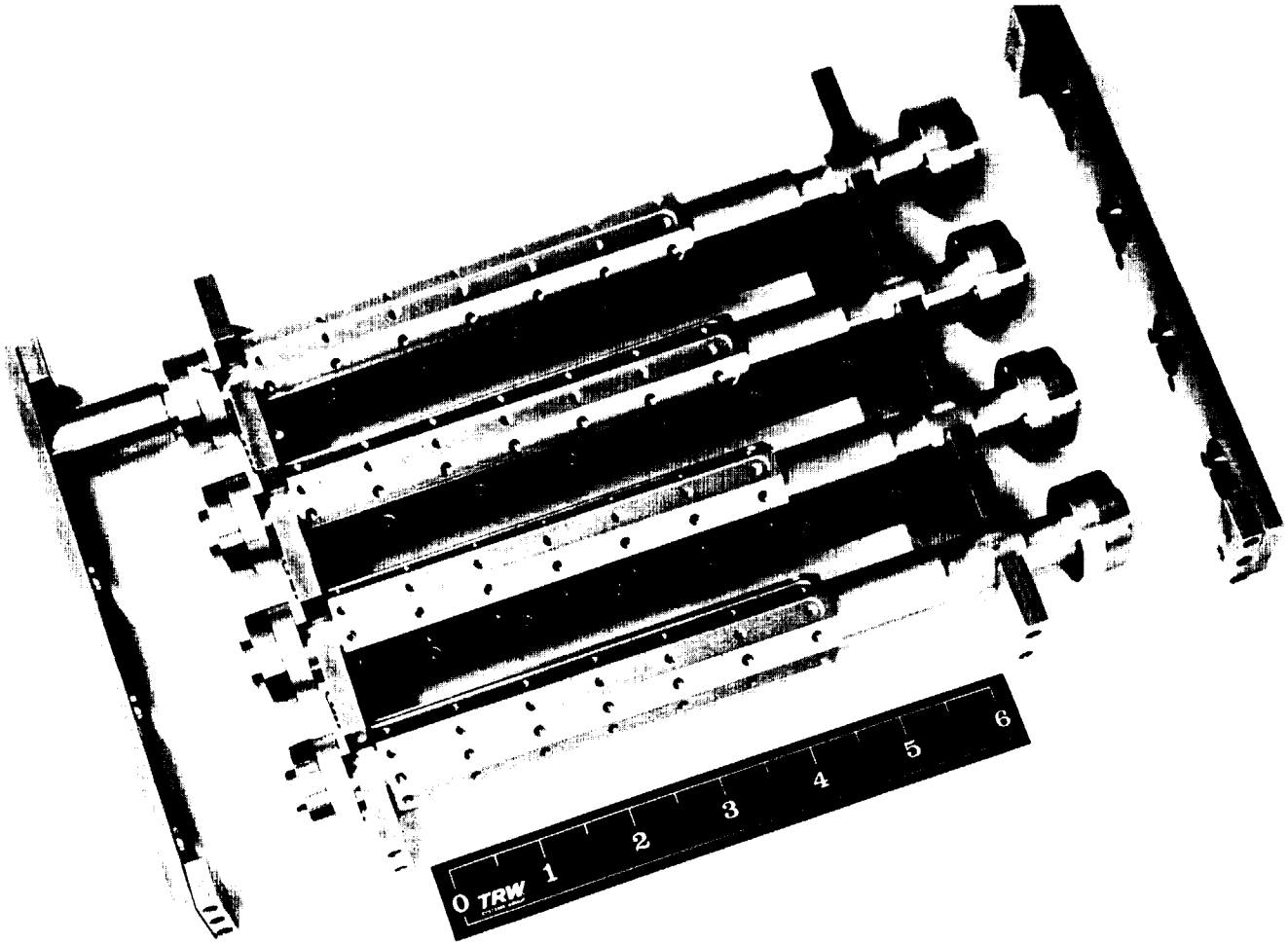

·e VI-6. Multipurpose sample holder partly assembled.

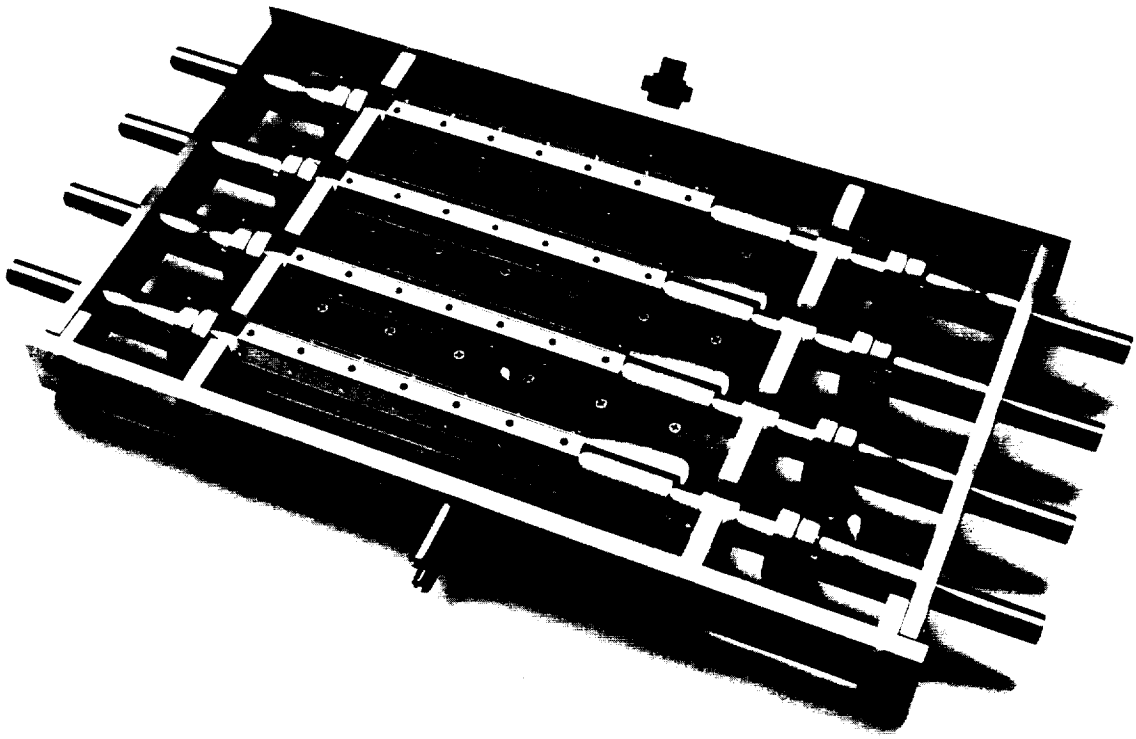

Figure VI-7. Photograph of completed multipurpose sample holder.

between them. They make good thermal contact with the water cooled back plate for cooling and good mechanical contact with slotted guide plates for registration. The rectangular flat copper plates screwed perpendicularly to the shields prevent ions from impacting the shield. Their sides are beveled so that very few atoms of sputtered copper will hit the samples. The sections of thin walled stainless steel tubing between the disconnect flanges and the end plates will minimize the thermal short between pipes, permitting their operation at widely spaced temperatures. The eight stainless steel tubes have been hydrogen brazed to the disconnect flanges and heliarced to the end plates. Special capture screws have been made for the disconnect flanges.

Figure VI-8 shows four sample substrates and a 4-40 screw. These substrates fit in the milled grooves of the sample pipes and are held in place by these reworked flat head machine screws which shadow shield a portion of each end of each sample from the ion beam. This is the concept shown in Section A-A of Figure VI-1.

The ruler in Figure VI-6 indicates approximately the portion of the sample holder which is exposed to the ion beam through the collector cut-out. The circular portion of the sample pipe is to accommodate semi-circular samples indicated conceptually in Section B-B of Figure VI-1. The smaller diameter portion at the end permits loading and unloading semi-circular samples without undue flexure.

Careful inspection of Figure VI-7 will reveal that the end of the flat sample section of the aluminum sample pipes has been undercut to prevent the ion beam from sputtering aluminum onto the adjacent semi-circular samples. Also visible in this figure is one lower track roller and both upper track guide pins. The sample holder rollers and guide pins and the tracks mounted across the 4 x 8 foot chamber behind the collector plate allow smooth sample holder ingress and egress and precisely position the holder parallel to the collector plate.

The front and rear of the entire sample holder assembly are shown in Figures VI-9 and VI-10. Eight cryogenic-type vacuum feedthroughs on the port plate provide supply and return sample temperature controlling fluid

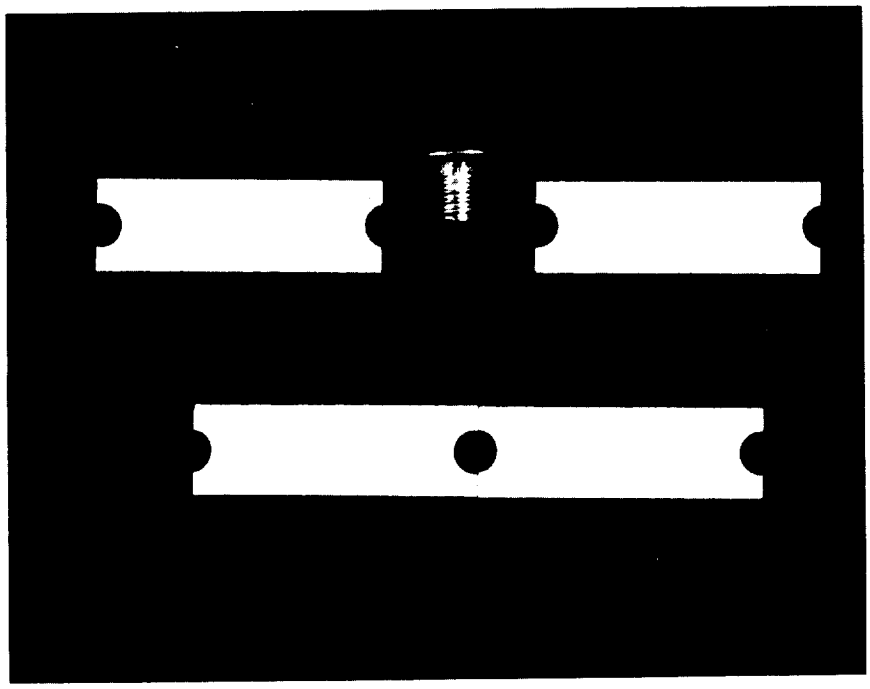

Figure VI-8. Four aluminum multipurpose sample substrates and a reworked flathead machine screw. Samples are mounted on holder end-to-end as shown by bottom two substrates.

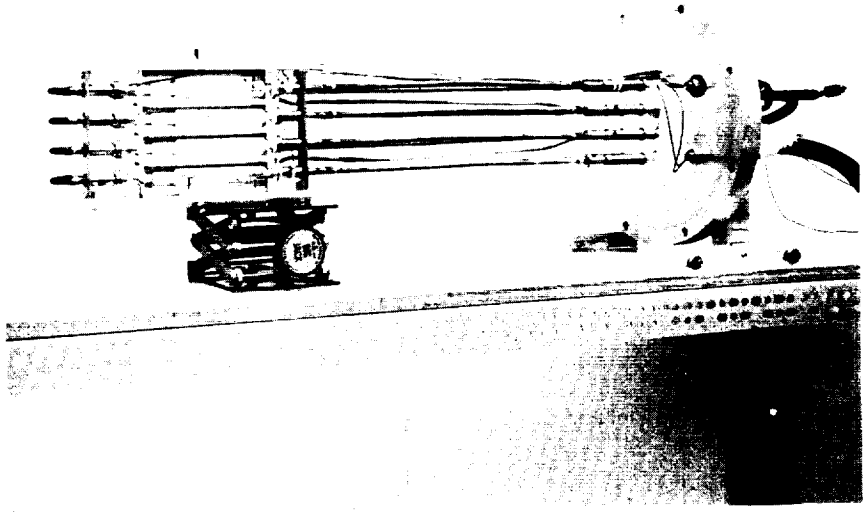

Figure VI-9. Front view of entire multipurpose sample holder assembly.

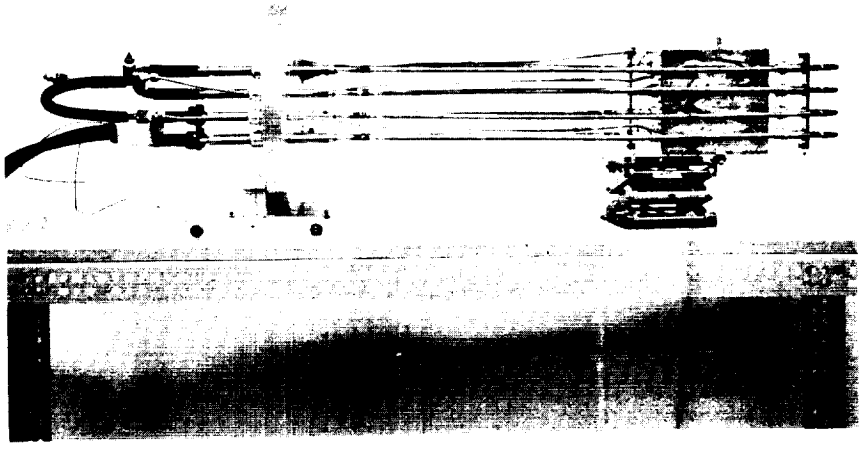

Figure VI-10. Rear view of entire multipurpose sample holder assembly.

paths for the four sample pipes. Two additional fluid feedthroughs are for water cooling the sample holder back plate. Stiff copper tubing is brazed to the feedthroughs and the sample holder fittings. Two eight pin electrical feedthroughs are available for electrical instrumentation. In the photographs thermocouple wire employed during the thermal test of the sample holder can be seen.

Initial use of the sample holder will be with approximately 20°C and approximately 100°C water as the temperature control fluids. These temperatures will be sufficient to allow approximate determination of the activation energy of chemical reactions and establish whether a broader temperature range and/or better temperature control would be a worthwhile investment.

A Haake Model No. 1280-1 constant temperature circulator was purchased on capital funds as a source of high temperature fluid. The circulator specifications indicate $\pm$ 0.01°C temperature control accuracy, a 2 KW stepless heater, and 28 ℓ/min discharge capacity.

The ~20°C water will be city water. City water temperature was recorded over an 11 day period and the water was always between 18 and 20°C. More important, the highest time rate of temperature change observed was 1.6°C/hr and that was atypical. Typically, during working hours, the temperature was constant within $\pm$0.5°C and time rates of change were less than 0.5°C/hr.

D. Thermal-Vac Test

The multipurpose sample holder was tested and found to have acceptable temperature control and vacuum performance. Furthermore, no evidence was found of sputtered metal atoms arriving at sample surfaces, and vinyl acetate appears to be an acceptable interface compound between copper sample substrates and the sample holder "pipes." Therefore, fabrication and test of the sample holder is complete.

The test consisted of mounting thermocouple equipped copper samples on hot and cold pipes and observing their temperature dependence on time and ion beam exposure. After the test, the sample holder was removed from the vacuum chamber and carefully inspected for evidence that the beam had hit all sample locations and that the various sputtering shields had prevented material from arriving at sample surfaces.

The Haake 1280-1 constant temperature circulator was used to circulate ~95°C water through two of the pipes in parallel in closed loop. With constant input power to the sample holder, i.e. beam on and constant or beam off, sample temperature was constant to $\pm$ 0.2°C. When the beam shutter was opened the sample temperature rose ~3°C within 1-1/2 minutes and then remained stable. When the shutter was closed it dropped ~3°C in a similar time period.

Since exposure times with the multipurpose sample holder will be several hours or more, a brief transient in sample temperature at the beginning and end of the exposure will be of no consequence.

The cold pair of pipes were also operated in parallel, but open loop with city water. Their temperatures remained constant within $\pm$0.3°C with constant input power. Opening and closing the beam shutter had the same effect as with the hot pipes.

E. Multipurpose Samples

Due to the large number of samples required, a rapid, inexpensive method for sample substrate fabrication was needed. The material selected for substrates was 6061-T6 aluminum because of its hardness, thermal conductivity, and machineability. The following method fits the manufacturing requirements. The sample substrates are sheared to size, jig punched, and then abrasive tumbled to debur before they are ready to polish, plate, coat, etc.

Figure VI-8 shows the substrate configuration and the reworked flat head screws which hold the samples in place.

The status of multipurpose sample preparation is indicated in Table VI-1.

Table VI-1. Status of Multipurpose Samples

TYPE	STATUS
3M401-C10	50 mounted for spraying
PV100	" " " "
Cat-a-Lac	" " " "
RTV-41	40 mounted for coating
RTV-566	40 prepared
Teflon FEP	have 2 and 5 mil sheet shock
Kapton	have 3 mil sheet stock
Copper	55 polished
6061-T6 Al	18 polished
Silver	50 plated (2-3 mil thick) on polished 6061-T6
Solder	70 mil billet rolled
Gold	30 plated on polished 6061-T6
7940 Quartz	have 20 mil sheet for approximately 5 samples
0211 Glass	have 6 mil sheet for approximately 8 samples
Z-93	60 prepared
S13G	60 prepared
6061-T6 Al	175 unpolished

F. Conclusions

The multipurpose sample holder system is complete and ready for use. Thermal-vacuum tests indicate completely satisfactory performance of the system.

VII. ANALYSIS OF CONTAMINANT SOURCES

Phase I included extensive effort in analyzing electrostatic rocket propellant effluents and their probable effect on various spacecraft surfaces. Two additional contamination sources, accelerator grid sputtering and discharge neutralizers, received attention during Phase II and are discussed in Subsections A and B. The previously developed diagram showing the bulk accumulation regions for mercury and cesium was improved during Phase II and is presented in Subsection C.

A. Sputtered Accelerator Grid Material

The negatively charged electrode in the ion optical system of electrostatic thrusters is customarily (mis-) named the accelerator grid. Usually, this electrode consists of holes in a metal plate and forms the exit plane of the thruster, as shown in Figure VII-1. Propellant (group 3) ions which are formed downstream of the thruster between the accelerator grid and the neutralization plane by charge exchange are attracted by the electrode's large negative potential. The impinging ions appear as accelerator "drain" current in the accelerator power supply, and after a few hundred hours of operation, sputtering patterns are clearly visible on the downstream face of this electrode which is often molybdenum. The magnitude of the resulting flux of molybdenum atoms may be estimated from the drain current and sputtering yield data:

$$\Gamma_o = S\,\Gamma_+ = S\,I_+(qA)^{-1} \qquad (1)$$

where

Γ_o = flux density of Mo atoms leaving the accelerator grid, atoms/cm^2-sec.

S = number of Mo atoms released per incident ions, atoms/ion

I_+ = accelerator drain current, amps

q = 1.6×10^{-19} coul/electron

A = area of accelerator grid, cm^2

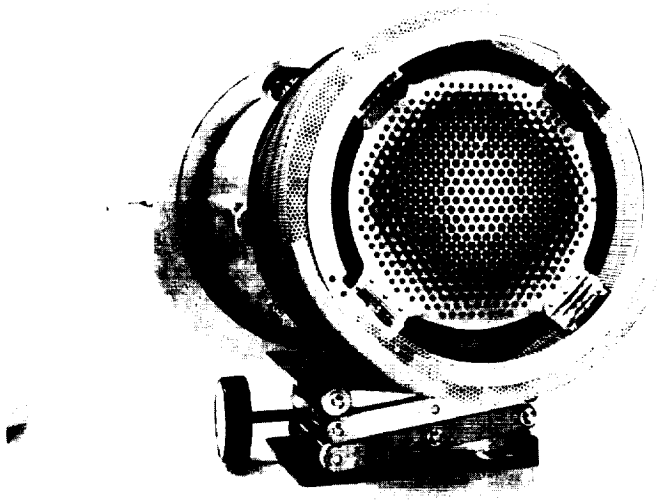

Figure VII-1. Photograph of 15-cm-diameter NASA/Lewis-type electron bombardment thruster. Charge exchange ion sputtering pattern on screen electrode is visible.

Mercury electron bombardment thrusters typically have 1 to 3 x 10^{-5} A/cm^2 drain current density. The sputtering yield of polycrystalline molybdenum by 2 Kev Hg^+ is ~2 (Ref. VII-1). Therefore $\Gamma_o \simeq 2 \times 10^{14}$ Mo/cm^2-sec.

To first order, the spatial distribution of this flux should be cosine. Since the distribution of unionized propellant flux from the thruster is also approximately cosine, the two fluxes may be directly compared. Taking the example above, it is found that flux of molybdenum atoms arriving at any location will be approximately 1/10 the corresponding mercury atom flux. However, mercury (and cesium) have high vapor pressures and so will reevaporate at a significant rate. In contrast, molybdenum or any other conceivable grid material has a very low vapor pressure, so virtually all accelerator grid atoms arriving at a spacecraft surface will be permanently deposited there. This fact means that in many situations sputtered accelerator grid material is more important than unionized propellant.

'Accelerator grid material layer thickness will grow at the rate

$$\frac{dx}{dt} = \frac{\Gamma_{ar}}{n} = \frac{\Gamma_o a^2}{n\, r^2} \cos\theta \qquad (2)$$

where Γ_{ar} = arriving grid material flux density, atoms/cm^2-sec

a = thruster radius, cm

n = atomic density of the grid material, atoms/cm^3

r = radial distance from center of thruster, cm

θ = angle between thrust vector and radius vector, degree

In the case of a 15 cm-diam mercury thruster with a molybdenum accelerator grid, for instance, a layer thickness growth rate of 1 Å/hr would occur at a target surface one meter from the thruster and normal to its 80° radius vector. In order for a mercury layer to grow more rapidly than this, the target surface temperature would have to be less than ~-75°C. At greater distances from the thruster, corresponding temperatures for equivalent Mo and Hg growth rates are even lower. If the target were a solar array, a surface temperature of -75°C would typically occur at 3 AU. Thus, at solar distances less than 3 AU, the deposition rate of Mo on illuminated (i.e. "warm") spacecraft surfaces is expected to exceed the net condensation rate of mercury. Note, too, that the layer growth rate employed in this example is significant: at 1 Å/hr it would only take a few hundred hours to produce an opaque molybdenum layer.

These analytical predictions have been at least qualitatively confirmed in ground based experiments[2] and by the surface contamination experiment on SERT II[3] which was launched February 1970.

A final consideration is whether this flux of molybdenum atoms is significant in the experiments completed and contemplated in this program, since these experiments employ an electrostatic thruster as a beam source. Of course, when atomic beam experiments are conducted the molybdenum flux is zero. In the case of ion beam experiments, evaluation of molybdenum flux significance requires calculation of the molybdenum arrival rate at the sample location and comparing it to the Hg^+ arrival rate. The thruster-sample distance is 71 cm, so the flux of molybdenum arriving at the surface is 2×10^{12} atoms/cm^2-sec. The Hg^+ arrival flux is typically 1×10^{15}, 500 times greater; therefore the molybdenum flux is negligible in the experimental situation. The reason that the ratio is so high is that in the experiments the samples are located on the beam axis.

B. Discharge Neutralizers

Discharge (plasma bridge) neutralizers using both mercury and cesium have been developed, and one or both of these types seem certain to see application in space. These neutralizers emit both atoms and ions (as well as electrons) and therefore constitute a potential source of contaminant particles. Typically they are located about 1 inch downstream of the thruster exit plane and just outside the primary ion beam with their axis approximately perpendicular to the ion beam axis. The atomic component is considered below, and it is shown that this efflux in a cone about the neutralizer axis may be of significant magnitude.

1. Neutral Efflux. The angular distribution of emitted atoms from the cylindrical neutralizer exit orifice must be of the type described by Clausing.[4] Csiky[5] argues that this distribution probably approaches that of a cosine, considering typical orific dimensions and flow conditions. That assumption is made in the following analysis.

A cosine distribution from a "point" source may be expressed as

$$\Gamma(r,\theta) = \Gamma_o \frac{a^2}{a^2+r^2} \cos\theta \tag{3}$$

where

$\Gamma(r,\theta)$ = the flux density of atoms at a point (r,θ), atoms/cm^2-sec

a = the source radius, cm

θ = the angle formed with the source axis

and Γ_o = the flux density at the source exit plane, atoms/cm^2-sec

Since it is common to express propellant mass use rates ($\dot{m}$) in grams/hour, Γ_o is calculated

$$\Gamma_o = \frac{\dot{m}}{\pi a^2} \cdot \frac{\text{AMU}}{1.67\text{x}10^{-24}\text{gm}} \cdot \frac{\text{particles}}{\text{AMU}} \cdot \frac{\text{hr}}{3.6\text{x}10^3\text{sec}} \tag{4}$$

Combining Eqs. (3) and (4) we obtain the desired expression

$$\Gamma(r,\theta) = 5.3 \times 10^{19} \frac{\dot{m}}{M(r^2+a^2)} \cos\theta \tag{5}$$

where

M = the atomic weight of the neutralizer propellant in AMU

$\dot{m}$ = the atomic component of mass flow through the neutralizer in grams/hour

A typical total mass flow rate for discharge neutralizers is 0.3 gm/hr. Part of this flow is emitted as ions, which may give rise to a modified angular distribution. However an estimate of particle current density arriving at a surface may be made by assigning the total neutralizer mass flow to $\dot{m}$ in Eq. (5). Then on axis ($\theta = 0$) Eq. 5 evaluates

Distance	Γ_{Cs}	Γ_{Hg}
20 cm	3×10^{14}	2×10^{14}
5 feet	5×10^{12}	3.3×10^{12}

The first distance quoted is the diameter of a JPL E-B engine. The second is the minimum distance between thruster and solar panel on the JPL Jupiter Flyby Mission study. Figure 7-4 and 7-6 of Reference 6 demonstrates that arrival rates of these (5-foot) magnitudes on the front surface of a solar array may lead to condensation beyond 2.5 AU and 1.6 AU for mercury and cesium, respectively. From another viewpoint, the Γ_{Hg} 5-foot value is equivalent to what one would expect at approximately 70° and 5-foot distant from the JPL 20 cm E-B thruster.

2. Charge Exchange in the Thrust Beam. In general, the atomic beam described above must pass through the thrust beam before spacecraft surfaces other than the thruster are encountered. If a substantial fraction of the atomic beam underwent charge exchange collisions, the cosine distribution assumed above would be seriously altered. Therefore calculations were made of the production rates of charge exchange ions from this source. These rates are negligible, even in the case of a Cs neutralizer used with a Cs thrust beam, which is the combination which has the highest charge exchange cross section.

3. Plasma Bridge Ions. Three questions arise with regard to the ion efflux from the discharge neutralizer: What is the ion energy, density, and angular distribution? At this time only the first question can be answered with confidence. A properly operating discharge neutralizer has a plasma bridge potential of approximately 10 volts and the ions in this plasma have approximately 1/2 eV of kinetic energy.[5, 7]

Since the energy threshold of sputtering yield is usually considered to be approximately 25 eV, these ions are only capable of causing erosion when attracted by negatively charged surfaces. (As a matter of fact, nearby accelerator plates, which are so charged, are often observed to erode preferentially in the neutralizer local. When the accelerator grid fields reach the plasma bridge, it is safe to assume that all escaping ions terminate on the grid.)

Probably the greatest threat from plasma bridge ions is that this plasma might extend to a solar array where charged conductors could draw significant ion or electron currents from it. This possibility should receive analysis.

C. Bulk Accumulation Regions of Hg and Cs

Fig. 3-1 of the Phase I Final Report[6] was modified to include a broader temperature range and lower arrival rates. Furthermore, more recent vapor pressure data was employed.[8] Figure VII-2 is the improved diagram.

D. Conclusions

1. Sputtered Accelerator Grid Material. Analysis of the sputtering of molybdenum from the accelerator electrode of mercury electron bombardment thrusters indicates that this is an important thruster effluent. At solar distances less than 3 AU, the deposition rate of Mo on spacecraft surfaces will usually exceed the net condensation rate of mercury because of surface temperature: The arrival rate of Mo will be $\sim 10^{-1}$ that of Hg^{o} but the reevaporation rate of Hg^{o} is $\sim 10^{17}$ greater than Mo. The same general conclusion will hold for any electrostatic rocket employing mercury or cesium propellant.

In contrast, in the atom and ion beam experiments completed and contemplated under this program the flux of molybdenum atoms arriving at the sample location is insignificant.

2. Discharge Neutralizers. Analysis of discharge neutralizers indicates that in a cone about its axis particle fluxes may be comparable to those from the thruster at high angles. The most potentially deleterious effect of plasma bridge ions is believed to be electrical, but this possibility deserves further analysis. These matters deserve consideration when choosing the orientation of a discharge neutralizer during spacecraft design.

3. Bulk Accumulation Regions of Hg and Cs. A more useful and up-to-date diagram has been prepared.

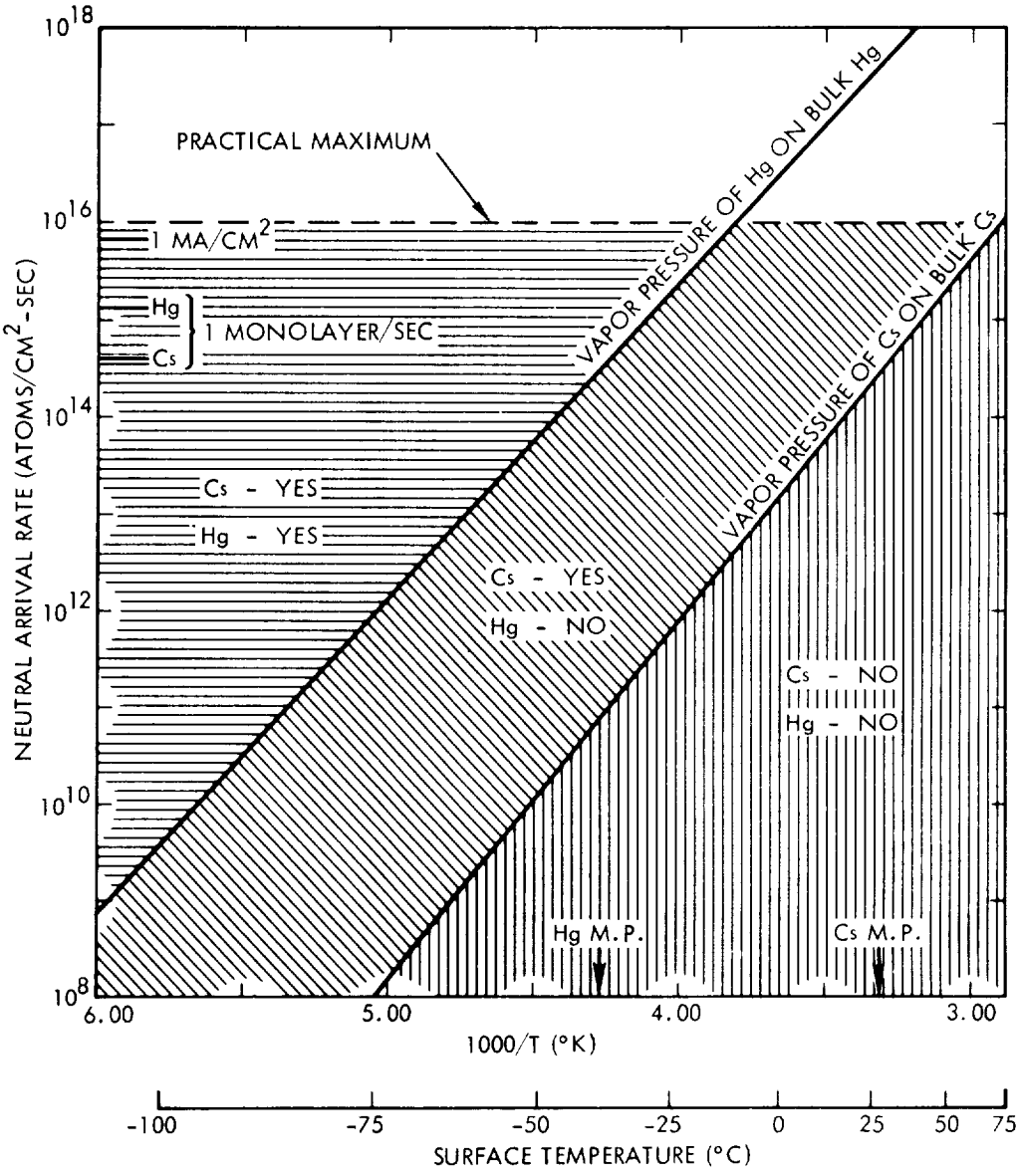

Figure VII-2. Bulk accumulation regions for mercury and cesium atoms on surfaces where adsorbed monolayers already exist.

E. Recommendations for Future Work

1. Sputtered Accelerator Grid Material. This problem clearly deserves additional attention. First the optical properties (α_s, ϵ_H) of opaque sputter-deposited molybdenum and other potential accelerator grid materials, e.g. stainless steel, should be obtained; second, knowledge of α_s, ϵ_H, transmittance, and electrical resistivity as a function of film thickness should be sought; finally the impact of this data on positioning spacecraft surfaces and appendages within the exhaust hemisphere of electrostatic rockets should be assessed.

2. Discharge Neutralizers. The foregoing discussion on discharge neutralizers raised questions as to the spatial extent and current carrying capacity of the bridge plasma. These subjects should be analyzed.

VIII. CONCLUSIONS

Each of the preceding sections of technical discussion contain specific conclusions drawn from results obtained. This section contains some (tentative) general conclusions to up-date and supplement those of the Phase I report.

A. Mercury Atoms

Apparently, organic spacecraft materials (silicones, polyesters, epoxies, polyimides, polyacetals, Teflon) do not react chemically with even an abundant supply of mercury. Some evidence is now available that mercury also has no effect on the optical properties (α_s, ε_H) of typical thermal control coatings; a definitive experiment is recommended. A reaction does occur between mercury and silver, but it is slow and the reaction products appear acceptable. Mercury reacts rapidly with soft solders (which are often used in solar array construction) and seriously affects their mechanical properties; atom beam experiments are recommended.

B. Cesium Atoms

Serious chemical reaction occurred between abundant cesium and Teflon FEP and Kapton H-Film (a polyimide). Reaction with Kapton is particularly worrisome because of its potential use as the foundation of lightweight, roll-up solar arrays suitable for powering electric rockets; further study of this reaction is recommended. Abundant cesium rapidly and severely attacks soft solder.

C. Ions

Typical thermal control coatings were exposed to large doses of mercury ions with the maximum kinetic energy likely to be encountered (3 KeV). Lower energy, high-divergence-angle ions are likely to have a similar effect, though perhaps at a lower rate. Cesium ions will surely affect the coatings affected by mercury ions and perhaps others. The results were that sample emittance was unaffected in every case, as was the absorptance of high absorp-

tance (black) samples, whereas the absorptance of white paints and RTVs were markedly increased. Thus ion impingement on unilluminated spacecraft surfaces (where the value of α is unimportant) is unlikely to cause thermal problems unless a thin coating is completely sputtered away. Black paints, illuminated or not, are also expected to be insensitive to ion bombardment. Further study of white paints and RTVs is definitely indicated.

Two glass samples were also exposed (quartz and 0211 microsheet) with no measurable effect on their optical properties. Therefore ion damage (Hg or Cs) to solar cell cover glass will probably proceed very slowly. (However, their optical coatings, if any, may be degraded by ion bombardment.)

D. Ion/Atom Mixtures

To date, experiments to determine the protection effect of mercury atoms impinging on a surface simultaneously with mercury ions suggest that the effect will not occur in many instances. However, this conclusion does not necessarily apply to cesium, since cesium adsorbs on most surfaces much more readily than does mercury.

E. Analysis of Contaminant Sources

Sputtered accelerator grid material is an important thruster effluent; for some surfaces and missions it will be more spacecraft design constraining than either propellant ions or atoms. Additional work is needed.

Discharge neutralizers emit a significant particle flux in a cone about their axis which should be considered in choosing their orientation during spacecraft design. Questions have been raised about the physical extent of the plasma bridge.

IX. RECOMMENDATIONS FOR FUTURE WORK

Each of the technical sections contain specific recommendations for future work. This section contains some general recommendations.

A. Chemistry

The major outstanding question in the chemistry area is whether energetic ions will affect the physical properties of typical organic spacecraft materials. Exposure of samples to mercury ions on the multipurpose sample holder followed by ex situ tests and analysis should answer this question.

A modest additional effort in studying the reaction of Kapton with abundant cesium may produce important information.

B. Metallurgy

The tolerance of soft solder to realistic quantities of cesium and mercury needs to be determined. This can be accomplished by exposing samples on the multipurpose sample holder to propellant beams.

C. Thermophysics

Mercury atom beam exposures of typical thermal control coatings should be made under conditions permitting bulk mercury condensation. If coating properties are unaffected then no further mercury atom experiments will be needed.

Mercury ion exposures of thermal control coatings should emphasize RTVs, white paints and non-glass materials typical of illuminated solar array surfaces. These experiments should include lower arrival rates and/or ion dose than employed to date.

The first cesium beam experiments should be atom beam exposures of typical thermal control coatings.

The optical properties of thin molybdenum films should be determined.

D. Ion Sputtering

Gross erosion rate measurements should be made on typical non-metallic targets with mercury ions. Protection effect experiments under conditions which permit bulk condensation, now in progress, should be completed. The next logical experiments would be with mercury ions bombarding a gold or silver target.

E. Analysis

Additional analysis should be made of the effects of sputtered accelerator grid material on spacecraft surfaces.

X. NEW TECHNOLOGY

To date no New Technology has been identified under this contract.

REFERENCES

I. Introduction

1. Hall, D. F., "Evaluation of Electric Propulsion Beam Divergence Effects on Spacecraft," 08965-6013-RO-00, Final Report, Contract No. NAS7-575, Sept. 1969, TRW Systems, Redondo Beach, Calif.

2. Hall, D. F., Newnam, B. E., and Womack, J. R., "Electrostatic Rocket Exhaust Effects on Solar-Electric Spacecraft Subsystems," AIAA Paper No. 69-271, Williamsburg, Va., 1969.

3. Hall, D. F., Newnam, B.E., and Womack, J. R., "Electrostatic Rocket Exhaust Effects on Solar-Electric Spacecraft Subsystems," Journal of Spacecraft and Rockets, Vol. 7, No. 3, March 1970, pp. 305-312.

4. Hall, D. F., and Kelley, L. R., "Experimental Techniques to Determine Electrostatic Rocket Exhaust Effects on Spacecraft Surfaces," AIAA 8th Electric Propulsion Conference to be held at Stanford University, September 1970.

II. Chemistry

1. Hanson, K. L., et al., "Feasibility Study 30 watts per Pound Roll-up Solar Array," 68SD4301, Final Report, JPL Contract No. 951970, June 1968, General Electric, Philadelphia, Pa.

2. Hall, D. F., "Evaluation of Electric Propulsion Beam Divergence Effects on Spacecraft," 08965-6013-RO-00, Final Report, Contract No. NAS7-575, Sept. 1969, TRW Systems, Redondo Beach, Calif.

III. Metallurgy

None.

IV. Surface Thermal Degradation Measurements

1. Hall, D. F., "Evaluation of Electric Propulsion Beam Divergence Effects on Spacecraft," 08965-6013-RO-00, Final Report, Contract No. NAS7-575, Sept. 1969, TRW Systems, Redondo Beach, Calif.

2. Crum, F., "Modification of a Beckman Spectrophotometer for Direct Measurement of Spectral Energy Distribution of Light Sources," Applied Optics Vol. 2, 1963, pp. 237-242.

3. Miller, W. D., and Luedke, E. E., "In Situ Solar Absorptance Measurements, An Absolute Method," Effects of the Space Environment on Materials; Vol. II, Society of Aerospace Material and Processing Engineers, 11th National Symposium and Exhibit, St. Louis, April 1967, pp. 75-84.

IV. Surface Thermal Degradation Measurements (cont'd)

4. Dunkle, R. V., et al., "Heat Cavity Reflectometer for Angular Reflectance Measurements," Progress in International Research on Thermodynamics and Transport Properties; American Society of Mechanical Engineers, 1962, pp. 541-67.

5. Johnson, F. S., "The Solar Constant," J. Metrology, Vol. 11, 1954, pp. 431-439.

6. Nelson, K. E., Luedke, E. E., and Bevans, J. T., "A Device for the Rapid Measurements of Total Emittance," Journal of Spacecraft and Rockets, Vol. 3, 1966, pp. 758-760.

V. Sputtering Experiments

1. Hall, D. F., "Evaluation of Electric Propulsion Beam Divergence Effects on Spacecraft," 08965-6013-RO-00, Final Report, Contract No. NAS7-575, Sept. 1969, TRW Systems, Redondo Beach, Calif.

VI. Multipurpose Sample Holder

1. Hall, D. F.,"Evaluation of Electric Propulsion Beam Divergence Effects on Spacecraft," 08965-6013-RO-00, Final Report, Contract No. NAS7-575, Sept. 1969, TRW Systems, Redondo Beach, Calif.

VII. Analysis of Contaminant Sources

1. Carter, G., and Colligon, J. S., Ion Bombardment of Solids, American Elseview Publishing, Inc., 1968, pp. 310-353.

2. Richley, E. A., and Reynolds, T. W., "Condensation on Spacecraft Surfaces Downstream of a Kaufman Thruster," NASA Technical Memorandum No. X-52746, January 1970.

3. Kerslake, W. R., et al., "SERT II: Mission and Experiments," Journal of Spacecraft and Rockets, Vol. 7, No. 1, Jan. 1970, pp. 4-6.

4. Loeb, L. B., The Kinetic Theory of Gases, McGraw Hill, 1934, p. 308.

5. Csiky, G. A., "Investigation of a Hollow Cathode Discharge Plasma," AIAA Paper No. 69-258, Mar. 1969.

6. Hall, D. F., "Evaluation of Electric Propulsion Beam Divergence Effects on Spacecraft," 08965-6013-RO-00, Final Report, Contract No. NAS7-575, Sept. 1969, TRW Systems, Redondo Beach, Calif.

7. Hall, D. F., Kemp, R. F., and Shelton, H., "Mercury Discharge Devices and Technology," AIAA Paper No. 67-669, Sept. 1967.

8. Honig, R. E., "Vapor Pressure Data for the Solid and Liquid Elements," Radio Corporation of America Review, Vol. 23, No. 4, Dec. 1962, pp. 567-586

APPENDIX A

MERCURY ATOM BEAM CALIBRATIONS

In order to obtain atom beam intensity data (and neutral fraction data in ion beams) it is necessary to either measure directly atom arrival rate or to know the total mass flow rate through the beam source (thruster). Direct measurement of atom flux is relatively difficult in the case of mercury, so the latter approach was recommended in the Phase I Final Report .

Three steps were required to implement this approach:

1) Make the propellant boiler isothermal and increase its radiation capacity.

2) Provide accurate boiler temperature control.

3) Conduct gravimetric calibrations

The boiler must be isothermal so that the propellant evaporation rate is not a function of propellant level. This was accomplished by brazing heavy copper shorting bars contiguously along the length of a cylindrical stainless steel container. Then the end plates of copper were brazed on. Finally, the Cal-rod heater was brazed in a helix around the copper bars.

The resulting boiler had a high heat capacity, even when empty. To provide reasonable operating conditions for the temperature controller, to permit reasonable boiler cool-down periods, and to dissipate heat conducted down the feed tube between the boiler and the engine manifold, a large radiator was affixed to the top of the boiler.

The difficulty in providing boiler temperature control is the need for high temperature resolution and the fact that during thruster operation the boiler is at high potential (typically 3 KV). These problems were solved by floating an API Model 732 digital set point time proportioning temperature controller at high voltage. This controller responds to thermocouple potential deviations from its set point as small as 1/5°C. Temperature control to $\pm$1/5°C provides boiler flux control of approximately $\pm$1% in the temperature range of interest.

Seven gravimetric boiler calibration runs were made with mercury to establish the relationship between boiler temperature controller set-point and mass flow.

These data are shown in Figure A-1. The vertical confidence bars represent weighing and "end effect" (finite run start and stop periods) errors, while the horizontal bars represent the controller dead band ($\pm$ 10 μV $\pm$ 0.2°C).

The reason for the "bad" data point at set-point 6.36 is not known. This was the first run made, and inadequate run length is responsible for the large error bars ($\pm$ 18%). One hypothesis is that the surface of the mercury in the boiler was oxidized and therefore its vapor pressure lowered. In view of the close adherence of the other data points to a linear relationship and the order in which they were obtained it appears safe to ignore the "bad" point at 6.36.

Subsequent thruster operation verified that the gravimetric calibration was reasonable and demonstrated the entire system was operating correctly. Acceptable "design point" thruster operation was achieved at set points between 7.50 and 7.55 which from Figure A-1 corresponds to 300 to 318 equivalent ma and 78.6% to 81% propellant utilization. This utilization is in the expected neighborhood for 15 cm Lewis E-B thrusters of its vintage.

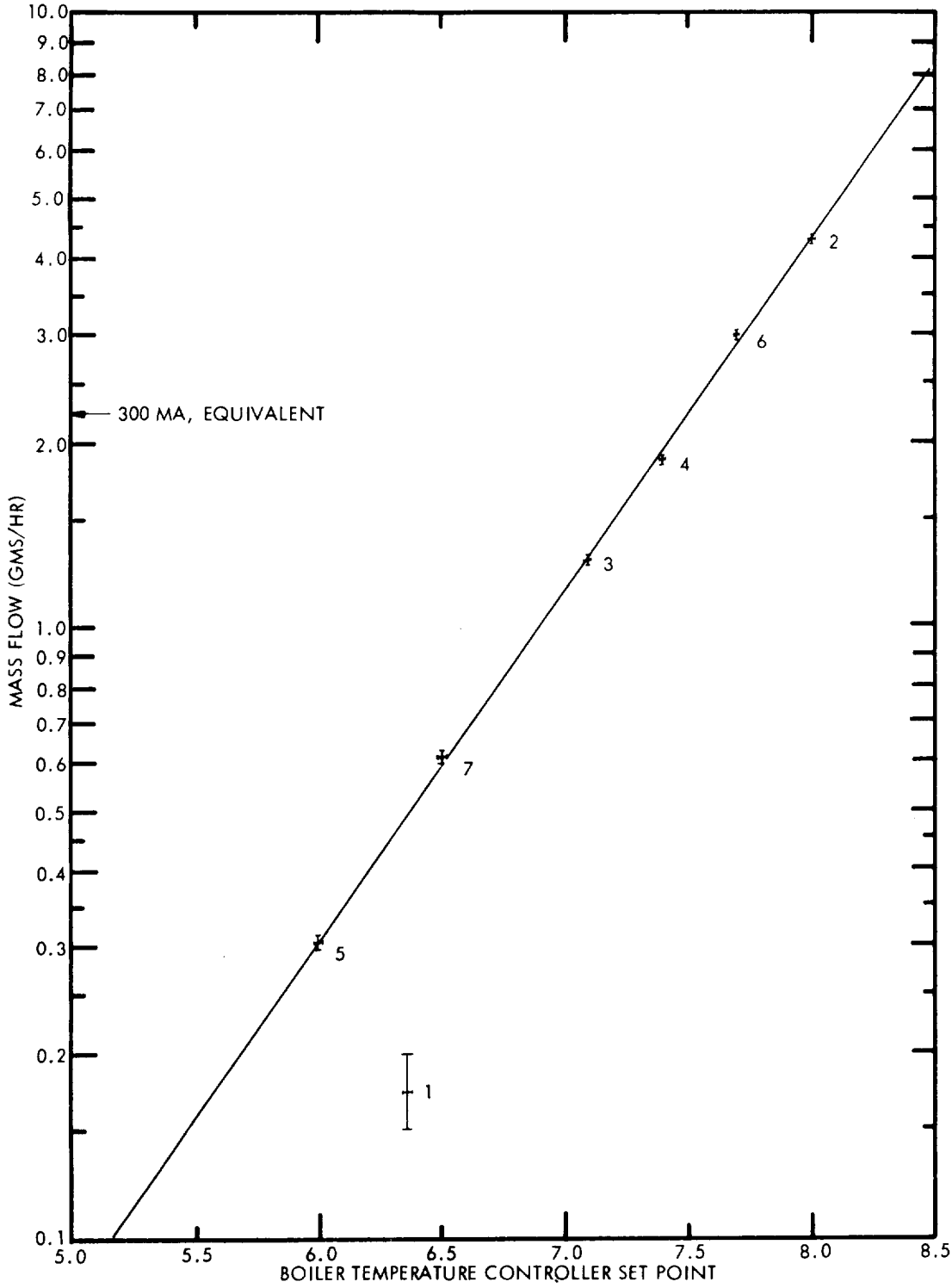

Figure A-1. Mercury mass flow from engine boiler vs temperature controller set point. Numerals indicate the order in which data points were obtained.

APPENDIX B

SPECTRAL REFLECTANCE DATA

The following data are described in Section IV.A.5.

TRW DESIGNATION: 454-69

MATERIAL: GOLD ON 6061-T6 ALUMINUM

SAMPLE #1

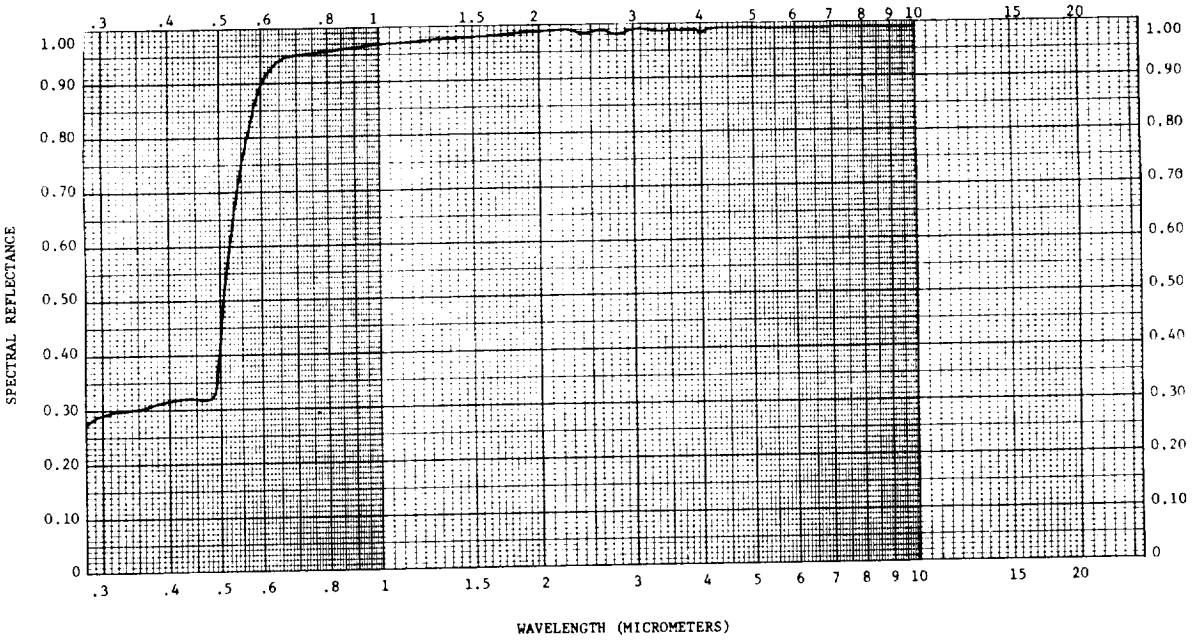

TRW DESIGNATION: 455-69

MATERIAL: GOLD ON 6061-T6 ALUMINUM

SAMPLE #2

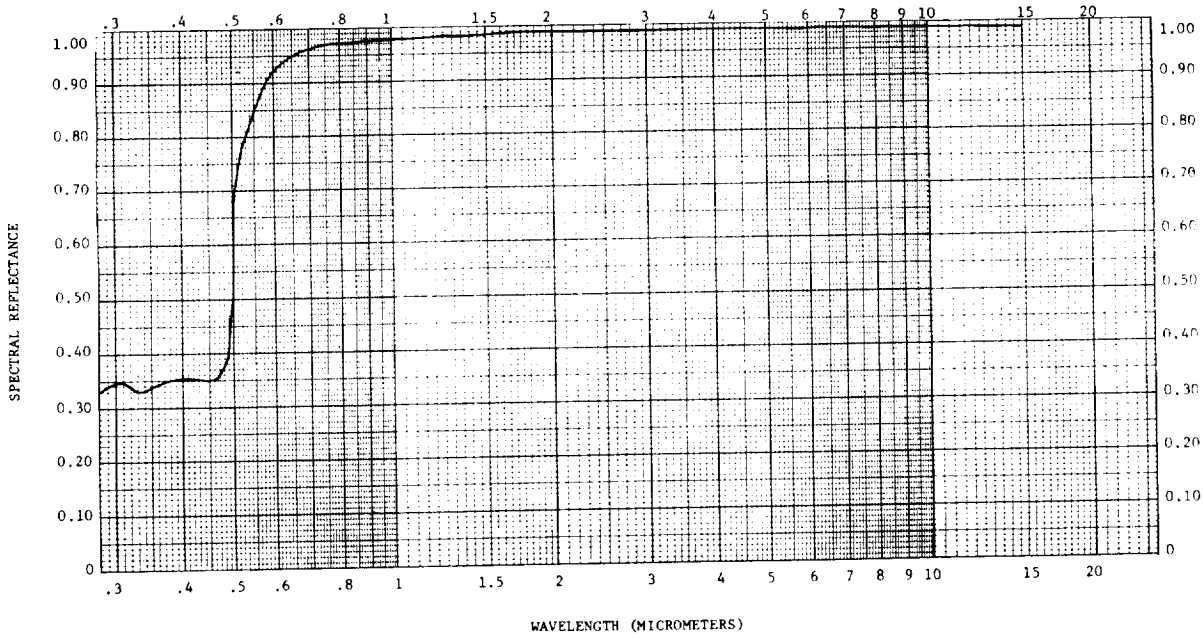

TRW DESIGNATION: 456-69

MATERIAL: S13G WHITE PAINT

SAMPLE #1

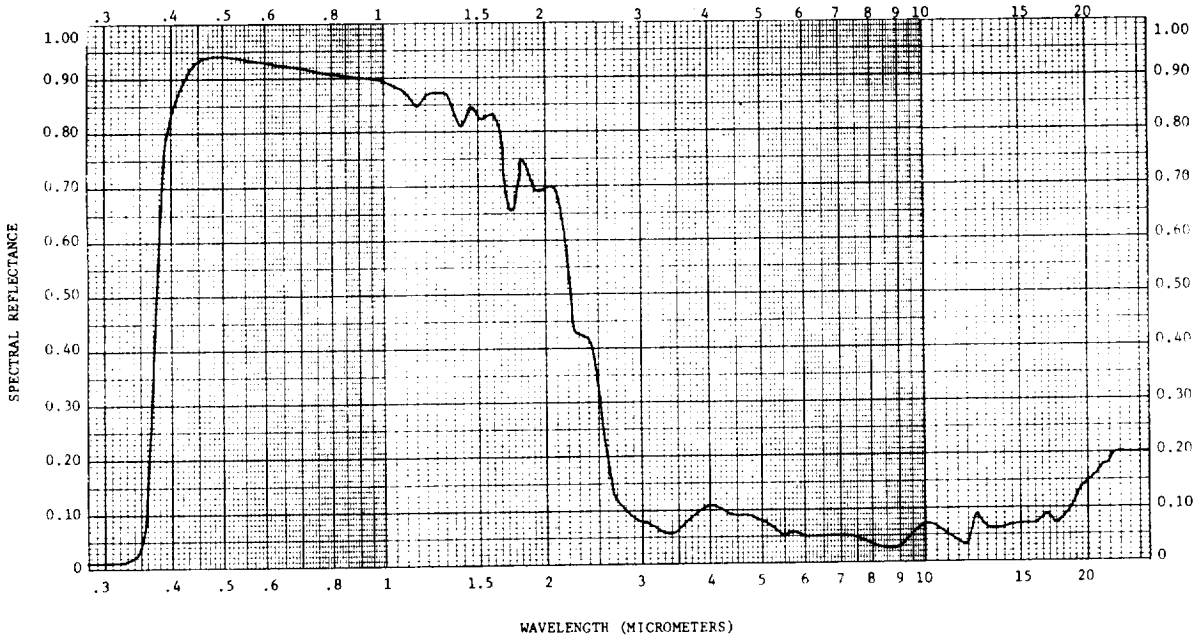

TRW DESIGNATION: 457-69

MATERIAL: S13G WHITE PAINT

SAMPLE #2

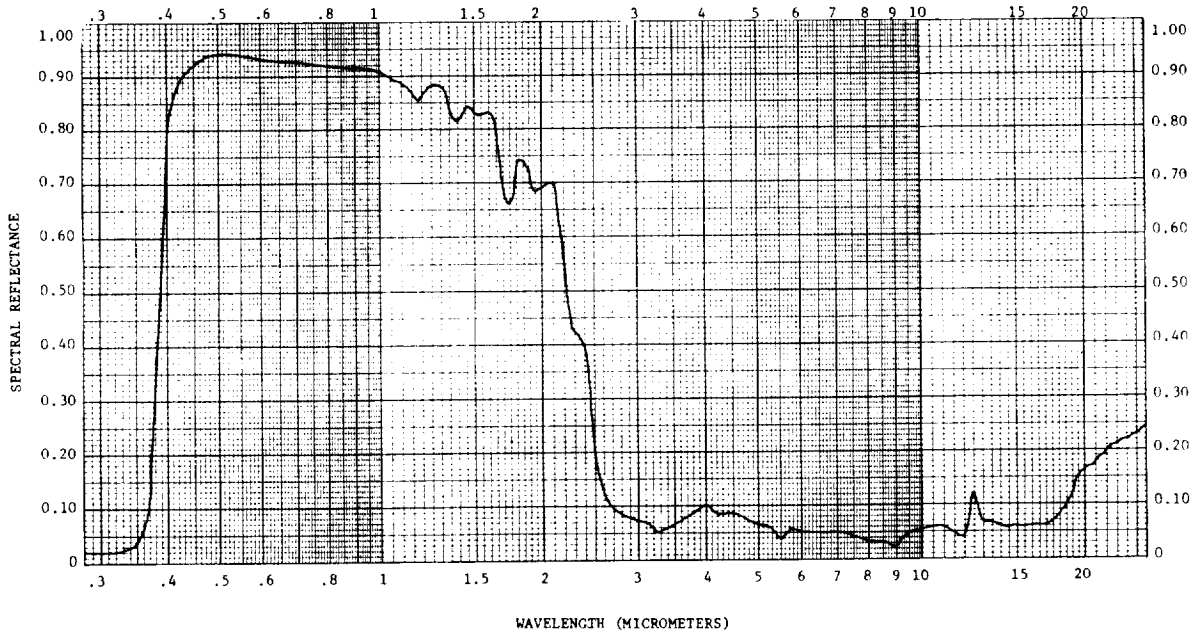

TRW DESIGNATION: 458-69
MATERIAL: PV100 WHITE PAINT
SAMPLE #1

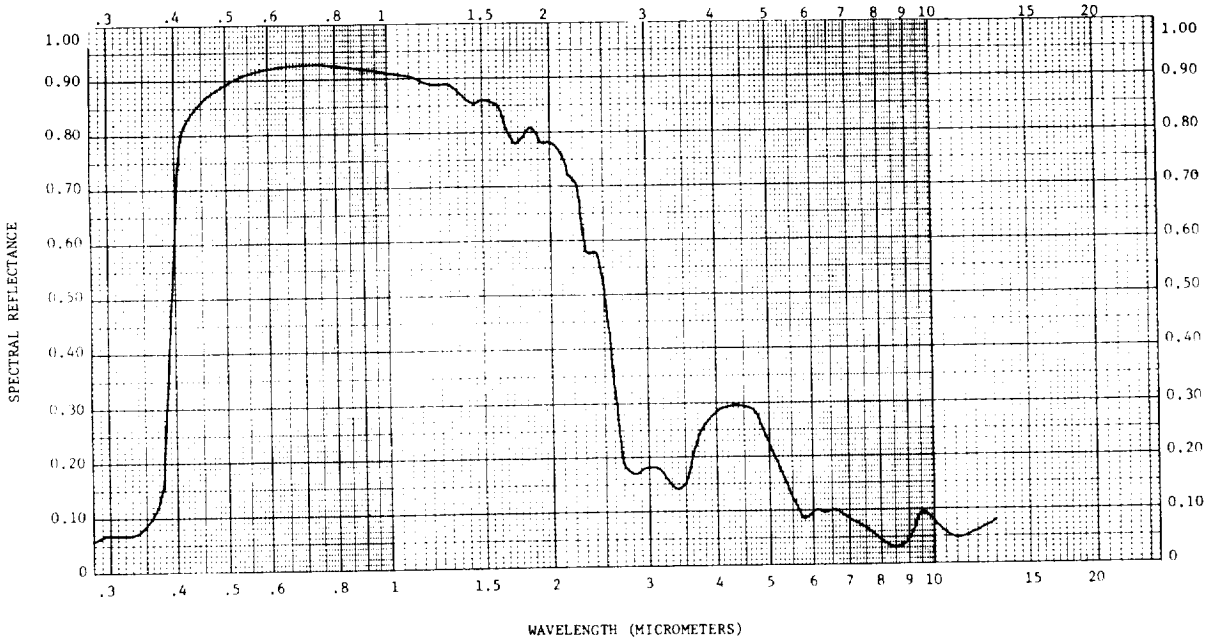

TRW DESIGNATION: 459-69
MATERIAL: PV100 WHITE PAINT
SAMPLE #2

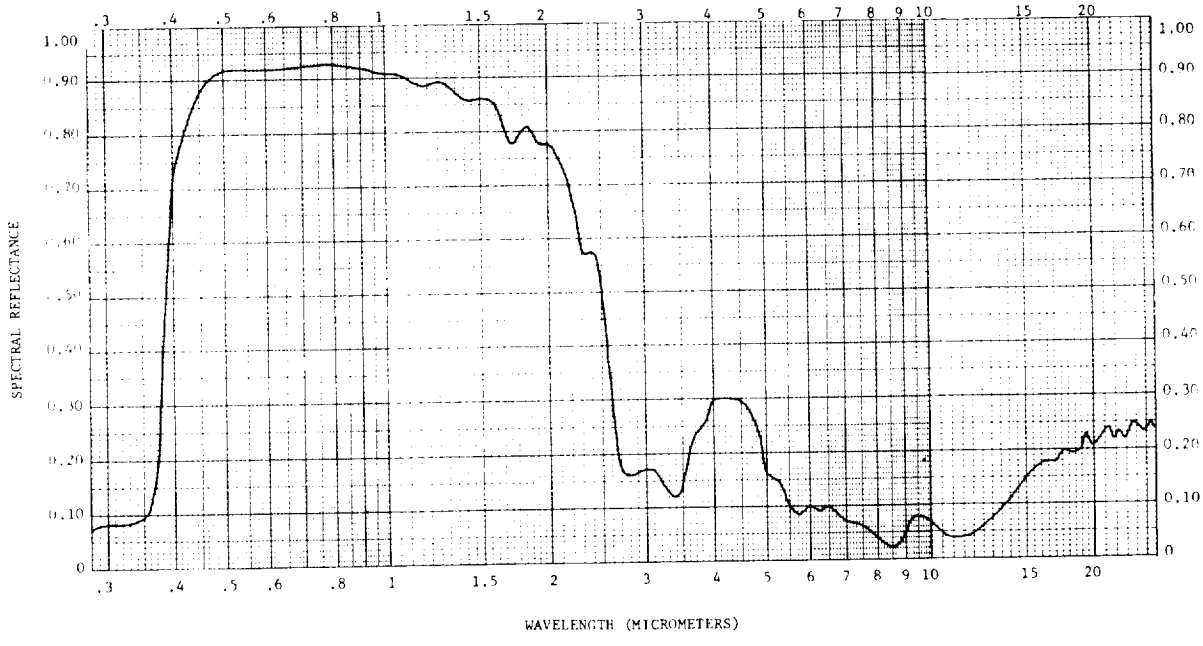

TRW DESIGNATION: 460-69
MATERIAL: Z-93 WHITE PAINT
SAMPLE #1

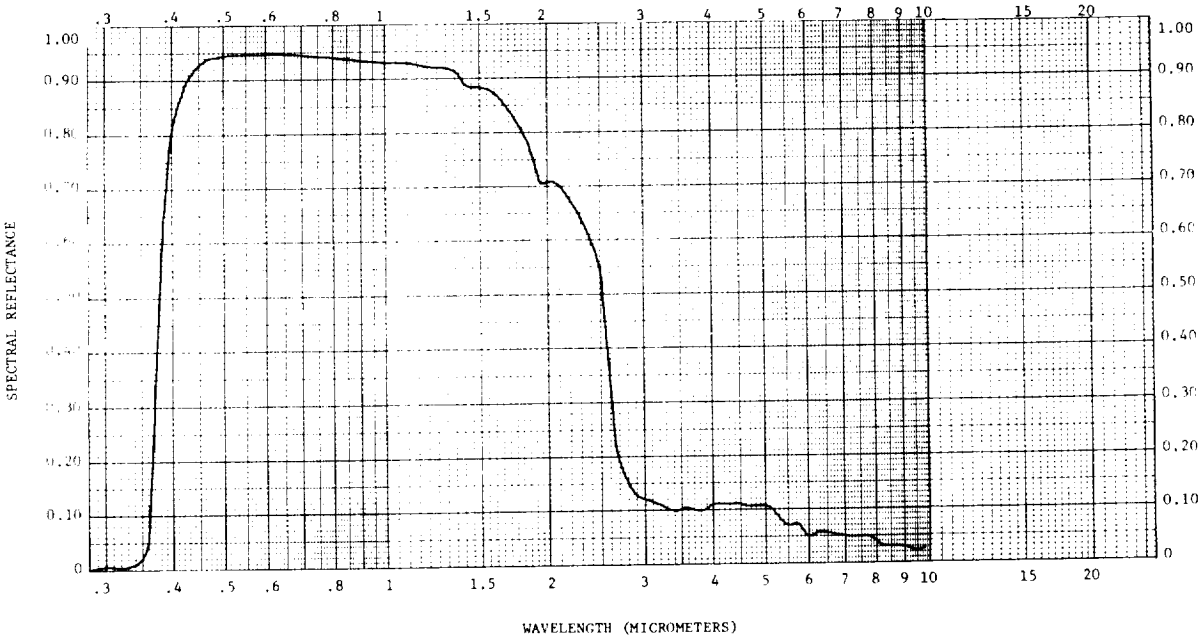

TRW DESIGNATION: 461-69
MATERIAL: Z-93 WHITE PAINT
SAMPLE #2

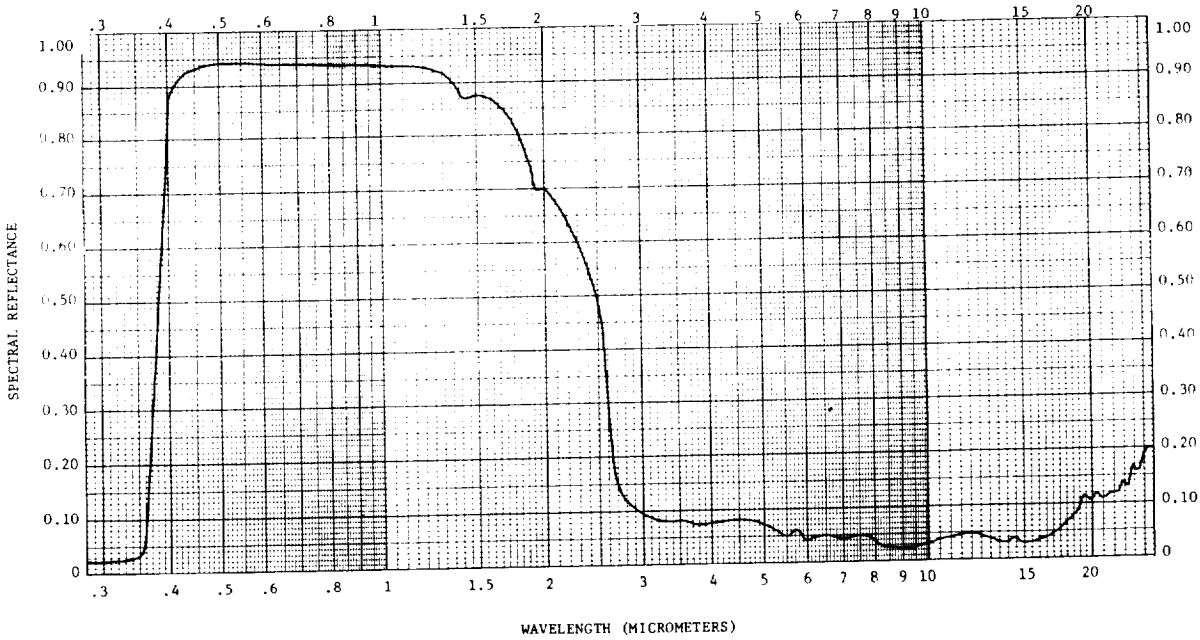

TRW DESIGNATION: 462-69

MATERIAL: BUFFED 6061-T6 ALUMINUM

SAMPLE #1

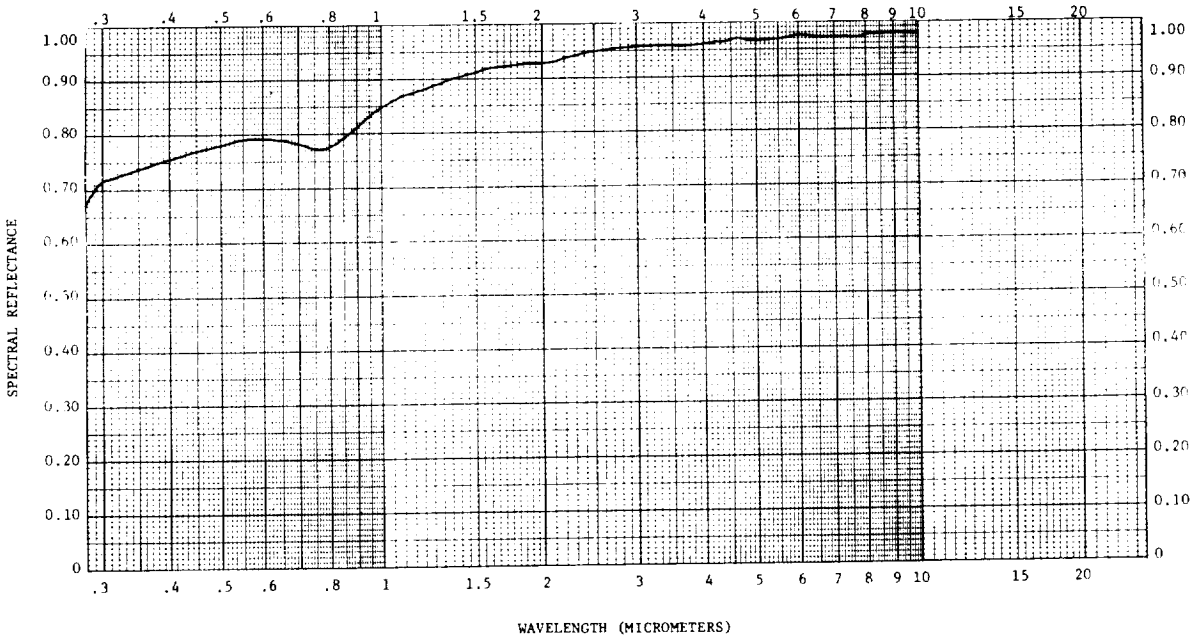

TRW DESIGNATION: 463-69

MATERIAL: BUFFED 6061-T6 ALUMINUM

SAMPLE #2

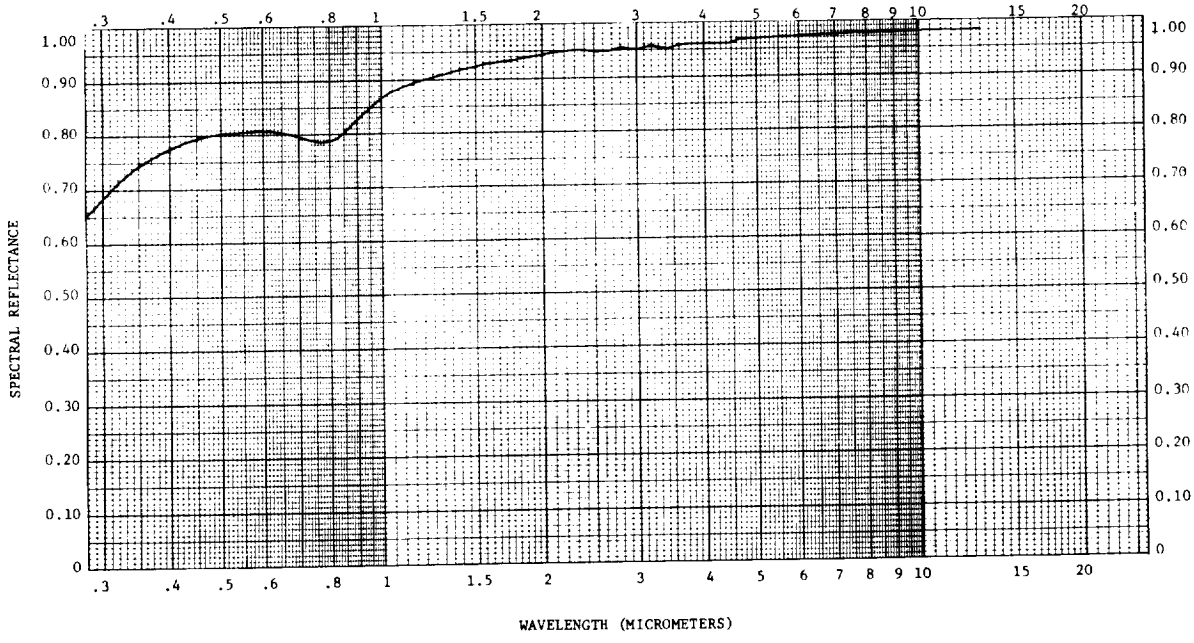

TRW DESIGNATION: 464-69
MATERIAL: 3M BLACK VELVET PAINT (401-C-10)
SAMPLE #1

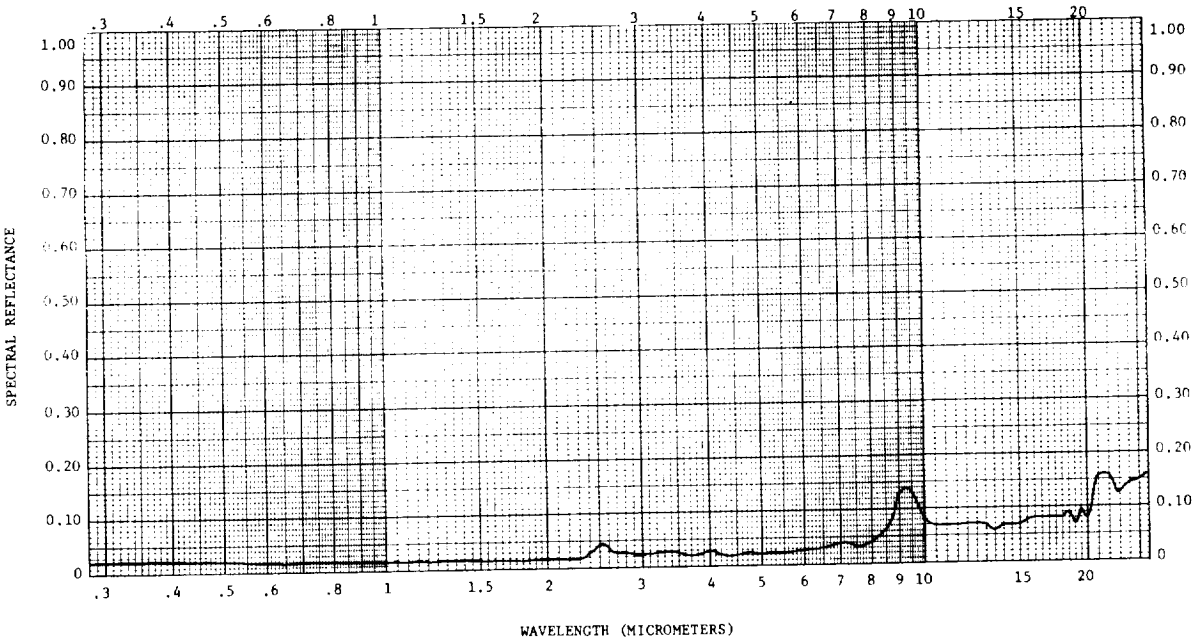

TRW DESIGNATION: 465-69
MATERIAL: 3M BLACK VELVET PAINT (401-C-10)
SAMPLE #2

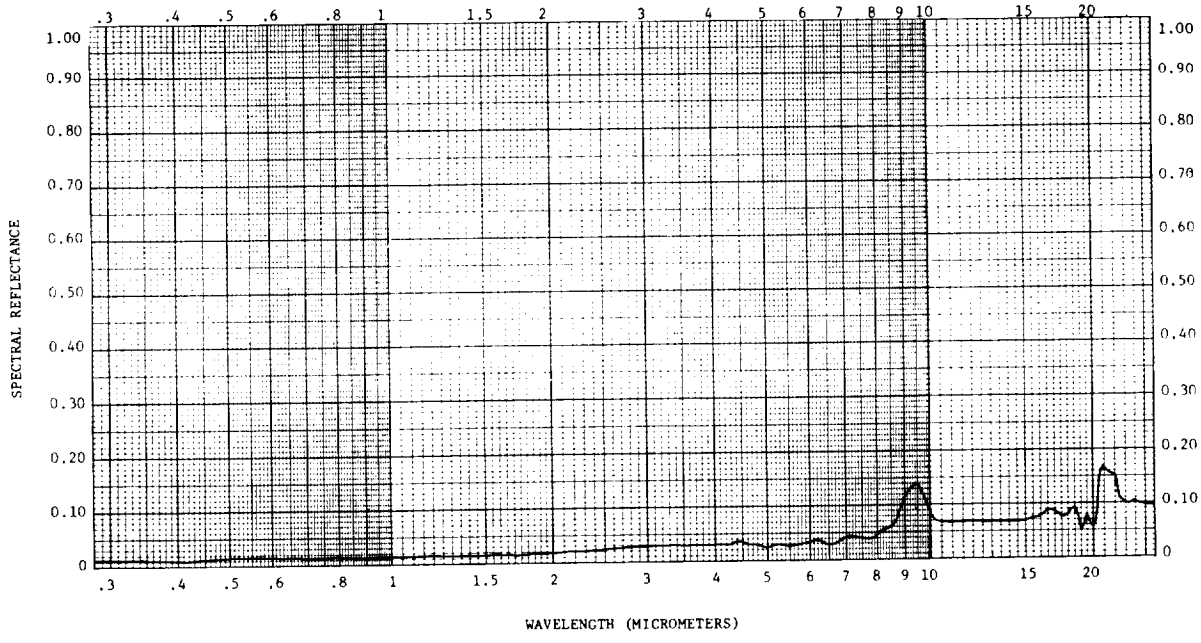

TRW DESIGNATION: 554-69

MATERIAL: SECOND SURFACE
ALUMINUM VACUUM DEPOSITED ON CORNING 0211 6-MIL-THICK MICROSHEET
SAMPLE #1

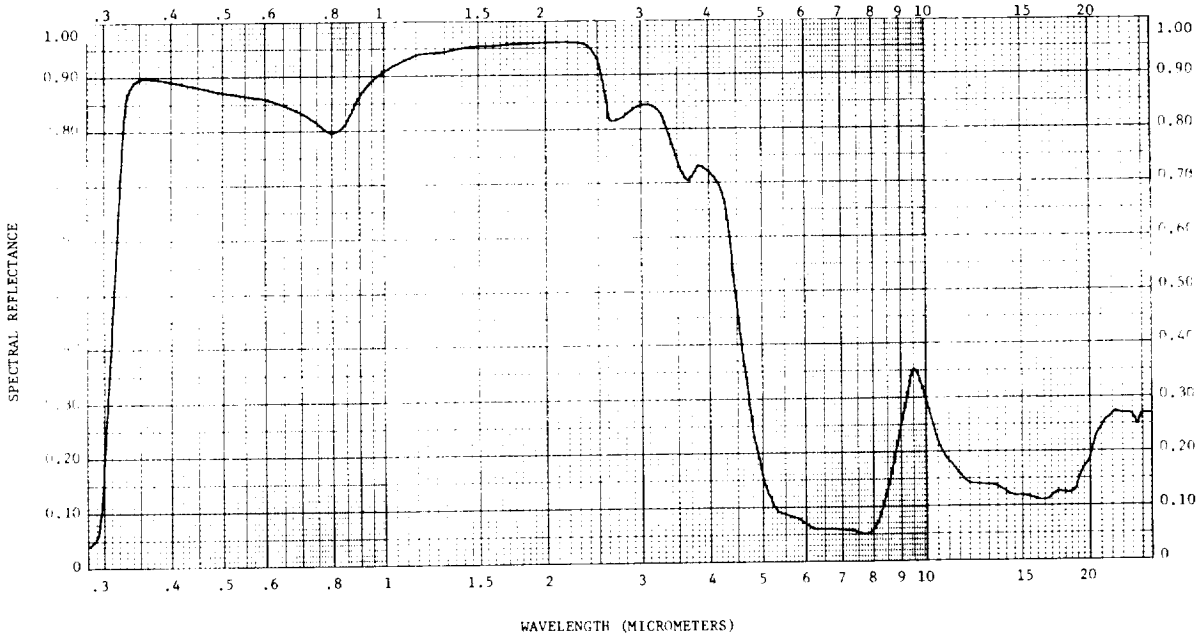

TRW DESIGNATION: 555-69

MATERIAL: SECOND SURFACE ALUMINUM
VACUUM DEPOSITED ON CORNING 0211 6-MIL-THICK MICROSHEET
SAMPLE #2

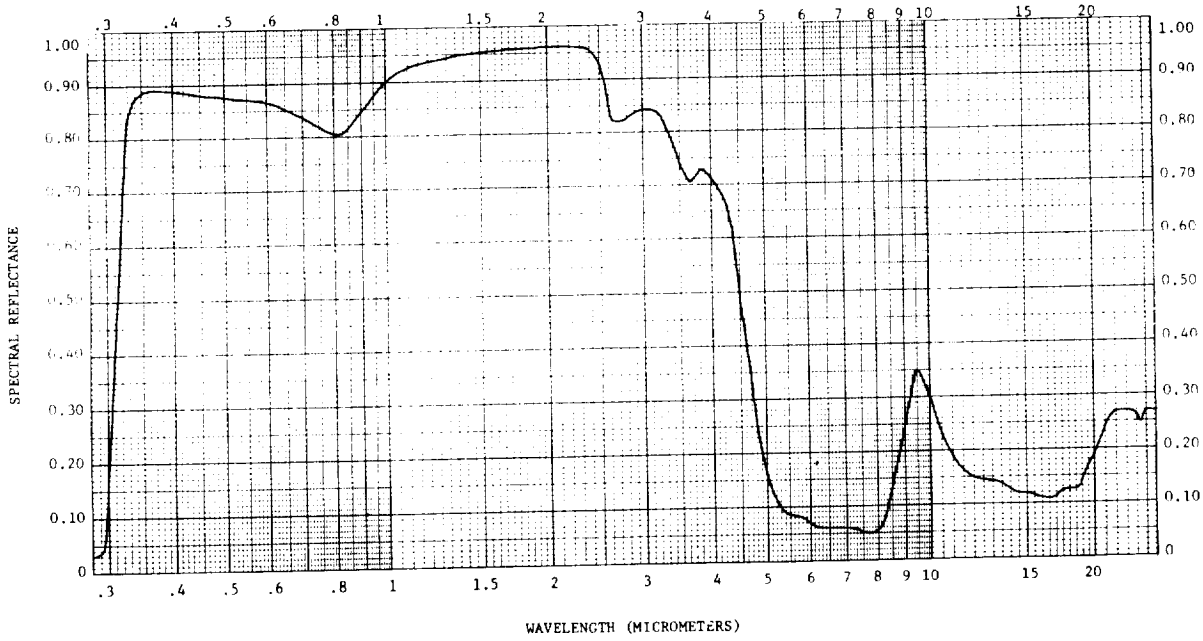

TRW DESIGNATION: 556-69

MATERIAL: SECOND SURFACE ALUMINUM

VACUUM DEPOSITED ON 20-MIL-THICK CORNING 7940 QUARTZ

SAMPLE #1

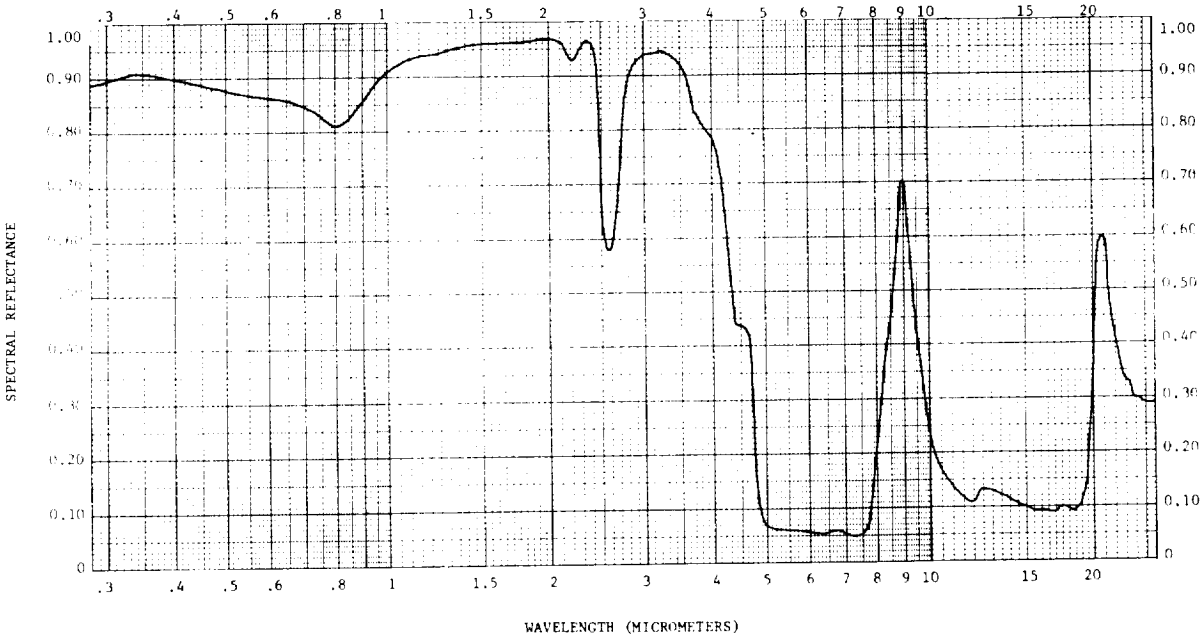

TRW DESIGNATION: 557-69

MATERIAL: SECOND SURFACE ALUMINUM

VACUUM DEPOSITED ON 20-MIL-THICK CORNING 7940 QUARTZ

SAMPLE #2

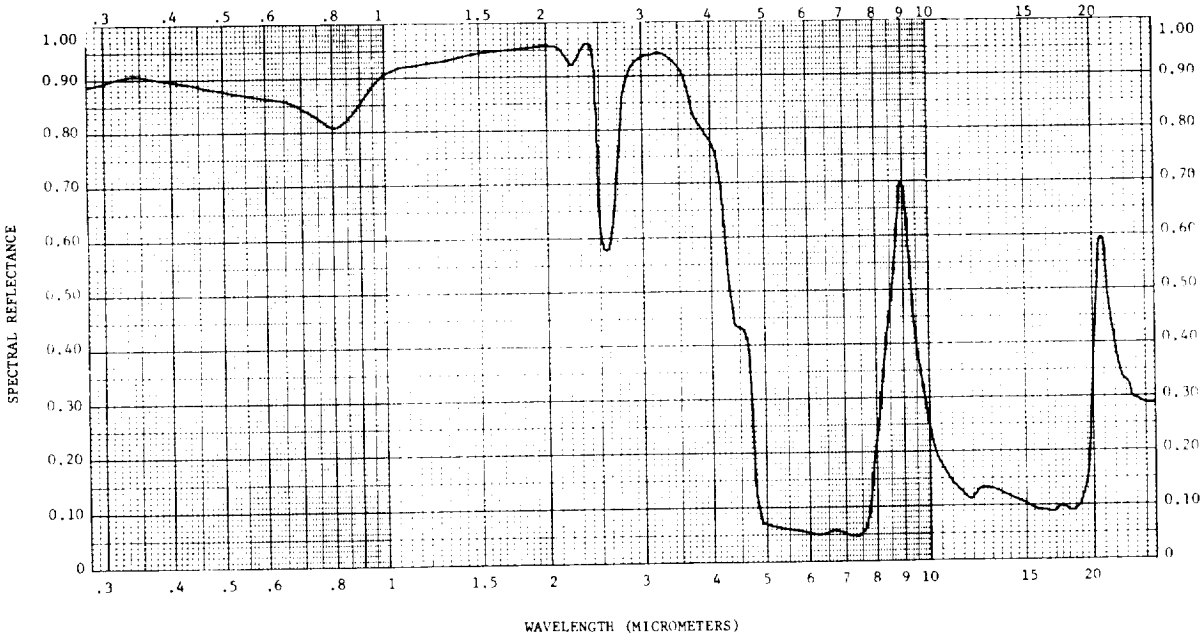

TRW DESIGNATION: 613-69A

MATERIAL: CAT-A-LAC BLACK PAINT

SAMPLE #1

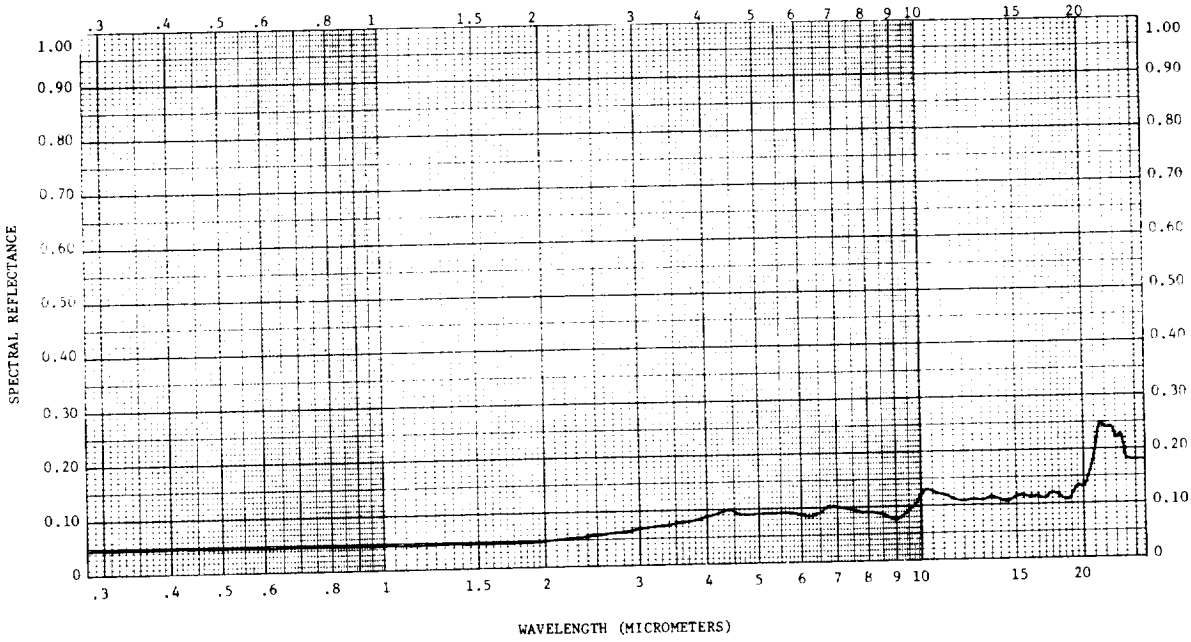

TRW DESIGNATION: 613-69B

MATERIAL: CAT-A-LAC BLACK PAINT

SAMPLE #2

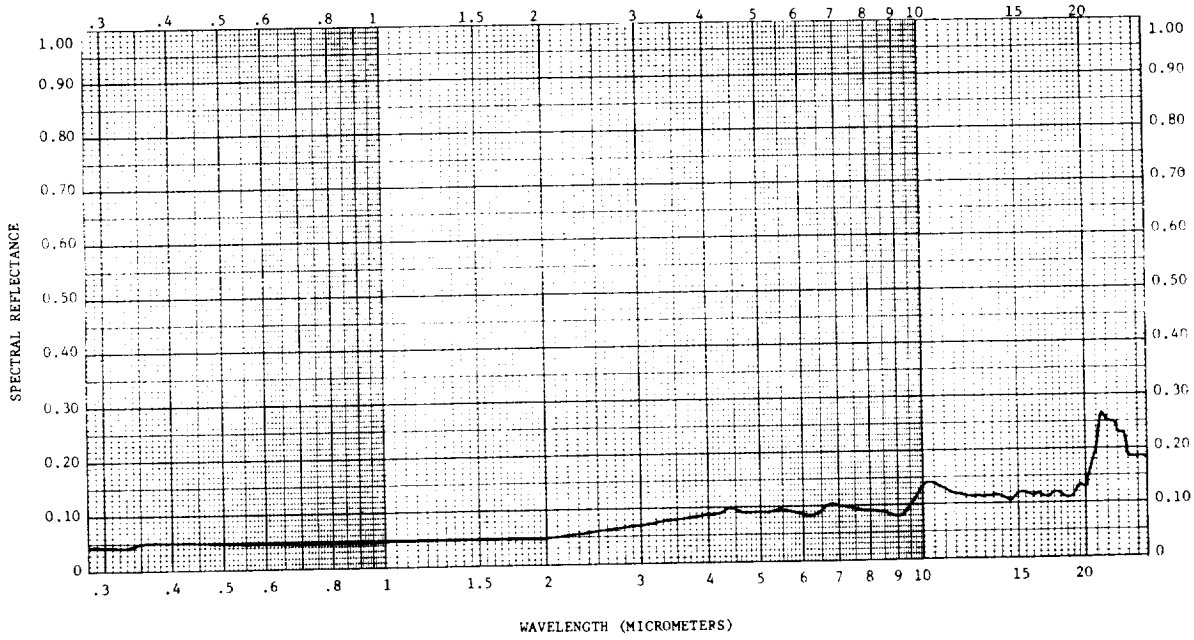

TRW DESIGNATION: 672-69
MATERIAL: RTV-41
SAMPLE #1

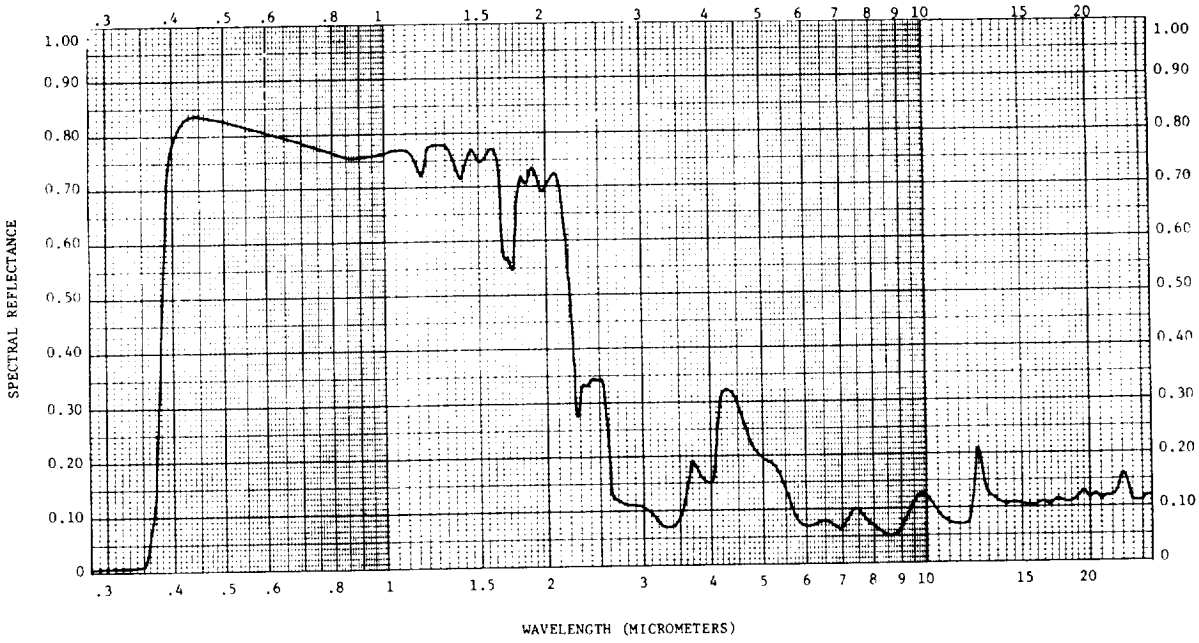

TRW DESIGNATION: 673-69
MATERIAL: RTV-41
SAMPLE #2

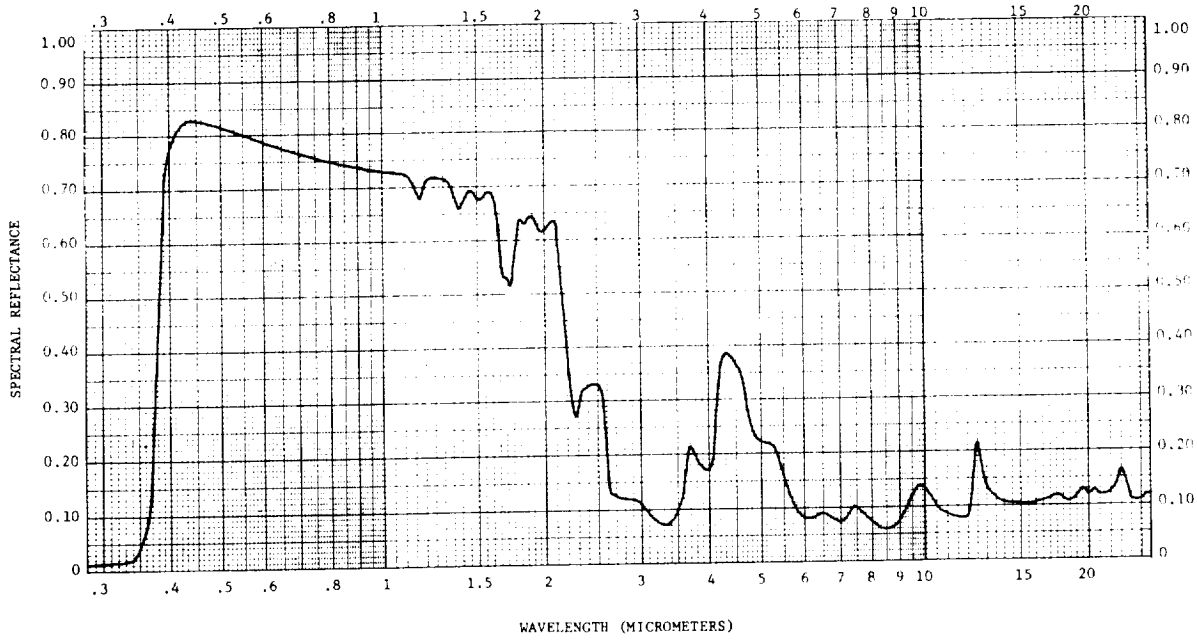

TRW DESIGNATION: 794-69

MATERIAL: RTV-566